MECHANICAL PROPERTIES

OF

UNSATURATED GRANULAR MATERIALS

MECHANICAL PROPERTIES

OF

UNSATURATED GRANULAR MATERIALS

By

ARASH KATEBI-ZAKI, M.Sc., B.Sc.

A Thesis

Submitted to the School of Graduate Studies

in Partial Fulfillment of the Requirements

for the Degree

Master of Applied Science

McMaster University

MASTER OF APPLIED SCIENCE (2004) McMaster University

(Civil Engineering) Hamilton, Ontario

TITLE: Mechanical Properties of Unsaturated Granular Materials

AUTHOR: Arash Katebi-Zaki, M.Sc., B.Sc. (Sharif University of Technology, Tehran, Iran, Amir-Kabir University of Technology, Tehran, Iran)

SUPERVISOR: Professor D.F.E Stolle

NUMBER OF PAGES: xvii, 149

Abstract

The mechanistic design of flexible pavement systems requires the specification of the mechanical properties of unbound granular base/subbase material. The influence of the degree of saturation, low confining pressure, and suction (measured through an SWCC test) on the monotonic and cyclic behavior of granular base/subbase was investigated to obtain a better understanding of granular base behavior corresponding to condition encountered in situ.

In order to achieve this understanding, a series of quick-undrained (UU) monotonic and cyclic triaxial tests were conducted on sand specimens (Material 1 and Material 2) at ambient temperature, with the degree of saturation ranging from 24% to 66%, and confining pressures from 4 kPa to 64 kPa. Additional tests were conducted under UU conditions to determine the effects of freeze–thaw on permanent deformation (plastic strain) and the memory of base material.

The results showed that shear strength and modulus of elasticity increase with increasing confining pressure, and decrease with increasing water content (degree of saturation), as expected. The stress-strain response of the specimens was generally ductile with higher confining pressure and degree of saturation causing greater ductility. The cyclic test results showed that there was a monotonic relationship between accumulated plastic strain and confining pressure, given that ratio of peak shear stress to confining presseure is constant. The research also showed that there is an almost linear relationship between increase plastic strain and moisture content after cyclic tests or freeze-thaw. Overall it was

found that the effect of saturation and change in suction on shear strength and modulus of elasticity is not as significant as the effect of confining pressure. However, it was found that the effects of saturation, suction, and confining pressure were almost equally important when it comes to plastic strain development during cyclic tests or freeze-thaw loading.

Acknowledgments

I would like to acknowledge the support of my research supervisor, Dr. Dieter F.E. Stolle who provided me with valuable insight, advice, and encouragement.

I would like to express my love and gratitude to my parents, Ali and Saltanat, for their continuous support. I also want to sincerely thank my wife, Shabnam, for helping me in editing my thesis.

And, I wish to thank Mr. Peter Koudys for his friendship, as well as his technical support at the geotechnical laboratory.

Table of Contents

List of Tables

List of Figures

List of Symbols

G_s	Specific Gravity
ρ	Bulk density
ρ_d	Dry density
ρ_w	Density of water
$\sigma_1, \sigma_2, \sigma_3$	Total stresses in the principle directions 1, 2, and 3
$\sigma_1', \sigma_2', \sigma_3'$	Effective stresses in the principle directions 1, 2, and 3
σ_n	Normal stress
σ_1^m	Maximum allowable major principle stress
σ_1^a	Applied major principle stress
σ_3^m	Minor principle stress or confining pressure for the triaxial test
τ	Shear stress
τ_f	Shear stress at failure
ϕ^b	Angle of internal friction with respect to matric suction changes
ϕ'	Angle of frictional resistance
ϕ_o	The value of ϕ for σ_3 equal to p_a
$\Delta\phi$	Reduction in ϕ for a 10 fold increase in σ_3
c'	effective cohesion
u_a	Pore air pressure
u_w	Pore water pressure
$\sigma_d = \sigma_1 - \sigma_3$	Deviator stress

$(\sigma - u_a)_f$	Net normal stress on the failure plane at failure
$(u_a - u_w)_f$	Matric suction on the failure plane at failure
χ	Parameter that depends on the degree of saturation and soil type
V	Specific volume
w	Gravimetric water content
w_f	Final water content
w_i	Initial water content
S_r	Degree of saturation
ε_t	Horizontal tensile strain at the bottom of the HMA layer
E_{AC}	Resilient modulus of the HMA
M_R	Resilient modulus
I_p	Plasticity Index
a	Hyperbolic stress-strain parameters
b	Hyperbolic stress-strain parameters
θ	Bulk stress
ψ	Suction
ψ_o	Reference stress is 1.0 kPa
π	Osmotic suction
K_o	Coefficient of lateral earth pressure
ε_p	Permanent Axial Strain
$\Delta\varepsilon_p$	Change in Plastic Strain

N_f	Number of cycles to failure
N	Number of load repetitions
R	Stress ratio

Abbreviations

CD	Consolidated –Drained Test
CU	Consolidated –Undrained Test with pore pressure measurement
CW	Constant Water Content Test
ESAL	Equivalent Single Axle Loads
FEM	Finite Element Model
FWD	Falling Weight Deflectometer
HMA	Hot Mix Asphalt
HVS	Heavy Vehicle Simulator
OPSS	Ontario Provincial Standard Specification
QC	Quality Control Tests
SWCC	Soil Water Characteristic Curve
UC	Unconfined Compression Test
UU	Triaxial tests conducted under undrained conditions

CHAPTER 1

Introduction

1.1 General

Many current pavement design and rehabilitation assessment tools are still based on empirical methods. However, the importance of mechanistic methods for the design and rehabilitation of pavements has been known for many years. Mechanistic methods basically have their roots in the mechanics of materials. Such methods rely heavily on the constitutive properties of pavement layers such as the resilient modulus. In this way a better understanding of pavement response can be achieved; i.e., the stresses, strains, and deflections in the various pavement layers.

The use of mechanistic instead of empirical methods also allows for better prediction of the degree of damage to a given pavement for any particular set of environmental and traffic loads. Such predictive capabilities enable pavement authorities to better quantify the effects of variation of layer material properties, layer thickness, temperature, etc. on the level of damage associated with seasonal changes and traffic loads. However, a complexity that is often overlooked is that a considerable amount of highway construction activity is carried out at relatively shallow depths where the soil is likely to be unsaturated and subjected to low stresses.

The rational design process assumes that the granular base and subbase

courses indefinitely maintain their original moduli. This holds reasonably well if moisture conditions remain constant with time, which is rarely the case given the variability of weather conditions typical to Ontario (from high humidity in August to deep winter frost penetration with severe spring thaw conditions). Therefore, the prediction of pavement response to unsaturated base/subbase requires an understanding of how the mechanical properties of base vary with changes in moisture content and temperature (freeze/thaw) corresponding to low confining pressures.

The experimental research reported in this thesis describes the effects of the degree of saturation, initial suction, temperature and low confining pressure on the mechanical characteristics of unsaturated modified base material. For the research, a modified Granular B material was compacted to a dry density of at least 1.87 g/cm^3 with the water content ranging between 4% and 10.5% by weight. These characteristics represent those of materials used in highways.

This chapter starts with a brief overview of the use of base/subbase material in the design of pavement structures, followed by an explanation of what is needed with respect to research on unsaturated bases, concluding with the objective of the thesis and details of its organization.

1.2 Use of Base Material in Highways

The base course is a layer of material immediately beneath the surface or binder course. Its purpose is to increase load-supporting capacity, allow quick

drainage of water and protect against frost action. Therefore, an appropriate base material requires certain physical properties that must be controlled within limits. These controlled properties, which are available in the AASHTO Guide for the Design of Pavement Structures (1993), are:

- Gradation
- Particle Shape
- Base Stability
- Permeability
- Plasticity
- Abrasion Resistance

A composition of crushed stone, crushed slag, or other untreated/stabilized materials often serve as good base/subbase material because of their high durability, high permeability, and low frost susceptibility.

The specifications which define the requirement for a suitable base material vary from one region to another. In Ontario, many authorities follow the guidelines provided in the Ontario Provincial Standard Specification (OPSS). Aggregates in Ontario for base/sub-base construction are designated as Granular A, B or M. Granular B aggregates are composed of clean, hard, durable, uncoated particles from deposits of gravel or sand, quarried rock. In this research, a modified Granular B aggregate, in which particles greater than the #10 sieve

(2 mm) were removed, was used for the tests conducted. Table 1.1 shows the MTO gradation requirement for the granular base material. It should be noted that the larger aggregate sizes were removed to ensure that sample diameter/largest particle size ratio was reasonable.

1.3 Research Objectives

The purpose of this research was to evaluate the effects of the degree of saturation, low confining pressures, freezing-thawing and initial suction on the monotonic/cyclic behavior of unsaturated modified base/subbase material.

Laboratory tests were conducted to evaluate the following:

- Change in undrained shear strength with a change in degree of saturation and confining pressure.
- Behavior of unsaturated modified granular material at different water contents and confining pressures.
- Effects of initial suction on shear strength parameters at low confining pressures.
- Change in modulus of elasticity (E_{50}) with a change in degree of saturation.
- Change in modulus of elasticity (E_{50}) with a change in confining pressures.
- Effects of water content/confining pressure on cyclic test results.
- Effects of freeze/thaw on cyclic test results.

- Effect of freeze/thaw on the memory of the mechanical properties.

A finite element sensitivity analysis was performed, using SAP 2000, to demonstrate the effect of base modulus of elasticity on surface deflection for an FWD test.

1.4 Organization of Thesis

The research presented in this thesis was primarily concerned with describing how the behavior of base/subbase material, under cyclic and monotonic conditions, varies with the degree of saturation at low confining pressures. In order to gain an understanding of why this variation occurs and justify the work that has been undertaken, it is necessary to present a review of the literature. Chapter 2 presents a brief discussion and short overview of the published research on pavement design. Chapter 3 offers a literature review on material characteristics, with Chapter 4 discussing unsaturated soil mechanics, matric suction, soil-water characteristic curves and unsaturated shear strength.

Chapter 5 presents a sensitivity analysis performed with a finite element computer program. Chapter 6 provides a brief description of the test equipment, materials and procedures used during the experimental part of the research, with Chapters 7 and 8 presenting detailed results for monotonic and cyclic testing, respectively. Finally, Chapter 9 lists the conclusions and observations that can be made from the study and provides recommendations for future research.

Table 1.1: MTO Gradation Requirements (OPSS, 1993)

Ministry Sieve Designation	% passing by mass			
	Granular A	Granular B		Granular M
		Type I	Type II	
150 mm	-	100	100	100
37.5 mm	-	-	-	-
26.5 mm	-	50-100	50-100	50-100
19 mm	85-100	-	-	-
13.2 mm	65-90	-	-	-
9.5 mm	50-73	-	-	-
4.75 mm	35-55	20-100	20-55	20-100
1.18 mm	15-40	10-100	10-40	10-100
300 μm	5-22	2-65	5-22	5-95
150 μm	-	-	-	2-65
75 μm	2-8	0-8	0-10	0-25

CHAPTER 2

Pavement Design

2.1 Introduction

The design of pavements involves three basic external parameters; i.e. the material and geometric characteristics of the base/subgrade upon which the pavement is placed, the applied surface loads and the environmental factors.

The base/subgrade upon which the asphalt layer is placed has a large impact on structural design. The stiffness of the base/subgrade helps determine the pavement layer thickness, the number of layers, and seasonal load restrictions. Traffic loads are used to determine pavement composition, layer type and thickness. Environmental factors such as temperature, moisture and ice formation can affect pavement durability, binder rheology, structural support and ultimately pavement life and failure (Erlingsson et al. 2002).

This chapter provides a summary of pavement design including loading concepts and environmental factors. The material characteristics will be discussed separately in Chapter 3 due to the need for a more detailed discussion as well as the overall appreciation of the nature of the research.

2.2 Loads

Load distribution is one of the primary functions of a pavement and the expected loads that a pavement can be exposed to play an important part in its

design. The loading that needs to be considered includes axle loads, the number of load repetitions, tire contact areas, and vehicle speeds.

According to the simplest rational design procedure, each individual load inflicts a certain amount of unrecoverable damage on a pavement which is cumulative over the life of the pavement. When this damage reaches some maximum value the pavement is considered to have reached the end of its useful service life. Therefore, structural pavement design requires a quantification of all expected loads that a pavement will encounter over its design life. This quantification is often expressed in terms of Equivalent Single Axle Loads (ESAL). This approach converts wheel loads of various magnitudes and repetitions ("mixed traffic") to an equivalent number of "standard" or "equivalent" loads, which usually corresponds to the 80 kN (18,000 lbs) dual tire single axle system (Irick et al. 1991, Huang 1993).

2.3 Environment

Environmental variations can have a significant impact on the properties of the pavement materials and the underlying subgrade, which can drastically affect pavement performance. Every environmental constituent (e.g., solar flux, heat, wind, humidity, etc.) has an incremental effect on a pavement. For instance, asphalt concrete shows visco-elastic-plastic behavior which is temperature dependent, whereas the stiffness and permanent deformation characteristics of

unbound materials show water content dependency (Erlingsson et al., 2002). There are several constituents that exert considerable influence, including:

Moisture - The moisture susceptibility of a material is reflected by its tendency to attract sufficient quantities of water to cause changes in its physical properties. Research studies have demonstrated that moisture susceptibility is related to the suction properties of soil and aggregate properties (Saarenketo et al., 1998). Certain types of soils can be highly expansive when wet and structural design must account for this expansiveness (Jones 1973, Holtz and Gibbs 1956). In general, high water content can have adverse effects on the monotonic and cyclic properties of the pavement materials.

Temperature Variations - The water content and the phase of water within granular materials are directly influenced by ambient temperature conditions (Harris, 1995). Cooler temperatures cause an increase in migration of water toward the ground surface by increasing the height of capillary rise in soils. Conversely, warmer temperatures reduce the height of capillary rise. This is frequently observed during construction performed when a cool season follows a warm season (McCarthy, 1998).

If the road has a high water content or access to free moisture, at freezing temperatures high suction properties can lead to significant frost action (Kono et al.1973, Guthrie and Scullion 2000), causing:

Frost heave - The crystallization of ice within the larger soil voids leading to the formation of ice lenses or veins, causes frost heaving. An ice lense grows

through capillary rise until the water supply is exhausted or until freezing conditions at the freezing interface no longer allow crystallization. As the ice lense grows, the overlying soil and pavement will "heave", possibly causing cracking of the pavement. This problem mainly occurs in soils containing fine particles (often termed "frost susceptible" soils). Clean sands and gravels, with small amounts of fine particles, tend to be non-frost susceptible. The degree of frost susceptibility is mainly a function of the percentage of fine particles within the soil (Knutsson et al. 1985, Holtz 1981).

Thaw weakening - Thawing refers to the melting of ice contained within the base/subgrade. As the ice melts during the spring and turns to liquid it cannot drain out of the soil fast enough and thus the base/subgrade becomes significantly saturated (weaker with less stiffness) and tends to lose bearing capacity. Therefore, surface loads may be quite detrimental to a pavement during thaw periods (Drumm et al. 1997).

2.4 Structural Design of Flexible Pavement

Flexible pavements are layered structures consisting of an asphaltic layer overlying granular base/subbase layers (typically unbound), which in turn are constructed over a prepared subgrade. The layered configuration is designed so as to reduce the imposed surface loading through the pavement layers to a much lower intensity that could be carried by the subgrade without permanent deformations.

A flexible pavement design procedure should provide a layered pavement structure that is capable of sustaining the anticipated heavy traffic loadings for a given design period. It is generally assumed that flexible pavements deteriorate or lose serviceability with time. According to the serviceability concept, pavements display certain distress modes that can fall into three main categories: fracture, distortion, and disintegration. Disintegration refers to distress in the asphaltic concrete layers caused by factors such as low stability, loss of fines, poor asphalt cement-aggregate bonds, etc. Fracture and distortion take the following forms:

- Permanent deformations (distortion mode)
- Load-induced fatigue cracking (fracture mode)
- Thermal-induced cracking (fracture mode).

The accumulation of inelastic permanent deformations associated with repeated wheel loadings, causes permanent deformation, which is a fatigue related distress mode. During the design process, the pavement structure is analyzed and modified as necessary to ensure that the critical distress modes will either be precluded or their effects reduced to tolerable functional levels for the selected design period (Erlingsson, 2004).

Structural design aims to determine the number, material composition and thickness of the different layers within a pavement structure. The two principal methods of flexible pavement design are empirical and mechanistic-empirical. Since this chapter is only meant to provide a brief overview of the different structural design techniques, for detailed analysis of the design methods the

reader is referred to:

- Empirical Method: The AASHTO Guide for Design of Pavement Structures 1993.
- Mechanistic-Empirical Method: The 2002 AASHTO Guide for Design of Pavement Structures.

2.4.1 Empirical Method

An empirical approach is based on the results of experiments or experience and requires making certain observations in order to ascertain the relationships between input variables and outcomes. It is not necessary to firmly establish the scientific basis for the relationships between variables and outcomes as long as the limitations with such an approach are recognized. In some cases, it is much more expedient to rely on experience than to quantify the exact cause and effect of certain phenomena.

2.4.2 Mechanistic - Empirical Method

A mechanistic approach explains phenomena only by reference to physical causes. In pavement design, the phenomena of interest are the stresses, strains and deflections within a pavement structure and the physical causes are the loads and material properties of the pavement structure. The relationship between these phenomena and their physical causes is generally described using mathematical

models, the most common of which is a layered elastic model.

Empirical elements are used, together with the mechanistic approach, when defining the values of the calculated stresses, strains and deflections that result in pavement failure. The relationship between loads and material properties, and pavement failure is described by empirically derived equations that compute the number of loading cycles to failure. The mechanistic-empirical pavement design method has certain basic advantages over a purely empirical one. It uses material properties that relate better to actual pavement performance, provides more reliable performance predictions, and accommodates environmental effects on materials (Erlingsson, 2004). It characterizes materials better allowing for improved use of available materials and, accommodation of new ones.

2.4.3 Mechanistic Models

This section briefly describes the mechanistic analysis procedures used for flexible pavement design

One of the more popular approaches to analysis of pavements is by layered elastic models. This approach makes some basic assumptions, such as:

- Each layer is homogeneous, isotropic, and linearly elastic
- Each layer has a finite thickness h, but the lowest layer is infinite in thickness

- A uniform pressure q is applied on the surface over a circular area of radius a.

Given these assumptions, the theory of elasticity is used to develop solutions for given surface loadings.

The finite element method (FEM) is a numerical analysis technique for obtaining approximate solutions to a wide variety of engineering problems. In the FEM analysis, the pavement is discretized into a number of elements. The FEM approach provides an approximate solution to the layered elastic model. Generally, a finite element model must assume some constraining values at the boundaries of the region of interest. Also, the choice of element geometry (size and shape), as well as interpolation functions, influence overall model performance (Huebner et al., 2001).

2.5 Failure Criteria

The empirical equations, used to compute the number of loading cycles to failure, are a part of the mechanistic-empirical design process. These equations are derived by observing the performance of pavements and relating the type and extent of observed failure to an initial strain under various loads. Fatigue cracking and rutting are two types of failure criteria. These are related to deformations in the pavement subgrade (Huang 1993).

CHAPTER 3

Material Characterization

3.1 Introduction

The mechanistic method of pavement design requires information on material properties as described in Chapter 2. The material properties to be used for analysis include the resilient moduli and the Poisson ratios of subgrade, granular base, and asphalt layer. Since the Poisson ratio has a relatively small effect on pavement responses, it can be reasonably assumed as 0.45 for subgrade soils and 0.35 for all other materials (Huang 1993). The properties of bituminous bounded materials depend on temperature, while the response of granular base/subbase material depends on the water content (Erlingsson and Magnusdottir 2002, Lekarp et.al. 2000, Said and Wahlström 2000, Said et al. 2000). This section describes the methods for estimating the resilient modulus of base material and the factors affecting it.

3.2 Resilient Modulus

During each loading cycle, the applied deviator stress and the corresponding strain is monitored. At the end of the loading phase, the maximum deviator stress is noted and the total strain corresponding to this stage is measured. At the end of the unloading period, the strains corresponding to the plastic strains are evaluated. The resilient modulus is then calculated as the ratio

of the maximum deviator stress to the resilient strains (total strains minus plastic strains).

$$M_R = \frac{\sigma_d}{\varepsilon_r} \tag{3.1}$$

3.3 Estimate of Resilient Modulus for Fine-Grained Soil

Owing to the complexity and equipment requirements of repeated load testing, it is generally preferable to develop approximate methods for the estimation of M_R. The AASHTO design guide (1993) suggests that the M_R of fine-grained soils can be estimated using:

$$M_R = 1500 \text{ CBR (psi)} = 10.41 \text{ CBR (MPa)} \tag{3.2}$$

in which CBR is California Bearing Ratio, which can be measured as per ASTM D1883 or AASHTO T193.

Although the CBR is widely used to characterize subgrade soils, and such a relationship may be useful in practice, it provides a measure of shear strength and compressibility that is not necessarily correlated to a measure of stiffness or modulus. Drumm et al. (1990) proposed an approximate method for predicting M_R from E_i, which is the initial tangent modulus or initial slope of the stress-strain curve under triaxial stress conditions and corresponds to small levels of stress or strain when the stress-strain curve assumed to be hyperbolic.

$$M_R = \frac{a' + b'(\sigma_1 - \sigma_3)}{\sigma_1 - \sigma_3} \tag{3.3}$$

where a', which is a function of ($(\sigma_1-\sigma_3)_{ult}$, %clay, I_p, S_r, γ_d, %passing #200) = material parameter for hyperbolic representation of resilient modulus-deviator stress relationship; and b', which is a function of (E_i, $(\sigma_1-\sigma_3)_{ult}$, w_l, %passing #200) = material parameter for hyperbolic representation of resilient modulus-deviator stress relationship; $\sigma_1-\sigma_3$ = deviator stress; E_i = initial tangent modulus; $(\sigma_1-\sigma_3)_{ult}$ = the asymptotic value of stress difference which is related closely to the strength of the soil. The values of E_i, and $(\sigma_1-\sigma_3)_{ult}$ can be calculated from the hyperbolic stress-strain relation which is described in the following section.

3.3.1 Hyperbolic Stress-Strain Relationship

If the results of soil deformation analysis are to be realistic and meaningful, it is important that the stress-strain characteristics of the soil be represented in a reasonable way. This is difficult because the stress-strain characteristics of soil are extremely complex, and the behavior of soil is nonlinear, inelastic, and highly dependent on the magnitudes of the stresses in the soil.

The hyperbolic stress-strain relationships were developed in an attempt to provide a simple framework capturing the most important characteristics of soil stress-strain behavior, using the data available from conventional laboratory tests.

It has been shown that the stress-strain curves for a number of soils may be approximated quite accurately by hyperbolae like the one shown in Figure 3.1 (Wong and Duncan, 1974). This hyperbola can be represented by an equation of the form:

Equation 3.4:

$$(\sigma_1 - \sigma_3) = \frac{\varepsilon}{\frac{1}{E_i} + \frac{\varepsilon}{(\sigma_1 - \sigma_3)_{ult}}} \tag{3.4}$$

If the hyperbolic equation is transformed to Equation 3.5 as shown below, it represents a linear relationship between $\varepsilon/(\sigma_1-\sigma_3)$ and ε:

$$\frac{\varepsilon}{(\sigma_1 - \sigma_3)} = \frac{1}{E_i} + \frac{\varepsilon}{(\sigma_1 - \sigma_3)_{ult}} = a + b\varepsilon \tag{3.5}$$

where, a and b are material parameters for hyperbolic representation of stress-strain response, corresponding to initial tangent modulus and unconfined compressive strength, respectively. E_i is the initial tangent modulus or initial slope of the stress-strain curve; and $(\sigma_1-\sigma_3)_{ult}$ is the asymptotic value of stress difference which is related closely to the strength of the soil.

To determine the best-fit hyperbola for the stress-strain curve, values of $\varepsilon/(\sigma_1-\sigma_3)$ are calculated from the test data and are plotted against ε. The best fit straight line on this transformed plot corresponds to the best-fit hyperbola on the stress-strain plot. When data from actual tests are plotted on the transformed plot,

the points are frequently found to deviate from the ideal linear relationship. The data for stiff soils, such as dense sands, usually plot on a curve which is concave upward. However the data for soft soils, such as loose sands, usually plot on a curve which is concave downward.

A good match is usually achieved by selecting the straight line so that it passes through the points where 70% and 95% of the strength are mobilized. In practice, only two points for each stress-strain curve (the 70% point and the 95% point) are plotted on the transformed diagram (Wong and Duncan, 1974). Figure 3.2 shows a schematic plot in terms of transformed parameters $\varepsilon/(\sigma_1-\sigma_3)$ and ε for medium-dense sand (Wong and Duncan, 1974).

3.4 Factors Affecting the Resilient Properties of Granular Materials

As illustrated by Drumm et al. (Equation 3.3), the resilient modulus is a function of deviatoric stress level (σ_d), degree of saturation (S_r), density (γ_d), fines content (%passing sieve #200), and material parameters for the hyperbolic representation of stress-strain response(E_i, $(\sigma_1-\sigma_3)_{ult}$). A literature survey of resilient moduli studies by other investigators indicates that these factors have a significant effect on the resilient response of granular materials. The factors are discussed further in the following section.

3.4.1 Stress Level

Some investigators (Fredlund et al. 1977, Rhee 1991, Kim 2001) have determined that the bulk stress level has the greatest effect on the resilient response of granular materials. The resilient modulus increases with confining pressure (cell pressure σ_3) and, is relatively unaffected by the magnitude of repeated deviator stress as long as the repeated stress does not cause excessive permanent deformation. AASHTO (2002) has adopted the bulk stress model as Equation 3.6 for base/subbase soils:

$$M_R = k_1 (\theta)^{k_2} \qquad (3.6)$$

where, $\theta = \sigma_1 + \sigma_2 + \sigma_3$ = bulk stress, with σ_1, σ_2 and σ_3 being the major, intermediate, and minor principal stresses, respectively; k_1 and k_2 are constants determined experimentally.

A typical plot of M_R versus bulk stress is shown in Figure 3.3.

Extensive testing of granular materials has indicated that both the number of stress repetitions and the sequence of the applied stresses have little, if any, effect upon the M_R value (Kim et al. 2001). This implies that one specimen can be repeatedly used to derive the constants of Equation 3.6. In general, after "conditioning" the specimen with about 1000 repetitions, M_R values may be calculated after 150 to 200 repetitions at each stress state. In addition, the load duration and frequency have little effect upon the granular aggregate.

3.4.2 Aggregate Properties and Specimen Diameter

Aggregate gradation, moisture content, and shape properties have significant influence on the mechanical response of unbound base layers. Aggregate particle shape can be expressed using three independent properties: form, angularity, and surface texture (Barrett, 1980; Masad, 2000). Form quantifies the dimensional proportions of an aggregate. Angularity refers to the sharpness or roundness of the corners, while texture refers to the small-scale asperities at the surface of a particle. Within a specific type of aggregate (mineralogy and classification) texture and aggregate shape significantly influence the resilient response of the granular material. Rough-textured and angular aggregates develop a stronger and stiffer mass by locking together while smooth-textured and rounded aggregate particles tend to slide past one another. Studies have proven that the intuitive and obvious is true: crushed aggregates, high in angularity and roughly textured, provide better load carrying capacity and a higher resilient modulus than rounded, uncrushed particles (Hicks and Monismith, 1971; Allen, 1973; Allen and Thompson, 1974; Barksdale and Itani, 1989; Thom and Brown, 1989).

Thom and Brown (1987) reported that resilient modulus generally decreases as the fine content increases. Hicks and Monismith (1971) found that resilient modulus decreases as fines content increases for partially crushed aggregates, but they found an opposite effect for fully crushed aggregates. The dry density decreases as the fine content increases. It may be inferred that

aggregate gradation and amount of fines has an indirect effect on the resilient behavior of unbound granular bases by affecting the impact of moisture and density of the system. A more direct impact of gradation on stiffness occurs due to the manner in which the fine particles fill the voids and impact the interaction among the coarser, angular particles. This can be visualized in the extreme when one compares a "floating matrix" where the the coarse aggregate floats in the fines – preventing interaction – with a lack of fines where only coarse aggregate interaction provides a resistance to movement. The intermediate case is where the coarse aggregate and fine aggregate blend is appropriately balanced to provide optimum density and maximum particle interaction (Kim, 2001).

The resilient moduli determined from specimens of the same maximum particle size (same gradation) were almost identical, independent of specimen diameter, confirming that the effect of specimen size is negligible when the ratio between the diameter of the specimen and the maximum particle size is greater than 6. However, for a given confining pressure, the resilient modulus decreases with an increase in the maximum particle size (Kim, 2001).

3.4.3 Suction Induced by Freeze/Thaw

The significance of suction in modeling resilient response is generally recognized (Bergan and Monismith 1973, Fredlund et al.1975, Brown and Pappin 1981, Cole et al. 1986). Fredlund et al. (1975) stressed the fundamental importance of including the pore air and pore water stress states as well as the

applied stress in the development of a resilient modulus model. Since the pore air pressure will tend to equal atmospheric pressure in a field situation, it can be considered essentially as a constant. The effect of suction, apart from the externally applied stresses, has been investigated by Cole et al. (1981) based on laboratory tests performed on soils from Winchendon, Massachusetts.

Examination of the data showed that the stress function exponent k_2 (Equation 3.6) is statistically independent of the suction. Furthermore, it was found that the effect of suction on the resilient modulus can be represented by making k_1, a function of suction. where A, is a regression constant and:

$$k_1 = \left[\frac{101.36 - \Psi}{\Psi_0} \right]^A \tag{3.7}$$

The value 101.36 represents atmospheric pressure in kPa, ψ is suction in kPa (expressed as a positive number) and ψ_o is a reference stress = 1.0 kPa.

Given appropriate conditions, the more frost susceptible soils will undergo more heave. The moisture uptake associated with frost heaving generally results in a decrease in the soil density along with an increase in moisture content, possibly to the point of complete saturation. This occurs to varying degree in the test soils, depending on their level of frost susceptibility (Chamberlain, 1983). Upon thawing, the suction is generally near zero, while during subsequent recovery we find a continuing increase in ψ (decrease in the moisture content) and an increase in dry density. Densification takes place not only upon thaw as the soil consolidates and any pore water pressure dissipates, but also under the action

of the cyclic loads imposed during testing.

3.4.4 Stress Duration and Frequency

Based on repeated loading triaxial tests with both variable and constant confining chamber pressure, Cole et al. (1986), Kim et al. (2001) reported that the resilient response of well-graded granular materials is independent of stress pulse duration and loading frequency.

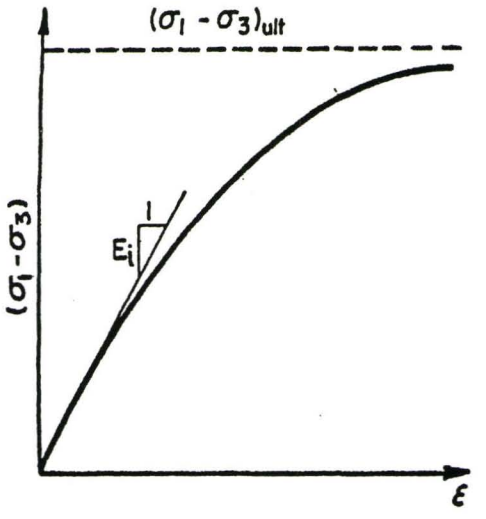

REAL

$$(\sigma_1 - \sigma_3) = \frac{\varepsilon}{\frac{1}{E_i} + \frac{\varepsilon}{(\sigma_1 - \sigma_3)_{ult}}}$$

Figure 3.1: Hyperbolic Representation of a Stress-Strain Curve

(Wong and Duncan, 1974)

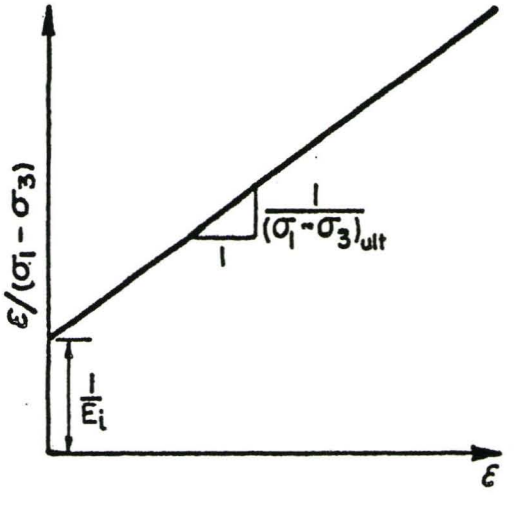

TRANSFORMED

$$\frac{\varepsilon}{(\sigma_1 - \sigma_3)} = \frac{1}{E_i} + \frac{\varepsilon}{(\sigma_1 - \sigma_3)_{ult}}$$

Figure 3.2: Transformed Plots for Sandy Material (Wong and Duncan, 1974)

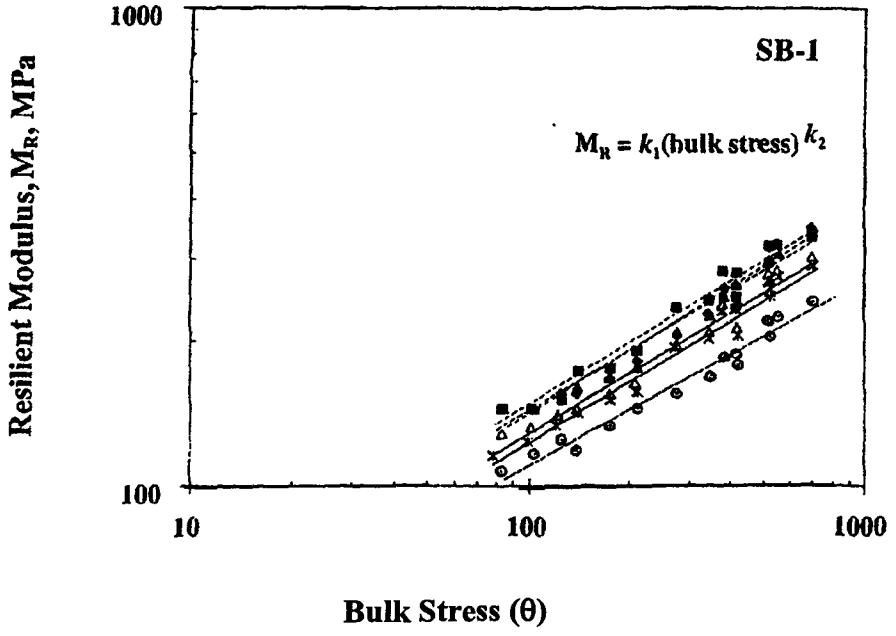

Figure 3.3: Variation in Resilient Modulus with Bulk Stress (Kim et al., 2001)

CHAPTER 4

Unsaturated Soil Mechanics

4.1 Introduction

A considerable amount of construction activity is carried out at relatively shallow depths where soil is likely to be unsaturated and subjected to low stresses. One particular example is the design and construction of roads and highways. The prediction of pavement response taking into account unsaturated base requires stress analysis techniques using a suitable stress-strain model. Current practice in analyzing problems at shallow depths, particularly with coarse-grained soils, is usually to ignore the unsaturated nature of the material. In effect, it is assumed that the influence of level of saturation may be considered to be negligible when compared to other factors.

Previous research into the behavior of unsaturated soils has shown that the suction induced by non-saturation decreases as the particle size, and hence void size, of the soils increase. The influence of suction induced in granular soils has largely been ignored because their magnitude is generally small relative to the stress levels imposed on the soil by self weight, or construction for most engineering activities, and traffic loading. However, for shallow depth activities (less than 2m) the stress levels will be less than 40 kPa. For example, in pavement design where a 20 cm HMA layer is laid down on top of a 40 cm base, the vertical pressure (σ_v) will be equal to γh, where, γ is the average unit weight of the hot

mix and base material, and h is the distance from the middle of the base to the top of the HMA. Assuming $\gamma = 20$ kN/m^3, and h = 0.4 m, the $\sigma_v = \gamma h = 20 \times 0.4 = 8$ kPa. The horizontal confining pressure is even smaller; i.e, $\sigma_h \approx K_o \sigma_v \approx 0.5 \times 8 =$ 4 kPa assuming that the coefficient of lateral earth pressure is 0.5. Given such low confining pressures, suctions induced in granular soils could have an effect on the soil behavior; particularly if the base/subbase has a high fraction of fines. The following section briefly reviews some of the literature on unsaturated soils to gain a better understanding of their behavior.

4.2 Soil Suction

Suction has been found to be an important property that affects the strength, compressibility, and stress-strain response of unsaturated soils. The relation between matric suction and water content is called a retention curve or soil-water characteristic curve (SWCC) (Fredlund and Rahardjo, 1993). Water is held in an unsaturated medium by forces whose effects are expressed in terms of the pressure of the water.

The total suction, ψ, of a soil is made of two components; the matric suction, which is the water pressure in a pore of the medium relative to the air pressure, $(u_a - u_w)$, and the osmotic suction, π:

$$\psi = (u_a - u_w) + \pi \qquad (4.1)$$

If the changes in osmotic suction are compared to those in matric suction when the water content is varied, the total and matric suction curves are almost the

same, particularly in the higher water content range. In other words, a change in total suction is essentially equivalent to a change in the matric suction; i.e., $\Delta\psi \approx \Delta(u_a - u_w)$.

The matric suction component is commonly associated with the capillary phenomenon arising from the surface tension of water, which is the result of the intermolecular forces acting on molecules at the air-water interface; i.e., the contractile skin. In soils, the pores with small radii act as capillary tubes that cause the soil water to rise above the water table. The capillary water has a negative pressure with respect to the air pressure, which is generally atmospheric (i.e. $u_a = 0$ gauge pressure) in the field. An increase in the radius of the curvature results in a decrease in the capillary height. In other words, the non-uniform opening along the capillary tube can affect the capillary height.

The development of capillary force in a soil is also affected by the pore size distribution in the soil. A non-uniform distribution results in hysteresis in the SWCC. Thus, at a given matric suction, the soil water content during the wetting and drying processes is different. In addition, the equivalent contact angle at an advancing interface during the wetting process is different from that at a receding interface during the drying process. The above factors, as well as the presence of entrapped air in the soil, swelling, shrinking or aging are considered to be the main causes for hysteresis in the SWCC. Hysteresis is very important where wetting and drying cycles occur, such as would be seen in the field. Figure 4.1 shows the typical soil-water characteristic curves for fine sand, glass beads,

volcanic sand, and silt loam, Figure 4.2 shows a typical wetting-drying SWCC.

Soil suction has been shown to be largely independent of material density in the medium to low saturation range (Heath 2002). Figure 4.3 shows the retention curve for different dry densities of sand. As can be observed in this figure, the results do not depend on the density of the specimen (Fredlund et al. 1997).

4.3 Unsaturated Shear Strength

A theoretical framework for unsaturated soil mechanics that parallels saturated soil mechanics is available in terms of stress state variables, such as net normal stress, $(\sigma_n - u_a)$, and matric suction, $(u_a - u_w)$ where σ_n is the normal stress, u_a is the pore-air pressure, and u_w is the pore-water pressure (Fredlund and Rahardjo 1993, Vanapalli 1997, Yoshimine et al. 1999). Several advancements have been made in the prediction of the strength behavior of unsaturated soils in recent years. These procedures use the soil-water characteristic curve, either directly or indirectly, along with the saturated shear strength parameters, c' and ϕ', to predict the shear strength function (Vanapalli et al. 1996, Fredlund et al. 1996, Öberg and Sällfors 1997, Khallili and Khabbaz 1998). The following section briefly summarizes some of these equations.

4.3.1 Equations

Bishop (1959) proposed a shear strength equation for unsaturated soils by

extending Terzaghi's principle of effective stress for saturated soils:

$$\tau = c' + \sigma' \tan \phi' \quad (4.2)$$

where, $\sigma' = (\sigma - u_a)_f + \chi (u_a - u_w)_f$; τ = shear strength of unsaturated soil; c' = effective cohesion; ϕ' = angle of frictional resistance; $(\sigma - u_a)_f$ = net normal stress on the failure plane at failure; $(u_a - u_w)_f$ = matric suction on the failure plane at failure; and χ = a parameter that depends on the degree of saturation and soil type. The value of χ was assumed to vary from 1 to 0, which represents the variation from a fully saturated condition to a total dry condition. Several investigators have however found limitations with respect to the quantification of the parameter χ, both theoretically and experimentally (Miao et al. 2001, Rassam and Williams 1999).

Fredlund et al. (1978) proposed a relationship to explain the shear strength of unsaturated soils in terms of two independent stress state variables:

$$\tau = c' + (\sigma - u_a)_f \tan \phi' + (u_a - u_w)_f \tan \phi^b \quad (4.3)$$

where, ϕ^b = angle indicating the rate of increase in shear strength relative to matric suction, $(u_a - u_w)$. The shear strength contribution due to matric suction, ϕ^b, was initially assumed to be linear based on the analysis of limited results published in the literature (Fredlund and Rahardjo 1993). Later, experimental studies performed over a broad range of suction values showed that the variation of shear strength with respect to soil suction is non-linear (Gan and Fredlund, 1988, Escario and Juca 1989). Equation 4.3 can be applied to both the linear and non-linear variation of shear strength with respect to suction. Figure 4.4 shows

shear stress v.s. normal stress for undrained triaxial tests.

As the soil moves from a saturated state to a drier state, the distribution of the solid, water, and air phases changes as the stress state changes. The wetted area of contact between the soil particles decreases with an increase in the soil suction. There is a relationship between the rate at which shear strength changes in unsaturated conditions and the wetted area of water contact between the soil particles or aggregates. In other words, a relationship exists between the soil-water characteristic curve and the shear strength of unsaturated soils.

Öberg and Sällfors (1997) proposed an equation for predicting the shear strength of primarily non-clayey soils such as sands and silts:

$$\tau = c' + (\sigma_n - u_a)_f \tan\phi' + (u_a - u_w)_f \left[S(\tan\phi')\right] \quad (4.4)$$

Examining Equation 4.4 and comparing to 4.2, the χ parameter proposed by Bishop is replaced by the degree of saturation. They state that this χ factor reflects the fraction of the pore area that is occupied by water (i.e. A_w/A_t) which is approximately equal to the degree of saturation, *S*. Equation 4.4 has not been experimentally verified through the measurement of shear strength and degree of saturation at the point of failure in the specimens. Implicit in this equation is the assumption that there is a one to one relationship between the degree of saturation, and the area of water contact along the shear plane in the soil.

4.3.2 Shear Strength versus Confining Pressure

The shear strength increases with an increasing effective confining pressure. The matric suction in the soil decreases with an increase in degree of saturation accompanied by a reduction in the volume. In undrained loading conditions for unsaturated soils, the increase in shear strength caused by an increase confining pressure is greater than the reduction of shear strength associated with the decrease in matric suction. In Figure 4.4, the diameter of the Mohr circles increase with an increase in confining pressure. The envelope defines a curved relationship between the shear strength and total normal stress for unsaturated soils tested under undrained conditions. Once the soil becomes saturated under the application of confining pressure a horizontal envelope develops with respect to the shear strength axis.

Under saturated conditions, where a single stress state variable, $(\sigma - u_w)$, controls the strength, an increase in the confining pressure will be equally balanced by a pore-water pressure increase. The effective stress, $(\sigma_3 - u_w)$, remains constant regardless of the applied confining pressure, σ_3. Once the soil is saturated, the undrained shear strength behavior is in accordance with $\phi_u = 0$ concept (Bishop, 1959 and Fredlund, 1989).

4.3.3 Effect of Confining Pressure on Angle of Friction

The Mohr envelope for almost all soils is curved to some extent, and the wider the range of pressures involved, the greater the curvature. Experimental

evidence has shown ϕ' is not constant for dense granular materials at low effective confining pressures. The following equation fits laboratory shear test data on compacted granular soils (Duncan et al. 1974):

$$\phi' = \phi'_o - \Delta\phi' \log_{10}\left(\frac{\sigma'_3}{p_a}\right) \tag{4.6}$$

$$\phi' = \phi'_c \qquad \text{when } \sigma'_3 > \sigma'_{3c}$$

where, ϕ'_o is the value of ϕ' for σ'_3 equal to p_a, and $\Delta\phi'$ is the reduction in ϕ' for a 10 fold increase in σ'_3. The values of ϕ'_c, and σ'_{3c} are the effective friction angle and confining pressure at critical state, respectively. The parameter p_a is atmospheric pressure (Wong and Duncan, 1974).

4.3.4 Variation of E_i with Confining Pressure

For all soils, except fully saturated soils tested under UU conditions, an increase in confining pressure will result in a steeper stress-strain curve and higher shear strength. Therefore, the values of E_i (initial tangent modulus) and q_f, increase with increasing confining pressure. This stress-dependency is taken into account by using empirical equations to represent the variations of E_i with effective confining pressure.

$$E_i = Kp_a\left(\frac{\sigma'_3}{p_a}\right)^n \tag{4.7}$$

where, the parameter K is the modulus number and n is the modulus exponent (Wong and Duncan, 1974).

4.4 Stress Paths

The successive states of stress in a test specimen or an in-situ element of soil can be represented by a series of Mohr circles or by a series of stress points, often corresponding to the stress on the plane of maximum shear. The curve connecting the relevant stress points is called the stress path, giving a clear representation of the successive states of stress (Craig, 1990).

4.5 Shear Testing Procedure

Modified laboratory tests can be used to establish the properties of an unsaturated soil. For example, a modified direct shear test or triaxial test can be used to measure the relationship between matric suction and shear strength. However, the equipment for such tests is costly, and is not available in most labs.

4.5.1 Triaxial Test

Various triaxial test procedures are used for unsaturated soils. These methods are usually given two-word designations:

1) Consolidated –Drained or CD test
2) Consolidated –Undrained or CU test with pore pressure measurement
3) Constant Water content or CW test
4) Unconfined Compression or UC test.

The CW test is a special case where only the pore air is kept in a drained mode, while the pore water is kept undrained during the shear test (Rampino et al. 1999).

4.5.2 Undrained Triaxial Tests

The procedure for performing an undrained test on an unsaturated soil specimen using the triaxial shear apparatus is similar to the procedure used for performing a typical undrained test on a saturated soil specimen. The unsaturated soil specimen is tested at its initial water content or matric suction. In other words, the initial matric suction in the specimen is neither relaxed nor changed prior to commencing the test. Both confined and unconfined compression triaxial tests can be conducted and the shear strength contribution due to suction can be interpreted in terms of total stress.

Matric suction changes in an unsaturated soil under undrained loading conditions are analogous to the changes in pore-water pressures in saturated soils under similar conditions of loading. Volume change in unsaturated soils under undrained loading is due mainly to the compression of air. Undrained pore pressures are assumed to be generated immediately after loading.

4.5.3 Unconfined Compression Test

The unconfined compression test is a special case of the undrained test, in which the soil specimen is sheared quickly by applying an axial compressive load in order to maintain undrained conditions until failure is reached (strain rate $\approx$ 1.2 mm/min). Theoretically, this should apply to both the pore-air and pore-water phases. The pore-air and pore-water pressures are not commonly measured during compression.

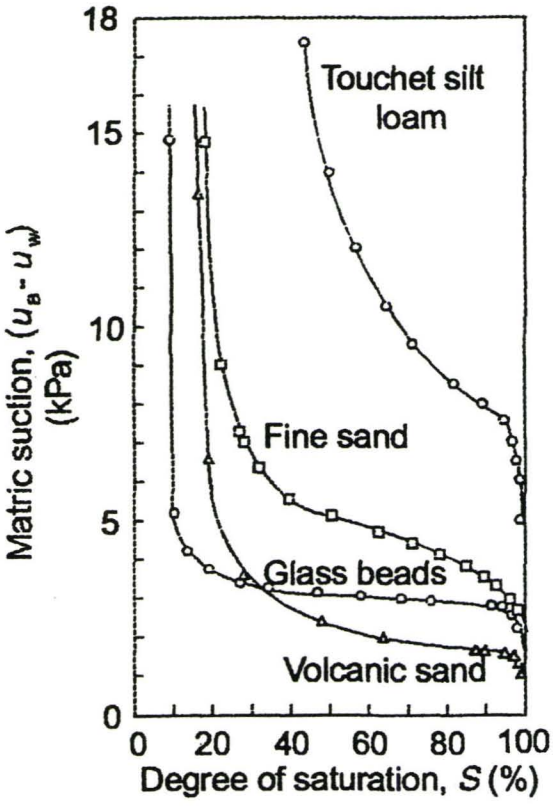

Figure 4.1: Typical Retention Curve for Different Materials (Barbour, 1998)

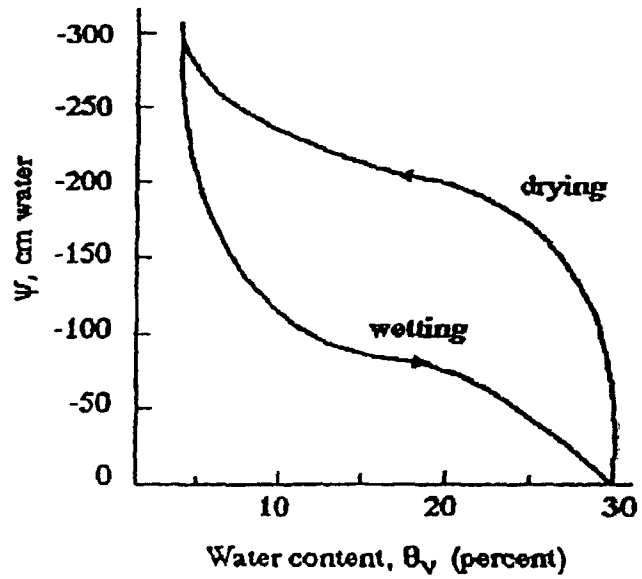

Figure 4.2: Drying-Wetting Hysteresis Curves (Fredlund and Rahardjo, 1993)

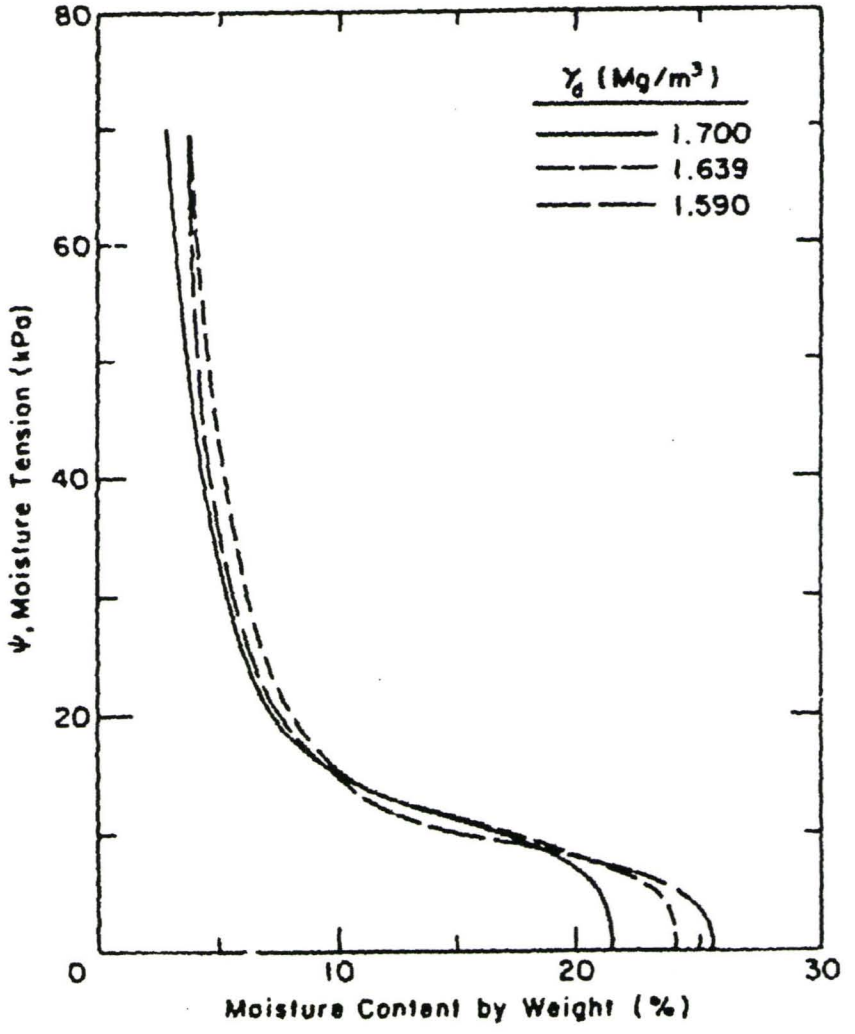

Figure 4.3: Water Retention Curve for Ikalanian Sand (Cole, 1986)

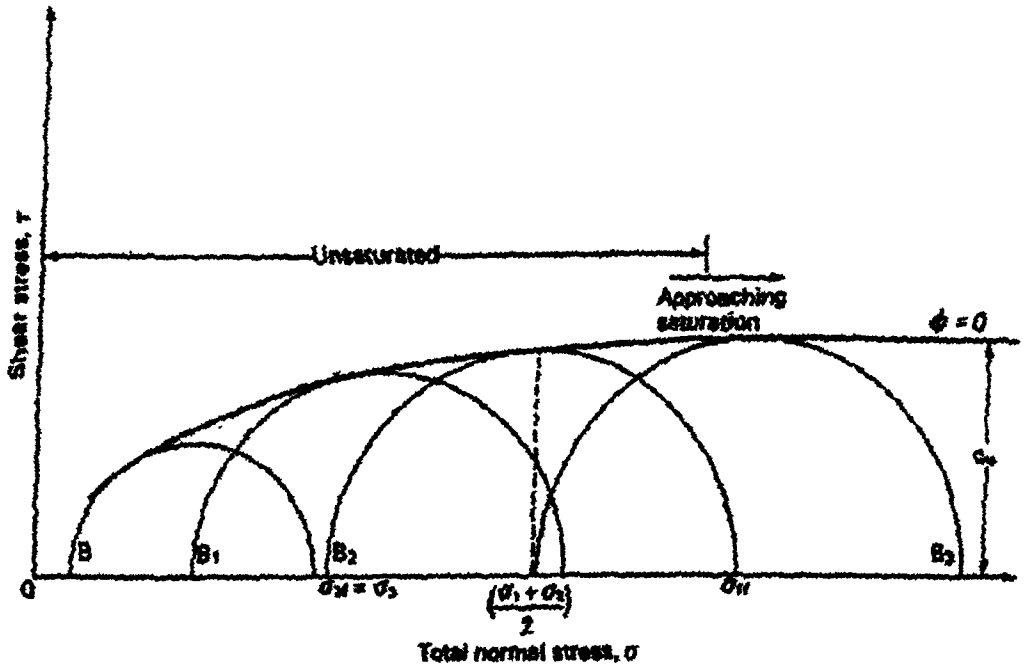

Figure 4.4: Shear Stress vs. Normal Stress ,UU Test

(Fredlund and Rahardjo, 1993)

CHAPTER 5

Sensitivity of Deflection to Base Modulus

5.1 Introduction

Deflection measurements have long been used to evaluate the structural capacity of the pavements whose properties depend on temperature and water content and to back calculate the elastic moduli of the pavement components. If allowable pavement surface deflections are available, they can be used to assess the need for seasonal load limits.

This chapter begins with a brief discussion of Falling Weight Deflectometer testing, and back calculation technique. Thereafter a computer analysis is performed to demonstrate how sensitive FWD test results are to changes in base modulus. An important reason for addressing moisture sensitivity of base materials is to examine if the effect of moisture changes can be detected by FWD testing. We know that changes in surface deflection measured by FWD can be affected by changes in Hot Mix Asphalt temperature-related properties or subgrade moisture-related properties. However, since this thesis focuses on the effect of base/subbase properties these changes are not taken into consideration in the example presented in this chapter.

5.2 Falling Weight Deflectometer

A FWD is a device that delivers an impulse to the pavement surface by

dropping a weight from a certain height. By varying the drop height and weight, a peak force ranging from 6.7 kN to 107 kN can be generated. The load is transmitted to the pavement through a loading plate, 300 mm in diameter, providing a load pulse in the form of a half sine wave with duration typically ranging from 25 to 30 ms. The magnitude of the load is measured by a load cell. Deflections are measured by velocity transducers mounted on a bar that can be lowered automatically to the pavement surface with the loading plate. One of the transducers is located at the center of the plate, while the remaining ones are placed at various offsets up to 2.25 m (Huang, 1993).

5.2.1 Back Calculation of Moduli

"Back calculation" is a mechanistic evaluation of pavement surface deflection basins generated by various pavement deflection devices. It takes a measured surface deflection and attempts to match it (within tolerable error) with a calculated surface deflection, generated from an identical pavement structure using assumed layer stiffnesses (moduli), which are adjusted until they produce a surface deflection that closely matches the measured one. The combination of assumed layer stiffness that results from this match is then assumed to be near the actual in situ moduli for the various pavement layers (Lytton, 1989).

5.3 Pavement Computer Model

A pavement comprising of HMA, base, and sub-base was modeled using a

finite element computer program called SAP2000. This static analysis was based on the assumption that all layers are linear elastic. Although HMA layers are viscoelastic and granular layers are nonlinear elastic, an approximate procedure is to assume them to be linear elastic (Huang, 1993). To illustrate the effect of some design factors on pavement responses, an elastic 3-layer system shown in Figure 5.1 was studied. Emphasis was placed on studying the influence of base layer modulus on measured response. Table 5.1 shows the modulus and Poisson ratio of different layers of pavement (Huang, 1993). Figure 5.2 shows the geometry of the 3-D model which was generated using solid elements.

5.3.1 Geometry

A 2 m x 2 m x 2.5 m symmetric model was found to be sufficient for the analysis after having initially tested a 10 x 10 x 10 m model. Any stresses outside the 2 m x 2 m area were found to be negligible. The circular plate with a diameter of 30 cm was instead represented by a 30 cm x 30 cm plate in the computer model. Since the model is symmetrical, symmetry was used and only a quarter of the problem was discretized.

Since any deflection beyond a depth of 2.5 m was found to be negligible, this depth was assumed to be sufficient for the model. To ensure that the assumption was correct, an analysis was completed for the case in which a spring whose stiffness was calculated from the $E_{sub\text{-}base}$ (Tomlinson, 1991) was placed under each node at a depth of 2.5 m. Since the results showed that deflections

were negligible, the springs were replaced by pinned supports at those points when performing additional simulations.

5.3.3 Loading

A 40 kN (9 kips) distributed load was applied to a 30 cm x 30 cm plate. This uniform load was applied to a 15 cm x 15 cm plate at the corner of the pavement model, which represented a FWD test.

5.3.4 Boundary Conditions

Figure 5.2 shows the geometry of the pavement model. In the x-z plane, the deflection in the y direction and rotation in the x and z directions were fixed for all nodes. The deflection of the nodes in the z direction was also fixed at z = -2.5. In the y-z plane, the deflection in the x direction and rotation in the y and z directions were fixed. In this case also, the deflection of the nodes in the z direction was fixed at z = -2.5. Where these two planes intersect (z-axis), the deflection in the direction of x, y and the rotation in all directions were fixed except for the node at z = -2.5 for which deflection and rotation was fixed in all directions.

5.4 Results

The main purpose of this analysis was to show how sensetive FWD test results are to changes in the base modulus. As shown in Table 5.2, and in Figures

5.3 and 5.4, the deflection in the centre of the plate increases by 7% when E_b decreases by 20%. Figure 5.3 shows a linear relationship between maximum deflection at the center of the plate and the base modulus of elasticity. As can be seen in this figure, with increasing modulus of elasticity the deflection decreases in a linear fashion. Figure 5.4 shows the maximum deflection vs. distance away from the center of the plate. In this case, there is a very slight upward curvature. The values of maximum deflection decrease in a linear fashion the further away the distance is from the center of the plate. It is important to recognize that changes in elastic modulus due to moisture changes must approach 20% in order to capture changes in peak deflection of the order of 7%. In other words, surface deflection is relatively insensitive to the properties of the base layer, which in turn implies that deflection measurements are not a good indicator of changes in the properties of the base/subbase due to possible changes in moisture.

Table 5.1: Properties of the Pavement Layers

Pavement Layers	Modulus of Elasticity (MPa)	Poisson Ratio
HMA	2758	0.45
Base	Variable*	0.35
Sub-grade	138	0.35

* Base modulus are: 138, 159, 171, 179, 207 MPa

Table 5.2: Deflection at the Center of the Plate

δ_{max} μm	Base Modulus MPa	E_b % Changes	δ_{max} % Changes
254.5	138	-20	+7
242.1	159	-7	+2
237.25	170.75	0	0
232.1	179	+7	-2
220.3	207	+20	-7

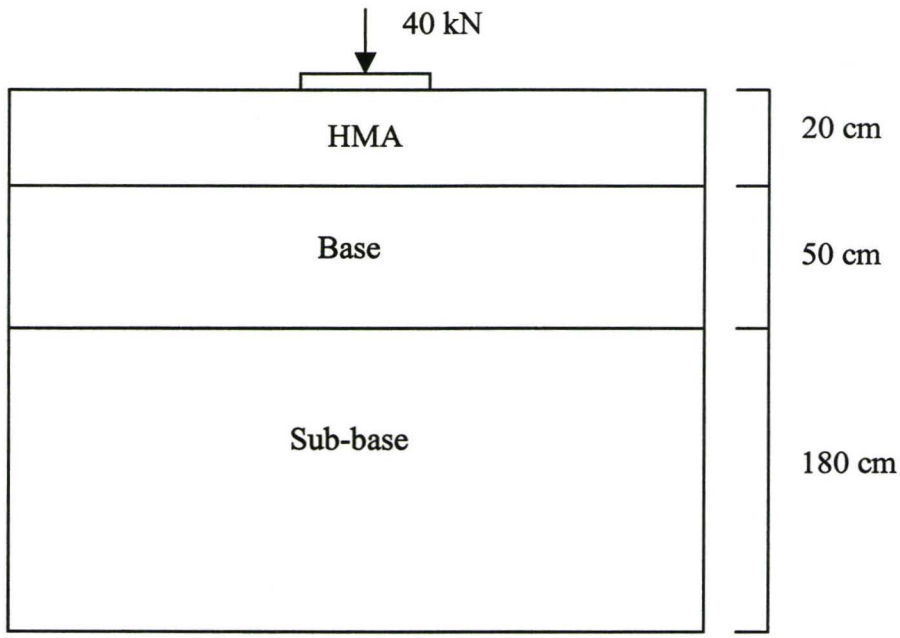

Figure 5.1: Elastic 3-Layer System

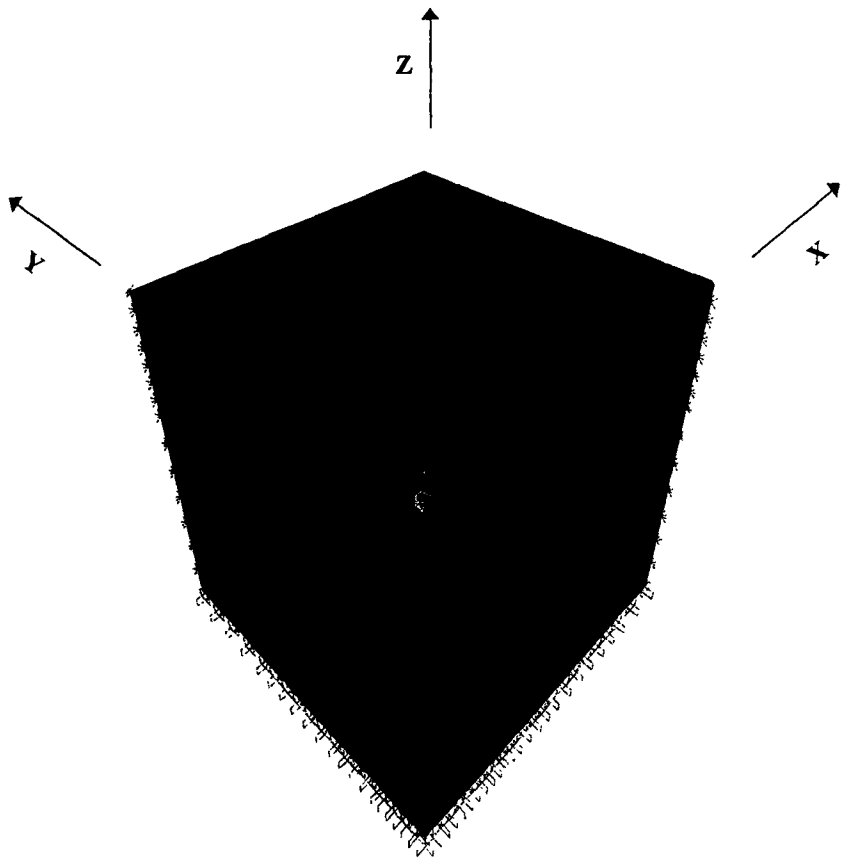

Figure 5.2: Computer Model

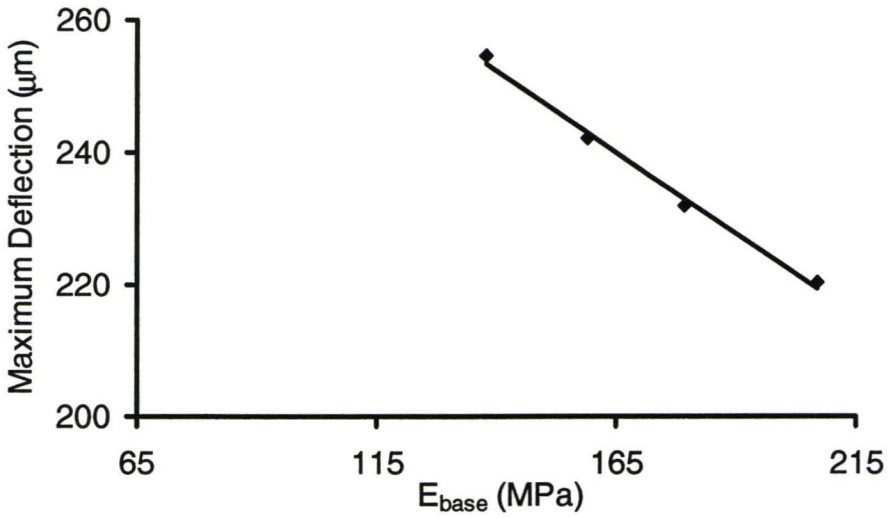

Figure 5.3: Maximum Deflections at the Center of the Plate vs. E_{base}

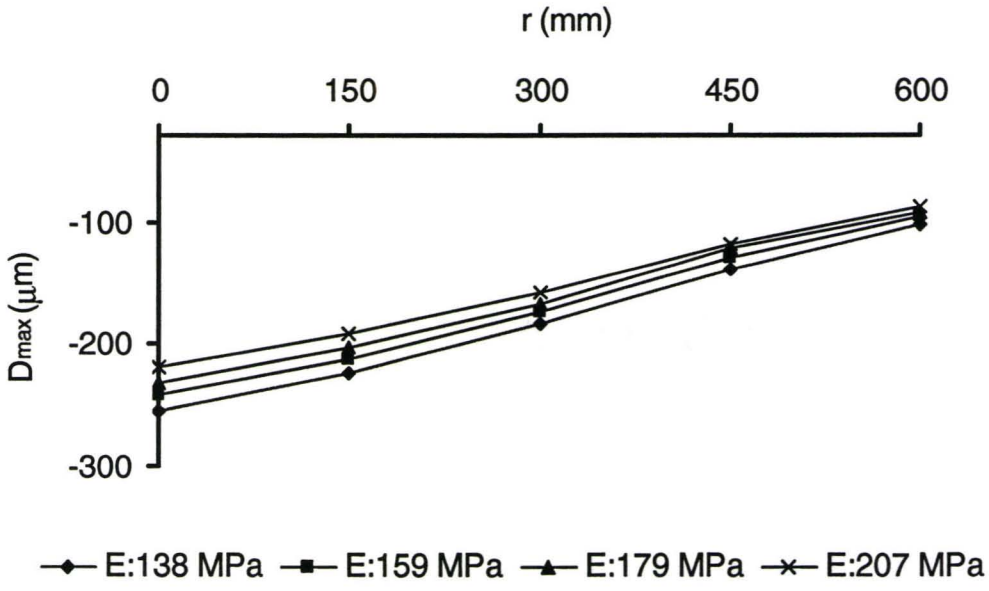

Figure 5.4: Maximum Deflections vs. Distance Away from the Center of the Plate

CHAPTER 6

Equipment, Materials, and Procedures

6.1 Introduction

The testing program in the present research was designed to identify the shear response of unsaturated modified granular material, using primarily the triaxial apparatus. This chapter describes the test equipment and materials used, as well as specimen preparation and testing.

6.2 Testing Program

Although it is recognized that base/subbase materials have particle sizes up to 150 mm diameter, for this research specimens were prepared using the fine portion of the granular base and compacted to achieve relatively uniform dry densities at varying water contents. Given the significance of the fine portion in the moisture sensitivity of granular bases, and the fact that the maximum specimen diameter was 38mm, the large fraction greater than the #10 sieve (2 mm) was removed. Consequently, although the parent material was a Granular B, the actual material tested no longer resembled that of a Granular B. An important reason for using smaller specimens was to make sure that stress changes within a sample from top to bottom due to self weight, did not exceed the confining pressures. Note that for 200 mm-high samples, the change in vertical stress from top to bottom is approximately 4 kPa, which would have corresponded to the

minimum cell pressure applied in the testing programme. The other reason for using finer aggregate was to allow the use of smaller samples that were easier to fabricate and monitor. It should be noted that the moisture sensitivity depends more on the finer fraction than on the coarser fraction.

Choosing only the fine portion of Granular B is a recognized limitation of the study but the testing is considered realistic in terms of identifying the representative properties that must be available during design, prior to construction.

To achieve the objectives of the research, a methodology had to be applied which would insure that specimens compacted under controlled conditions would possess consistent properties. The variables that were controlled during the tests included initial dry density, water content, degree of saturation and suction as well as, the confining pressure, rate of strain and level of stress (for cyclic loading). Variables that were measured during the tests, or calculated after testing was completed were: strain and deviator stress, undrained compression modulus, initial total suction, shear strength parameters, and plastic strain under cyclic loading (before and after freezing/thawing). The variables that were neither controlled, nor measured, nor calculated were pore water and air pressure, matric suction change during shearing and volume change during shearing.

The testing programme included:

1) Undrained conditions during shearing and the application of confining pressure (UU).

2) Tests that were conducted on 2 types of material specimens at wet of optimum, optimum, and dry of optimum water content.
3) Cyclic loading.
4) Some specimens being tested with 5 cycles of loading/unloading, then frozen and thawed, and put through 5 more cycles of loading.
5) A soil water characteristic curve test that was conducted on Material 1 (drying curve).
6) Testing the specific gravity of sand according to ASTM D854.

6.3 Equipment

A regular triaxial cell with the confinement applied using a compressed air system was used for tests performed at low confining pressure. This cell was installed in a "Wykehham-Farrance" 10 kN load frame, which was used to shear the specimens. Confining pressure was applied via an air pressurizer tank. The displacement rate during loading was 1.14 mm/minute. It should be noted that the 64 kPa pressure was considered a reference pressure.

Pressure System – To achieve low confining pressure, only air was applied in the cell. Final adjustments and control of the air pressure were made with an "AB High Performance Pressure Transducer" system. This system was used only because of very low confining pressures. A latex rubber membrane separated the soil specimen from the pressurized air. It was found that it was advisable to use a double membrane since in some cases the (inner) membrane could develop leaks.

Measurment Devices - Transducers were used to determine loads, displacements, and cell pressure. For small loads, a 250 lb load cell was used and it was connected rigidly to the top of the load frame. The loading ram then connected the measuring device to the specimen at the top cap. All load devices were externally mounted due to the limited space inside the triaxial cell. Axial displacements were measured with a displacement transducer. The transducer was mounted directly to the loading ram and movement of the loading ram was measured relative to the top cap of the cell. One pressure transducer, with a capacity of 0-100 psi, was used to measure the cell pressure (i.e., the confining pressure). Electronic information from the load cell, pressure transducer, and displacement transducer was collected automatically at 5 second intervals by a data acquisition software package

6.3.1 Compaction Equipment

Figure 6.1 shows the compaction equipment, which consisted of a compaction mold and tamper. The mold had an inside diameter of 38 mm and enough height to compact a 100 mm-tall specimen. A compaction force was applied by a hand-tamper with a drop weight. The diameter of the specimen was obtained by a and the height was measured by a dial gauge.

6.4 Materials

6.4.1 General Properties of the Materials

A. Granular Materials

All virgin granular materials used for the study met the gradation requirements of the Ontario Ministry of Transportation given in Table 1-1. Each type of granular base/sub-base material was air-dried and then screened into different-sized fractions. The fractions were then recombined in a way so as to meet the grading requirements for this research. The particle size distribution of the sand is provided in Table 6-1.

In the tests conducted during the research, a blended mixture of fine-grained coarse aggregate, consisting of two types of materials with D_{10} = 0.085 mm, D_{30} = 0.2 mm and D_{60} = 0.6 mm, was used. Classification of the material according to AASHTO and Unified system is fine sand, and SW, respectively. Material 1 was a well-graded mixture of sub-rounded fine to medium crushed silica sand composed of 100% shield material that came from the LAFARGE PIT at Hwy 5 at Dundas. Material 2 was a well-graded mixture of fine to medium crushed silica and lime sand mostly composed of shield with some limestone. The source chosen was the CBM ABERFOYL PIT, located 1 km north of Hwy 401 on Hwy 6. The reason for using both types of material is that it was believed that the surface charge characteristics could lead to different moisture sensitivities, which would mean that an additional variable was included. Figures 6.2 and 6.3 show the microscopic pictures of Materials 1 and 2 at a magnification factor of X 40.

The former contained more round-shaped particles while the latter contained flakier, medium-size particles. Material 1 has a maximum dry density of 1.99 g/cm^3 with a water content of about 8.6%, with Material 2 having a maximum dry density of 1.98 g/cm^3 with a water content of about 9.5%. The specific gravity, G_s, was measured according to ASTM D854 and was found to be 2.68.

6.5 Procedures

The following sections outline the techniques used when mixing, compacting, and installing specimens.

6.5.1 Mixing

The sand that was to be used was initially sieved and then prepared according to Table 6.1 by adding measured weights of each sieve size. For the earlier samples, the sand was poured through a splitting device until an even mixture was produced. However, at a later stage the sand was simply mixed with care for a couple of minutes to get an even mixture. The sample was then dried in an oven at 105°C to achieve zero water content. Distilled de-aired water was used to control the effects of osmotic suction and decrease air content in the soil solution. The amount of water required to achieve the desired dry density was then added to the sample and it was covered by cling-wrap to avoid water evaporation. Four moisture content tests were conducted both before and after shearing the samples. Any changes in water content during sample preparation, installation and shearing were found to be negligible.

Once the amount of water was determined from compaction curves, 155 g of air-dried material was poured into the bowl. The water was then added to the aggregate and mixed carefully with a spoon. Finally, the bowl was covered with cling-wrap to minimize either the loss or gain of moisture.

6.5.2 Compaction/Sample Preparation

Previous studies on suitable sized triaxial specimens, e.g., Anderson (1997) suggest that for granular soils, the specimen diameter has no effect on test results if it is at least six times the maximum particle size. Given the grain size distribution adopted, this requirement was attained. Samples 36 mm in diameter and 76mm high were compacted in 4 equal layers, with 25 and 35 impacts for each layer to achieve the target dry density, 25 impacts were required for samples with 7% to 10.5% and 35 impacts were used for those with 4% water content.

During sample preparation a mold was placed on top of the base plate and the porous stone was placed inside. The mold was then lined with a latex membrane and then a certain amount of sand was compacted. During compaction, no vacuum was applied to the sample. Once this process was completed, the loading cap was put on top of the sample. After compaction, the mold was removed however the membrane remained to allow the vacuum to develop proper levels of confinement. The specimen dimensions were measured quickly and thereafter, the volume of the sample and dry density were calculated. If the target dry density was not achieved, another sample was prepared. Once the target value

was achieved, the sample was covered with a second membrane. After shearing the samples, they were weighed to get the exact value of soil mass and dry density.

6.6 Procedures for Testing

As mentioned previously, the confining pressure was applied over a 2-3 minute period, and the initial load was set. The measuring equipment was zeroed appropriately and shearing commenced. When loaded cyclically, the applied deviatoric stress was $(\sigma_d)_f/3$. These specimens were subjected to 10 cycles. Some specimens were tested with 5 cycles of loading/unloading before freezing, and another 5 cycles after freezing and thawing. After the first 5 cycles of loading, the cell and the sample were placed inside a freezer (average temperature of –7°C) for a period of 18 to 22 hours. Thereafter they were removed and placed outside at room temperature for an additional 18 to 22 hours to thaw. After thawing, another 5 cycles of loading were applied to these samples. It should be noted that this entire process was conducted at constant cell pressure.

6.7 Quality Control

All specimens were compacted to specified water contents, dry density, and therefore target degrees of saturation. The amount of water and soil was estimated from the compaction curves. In order to gain confidence in the specimen preparation procedures, a Quality Control (QC) program was initiated.

The QC program was conducted with three specific objectives. The primary objective was to ensure that compaction techniques would reproduce specimens of water content, dry density, and degree of saturation. The second objective was to examine changes in water content that occurred during preparation and testing. The final objective was to make sure that the physical characteristics of the triaxial specimens were in good agreement with the target values specified. The results led the author to choose the procedure for sample preparation which was described in Section 6.5.2.

The first check was to ensure that procedures for mixing and compaction would produce reliable, repeatable results. For this purpose, QC specimens were prepared in the way described in Section 6.5.2. To achieve an even distribution of water throughout the sample, the sand was mixed carefully with the water specified and then covered. Specimen preparation followed the procedure outlined by Anderson et al. (1997) for triaxial testing of unsaturated granular soils at low confining pressure.

The usual procedure was to prepare 3 to 4 QC specimens at each degree of saturation. "Target", or ideal, water content, dry density, and degree of saturation were identified before mixing the material. After the material was prepared and mixed sufficiently, the QC specimens were compacted. Immediately after the specimen was prepared, the dimensions, weight, and water content were determined and compared to target values.

The second check was made by comparing initial and final average water

contents of triaxial specimens to target values. Initial water content refers to the average water content of mixed sand before testing. Final water content refers to the average water content of a sheared specimen. The final water content was then compared to the initial water content.

The final check was made to ensure the consistency of triaxial specimen characteristics within a group of specimens compacted to the same target degree of saturation. This was done by establishing the average initial degree of saturation and dry density, using the final water content determined by the above method. This average water content was then used along with the void ratio to determine the average dry density of the specimen. Similarly, the average degree of saturation was calculated using a specific gravity of 2.68, the average final water content, and the voids ratio. Equation 6.1 summarizes the relations used in determining these characteristics:

$$\rho = \frac{M}{V}, \qquad \rho_d = \frac{G_s \rho_w}{1+e}, \qquad S_r = \frac{G_s}{e} w, \qquad n = \frac{e}{1+e} \tag{6.1}$$

where, ρ = bulk density (g/cm^3); M = mass of moist soil (g); V = volume of moist soil (ml); e = voids ratio; n = porosity; and A = air content.

With practice, the technique was improved thereby resulting in more uniform groups of specimens. At lower target water contents, it was more difficult to achieve an even distribution of moisture throughout the sample. The main goal in doing QC was to gain confidence in achieving "consistent" results, not necessarily "perfect" results, which of course would have been most desirable. As

long as the preparation techniques produced specimens with predictable characteristics, the techniques were considered acceptable. Specimen preparation was quite repeatable with good consistency being achieved for both water content and dry density. This is important since strength and stiffness depend largely on the water content and dry density of base/subbase material.

The second important check was made by comparing average initial and final water contents of sheared specimens to the original target values. This procedure was used to identify changes in moisture occurring during the time period between compaction and the end of shearing. If large moisture losses occurred, substantial changes in suction and strength would have been expected. The difference in the average initial and final water contents ranged from 0.3% to 0.6%. In other words, the average moisture lost was 0.4% water content. This relatively small amount was attributed to evaporation during the preparation procedures (compaction, installing and removing the specimen) and not to the loss of moisture, during shearing, through drainage or leakage.

The mass of the water and solid particles of the specimens should remain constant from the beginning to the end of a test. Three samples were prepared initially by applying suction and the results showed that water content changed on an average from 10% to 7%. Since the initial suction of the sand made it sufficiently stable, all the samples were prepared with no application of suction.

The final check was made on triaxial specimens compacted to the same target moisture content. It should be noted that in almost all cases the compacted

dry density was equal to the target value of 1.87 g/cm^3. All specimens could therefore be considered to have the same density and as a result, it was assumed that any deviation in strength and stiffness would not be attributed to density.

6.8 Soil Water Characteristic Curve (SWCC)

A 1400/1405 Tempe Pressure Cell was used to test and determine the relationship between degree of saturation and suction, which is referred to as the "Soil Water Characteristic Curve". A 1405 Tempe Cell, consists of 3 parts: top and base cap assembly, the brass cylinder, and the porous ceramic plate. The porous Ceramic Plate can vary in bar rating according to the user's choice and the type of application.

Initially, the soil sample and the porous ceramic plate were saturated with water. Air pressure was then applied to the Tempe Pressure Cell to effect the extraction of moisture from the soil sample under controlled conditions. For all extraction work, a source of regulated air pressure was required. Compressed air from a compressor was used for the test and pressure control was achieved using the triaxial apparatus.

It was essential to fully saturate and de-aerate the porous plate before placing the Tempe Cell in operation. This was accomplished by saturating the plate in a vacuum desiccator with de-aerated distilled water. The saturated porous plate was thereafter installed in the cell and once in place, water was poured into the cell. The next step was to measure the volume of the cell. Based on the

required dry density, the amount of sand needed was weighed and poured into a beaker. Some de-aerated water was added to the sand such that it was completely covered. This was then boiled and vacuumed in order to release any air that was trapped within the pores of the sand. The sand was then poured into the cell, which was filled with water. Finally, the top part of the Tempe Cell was reattached and fastened in place. The Tempe Cell was connected to the pressure supply source and the pressure in the cell was raised to the desired level.

This process was repeated at higher pressure values. By noting the difference in weight, it was possible to find the change in weight from one soil suction value to another. At the end of a run, the sample was dried at 105° C. The changes in weight were interpreted in terms of water content by weight of soil. Since the volume of the soil sample was well defined, the water content could also be related to the volume of soil. By plotting the change in water content at each equilibrium value, against the soil suction, it was possible to develop the relationship of soil suction versus water content or degree of saturation for each soil.

Table 6.1: Grain Size Distribution

Sieve Designation	% Passing by mass
2.5 mm	100
1.25 mm	80
315 μm	44
75 μm	3

$D_{10} = 0.085$ mm

$C_u = 7$

$D_{30} = 0.2$ mm

$C_c = 0.8 \approx 1$

$D_{60} = 0.6$ mm

AASHTO System Classification: Fine Sand

Unified System Classification: SW

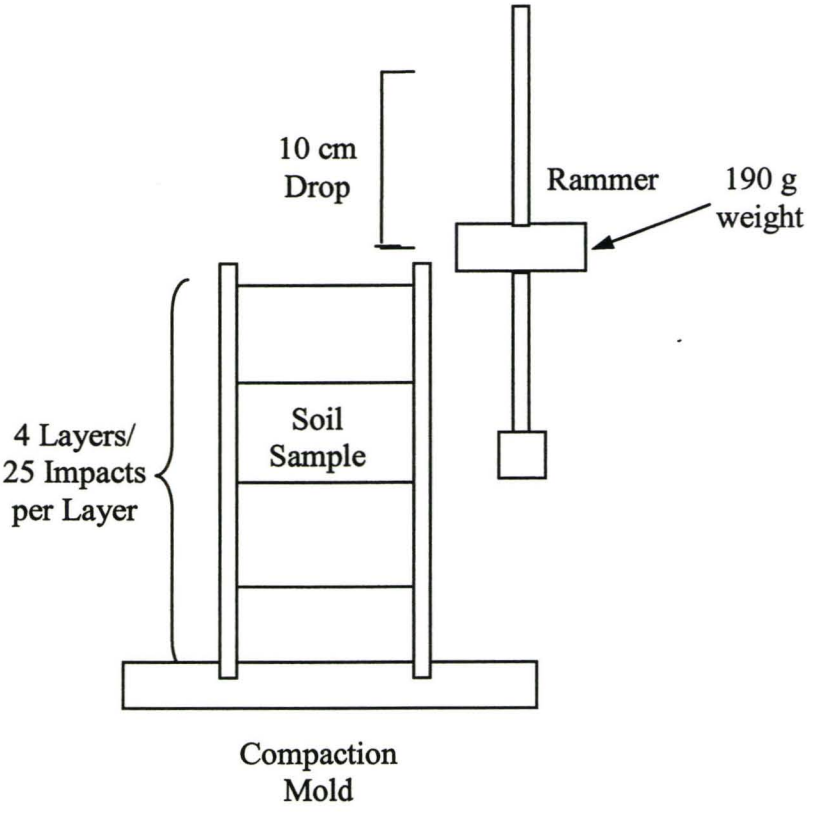

Figure 6.1: Compaction Equipment

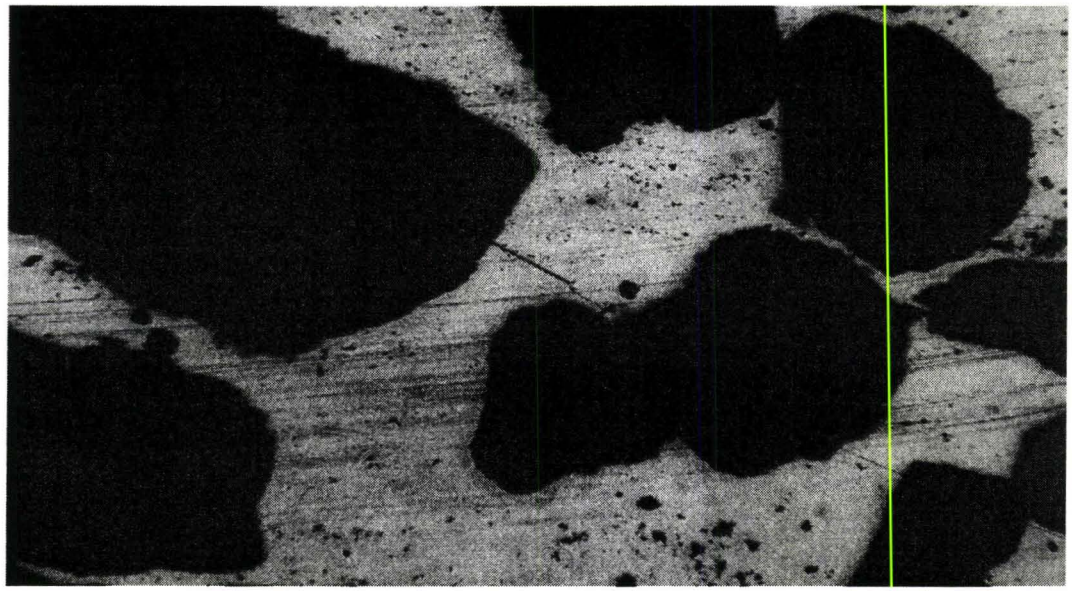

Figure 6.2: Microscopic Picture of Material 1

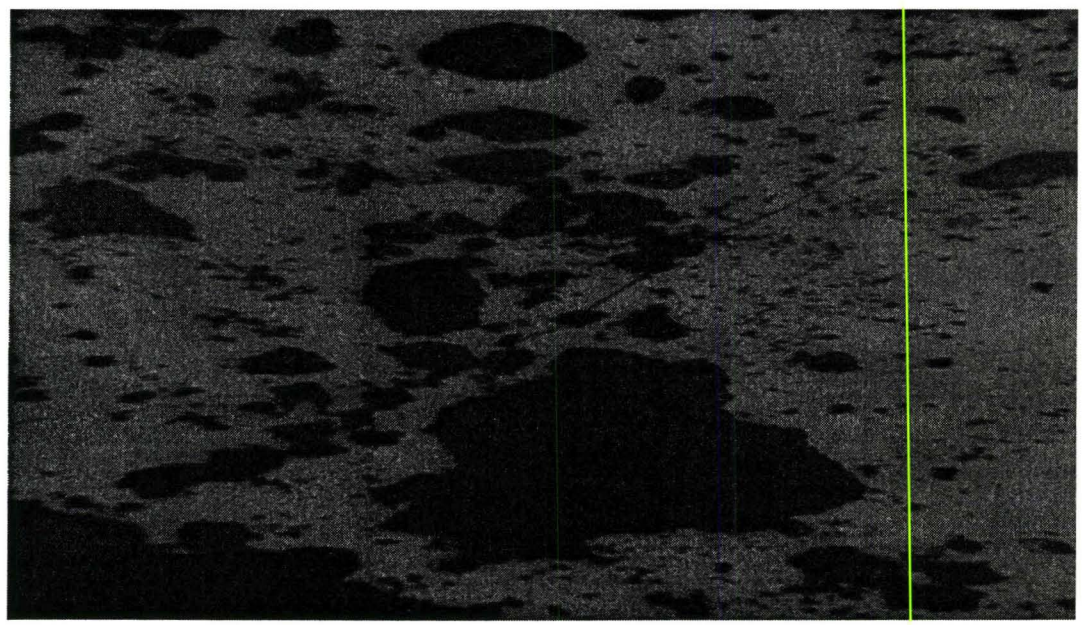

Figure 6.3: Microscopic Picture of Material 2

CHAPTER 7

Results and Discussion of Monotonic Triaxial Tests

7.1 Introduction

This chapter describes the results of a series of monotonic undrained triaxial compression tests on unsaturated modified aggregate, and demonstrates how the shear strength and secant modulus of elasticity of unsaturated base responds to changes in water content, degree of saturation, and confining pressure. Shear strength and the secant modulus are then related to the total nominal initial suction. Due to the compressibility of the air phase, the tests could not be considered "constant volume" tests. Results were obtained for specimens with average degrees of saturation of 24% to 67%, confining pressure ranging from 4 kPa to 64 kPa.

7.2 Monotonic Test Results

The results regarding the compaction curve, stress path, retention curve, hyperbolic stress-strain relationship, and monotonic loading tests are presented in this section.

7.2.1 Compaction Curve

Figures 7.1 and 7.2 show the relationship between dry density and moisture content for Materials 1 and 2, respectively. The optimum water contents

for these materials were found to be 8.6%, and 9.5%, respectively. As mentioned in Chapter 6, the soil was compacted inside a 76 cm^3 mold by a rammer consisting of a 190 g mass falling freely through 100 mm, in 4 equal layers receiving 25 blows with the rammer. The total compaction energy is calculated as:

$$E/V = \frac{mgh}{V} \tag{7.1}$$

where, E = compaction energy (J); V = volume of the soil (cm^3); mg = weight of the falling mass; and h = falling height.

After substituting in the appropriate value we have:

$$E/V = \frac{0.19 \times 9.81 \times 0.1 \times 4 \times 25}{76} = 0.244 \ \ J/cm^3 \tag{7.2}$$

In the standard Proctor test, the volume of the mold is 1000 cm^3 and the soil is compacted by a rammer consisting of a 2.5 kg mass falling freely through 300mm. The soil is compacted in three equal layers, each layer receiving 27 blows with the rammer; thus one has,

$$E/V = \frac{3 \times 27 \times 2.5 \times 9.81 \times 0.3}{1000} = 0.6 \ \ J/cm^3 \tag{7.3}$$

As can be observed here, the test compaction energy is 2.45 times less than that corresponding to the standard Proctor. Figure 7.3 shows typical dry density-water content curves for different compaction efforts. According to this graph, a higher compactive effort results in a higher value of maximum dry density and a lower value of optimum moisture content. However, the values of air content at

maximum dry density are approximately equal and range from 5% to 10% (Craig, 1990). Using the maximum dry density, optimum water content, and the specific gravity (G_s) for Materials 1 and 2, the air content is 8% and 7%, respectively which falls within the range reported by Craig (1990).

7.2.2 SWCC

Figure 7.4 shows the relationship between suction and S_r for Material 1. As expected, the suction decreases as S_r increases. The bubbling pressure for this material is estimated to be approximately 3.5 kPa, which is in accordance with the characteristic retention curves for sandy material. The results achieved in this study are consistent with the typical retention curves shown in Figures 4.1 and 4.3.

7.3 Effects of Saturation Level

Figure 7.5 shows the stress-strain relations for varying water content and confining pressures of 4 kPa, 16 kPa, and 64 kPa. As expected, for all cases the deviatoric stress at failure increases with increasing confining pressure, regardless of the original water content. It should however be noted that the slope of the curves (initial secant modulus) tends to become flatter as the water content is increased. Consequently, the material becomes less stiff as the water content increases.

Figure 7.6 indicates that at a given water content, normalized strength and

ductility tend to decrease with increased cell pressure. At low confining pressures, an abrupt change in stiffness occurs at about 0.25% to 0.5% strain. For higher confining pressures, the shape of the normalized stress-strain curve shows yielding but much greater ductility throughout shearing. It should be noted for a saturated drained response or the response of dry cohesionless material one would expect that q/p relation stays approximately constant; what we see here as a curved/convex up yield surface.

Figure 7.7 shows the relationship between q_f and σ_3 which seems to be linear in nature. As σ_3 increases, the value of q_f also increases. Furthermore, as S_r values increase, the value of q_f decreases, which is consistent with strength decreasing as water content goes up. Note that for increasing values of S_r, the slope of the resulting graphs decreases. When σ_3 is 4 kPa, the values of q_f are too close to distinguish from each other. In other words, at lower confining pressure, the degree of saturation sensitivity appears to be decreasing. The convergence of all curves to a point is interesting and should be investigated further.

Figure 7.8 shows the relationship between q_f/p_f vs. confining pressure for varying water content (degrees of saturation) for Materials 1 and 2. As can be observed in this figure, when confining pressure increases, the values of q_f/p_f decrease.

7.4 Effect of Confining Pressure

Figure 7.9 compares normalized stress-strain curves for water contents of

4%, 7%, and 10% and cell pressures of 4 kPa, 16 kPa, 64 kPa. For the low confining pressure (4 kPa), the effect of changing water content is minimal but for higher confining pressures, however increasing water content normalized q_f decreases. This almost indicates a relation for failure and that the same failure curve exists. It seems that the failure level is slightly dependent on the water content.

Figure 7.10 shows the relation between, $q_f=(\sigma_1-\sigma_3)/2$, and $p_f = (\sigma_1+\sigma_3)/2$, which appears to be linear in nature although one might expect a slight curvature due to the material being in an unsaturated condition. This is clearer for samples with higher water content (7%, 10%). With increasing σ_3 the slope becomes slightly flatter due to decreases in suction at the specimen. It should be noted that the envelopes for 8.6% and 9.5% water content have higher values of dry density that justify the higher shear strength. In the q_f-p_f figure, Material 2 has slightly higher values of q_f than Material 1, which can be related to larger amounts of angular aggregates resulting in a higher angle of shearing resistance. Also in this figure, Material 2 shows less sensitivity to changing water content than Material 1. Angular aggregates with good particle interlock may reduce the lubrication effect of water content and reduce the effect of increasing water content on reduction in shear strength.

Figure 7.11 shows the relationship between q_f and initial suction, which was estimated from the SWCC. By observing the graphs of σ_3 for 4, 16 and 64 kPa, one can see that there is a linear relationship between q_f and initial suction.

As σ_3 increases, the value of q_f increases, as expected. Also, as σ_3 values decrease, the slope of the resulting graphs also decreases. This shows that the effect of confining pressure on q_f is more important than that of water content for low confining pressures (4 kPa, and 16 kPa).

7.5 Discussion of the Effect of Confining Pressure

Recall from Chapter 4 that the deviator stress at failure can be related to the cohesion of the soil, and a contribution from both the net mean stress and the matric suction:

$$\tau = c'+(\sigma_n - u_a)_f \tan\phi'+(u_a - u_w)_f \left[S_r(\tan\phi')\right] \quad (7.4)$$

If this equation is compared with the Mohr-Coulomb criteria, one observes that the σ_n is replaced by $[\sigma_n - u_a+((u_a-u_w)\times S_r)_f]$. Heath et al. (2002) used this idea to normalize the behavior of unsaturated granular pavement materials. In his studies, he added the effective suction, $((u_a-u_w)\times S_r)_f$, to the effective confining pressure, thus giving:

$$q_f = p_f \times \sin\varphi \quad (7.5)$$

where, $\varphi = \varphi_o - \Delta\varphi \log(\sigma_3/p_a)$, and, $\sigma_3 = [(\sigma_3)_{applied} + ((u_a-u_w)\times S_r)_f]$.

Therefore, depending on the effective suction, the values of σ_3 can increase or remain unchanged. For example, for dry material even though suction is very high the effective suction is negligible. As can be observed from Equation 7.5, when suction increases so does σ_3 and φ, $\sin\varphi$, q_f/p_f all decrease.

This phenomenon can be explained in another way. According to Figure 4.4, the diameter of the Mohr circle increases with an increase in confining pressure. The failure envelope defines a curved relationship between the shear strength and total normal stress for unsaturated soils tested under undrained conditions. Evidently, the value of q_f/p_f decreases with increasing confining pressure. In undrained tests on unsaturated soils, the increase in shear strength caused by a rising confining pressure is greater than the decrease of shear strength associated with declining matric suction. Once the soil becomes saturated under the application of confining pressure, a horizontal undrained failure envelope develops with respect to the shear strength axis (i.e. $q_f/p_f = \sin\phi_u = 0$).

The stress-strain response of unsaturated granular material is affected by the applied confining pressure as illustrated in Figure 7.5 and Figure 7.7. As can be observed, when the confining pressure is increased, the q_f observed at a given degree of saturation increased. Undrained shear strength arises from both matric suction and net mean stress acting in the soil. This applies whenever the air voids in an unsaturated soil are highly interconnected. However, if the air voids are occluded or become completely compressed, only small changes in shear strength can be expected with further increases in cell pressure (net mean stress).

Increasing confining pressure causes an immediate decrease in the suction experienced by unsaturated soils. The decrease in suction is a function of the confining pressure applied and the initial suction (Tang 1996, Wan et al. 1995). For saturation below 50%, where the air phase is dominant in the macropores

(inter-connected pores), an increase in total stress causes compression of the void spaces, flattening of the air-water interfaces and a decrease in matric suction, which tends to reduce shear resistance. Furthermore, increased confining pressure increases the total and effective stresses carried by the soil skeleton, thus increasing the shear resistance. These two mechanisms (decrease in suction and increase in effective stress) act against one another, but the net effect is to produce strength increases which, are greater than or equal to zero.

When shearing at a sufficiently high confining pressure, compression and solution of the air will result in the occlusion of pores. This occlusion causes a reduction in the rate of effective stress increase, which continues until increases in cell pressure no longer produce increases in either effective stress or shearing resistance. As the cell pressure rises, there is a gradual transition from linearly increasing shear strength ($\phi > 0$) to constant shear strength ($\phi = 0$, full saturation).

7.6 Effect of Confining Pressure on Normalized Shear Strength

Figure 7.6 shows the relationship between q_f/p_f vs. strain for different confining pressures and at a constant water content. As can be observed, with increasing confining pressure the value of normalized shear strength decreases and the behavior becomes more ductile. Figure 7.8 also shows that q_f/p_f decreases with increasing confining pressure for constant water content, and this is evident in all cases. This can be justified by using Equation 7.8 where, as confining pressure increases the values of ϕ and q/p decrease.

7.7 Effect of Water Content on Normalized Shear Strength

Figure 7.9 compares normalized stress-strain curves for water contents of 4%, 7%, 8.6% and 10% and cell pressures of 4 kPa, 16 kPa, and 64 kPa. For low confining pressure (4 kPa), the effect of changing water content is not very significant but, with rising confining pressure it is evident that normalized q_f $(q/p)_f$ decreases as the water content increases. As can be seen, with an increasing degree of saturation the effective suction decreases therefore the effective confining pressure decreases leading to higher ϕ, and q/p values. As can be interpreted from Equation 7.4, a change in suction is not as effective as a change in effective stress when it comes to producing an increase in shearing resistance. This would explain the reason why, at low confining pressure (4 kPa, and 16 kPa) and increasing water content (decreasing suction), the changes in q_f are not very obvious.

7.8 Variation of Deviator Stress with Initial Suction

Figure 7.11 shows the strength envelope where the peak, q_f, is plotted against initial suction, for different confining pressures. Separate envelopes were drawn for each confining pressure. One observes that strengths became higher with increasing σ_3, as expected. Since all specimens were compacted to the same dry density, each average degree of saturation corresponded to some particular water content, which controls the matric suction in the soil.

The initial suction was taken to roughly represent the suction during

shearing. Figure 7.11 plots q_f vs. total initial suctions that were obtained by relating the initial water contents of the specimens to the SWCC. As confining pressure increases so does the shear strength. Each envelope rises at approximately the same slope for $\sigma_3 = 16$ kPa and 64 kPa, whereas for $\sigma_3 = 4$ kPa increasing suction does not produce continuously increasing shear strength. However, if suctions are localized then we may not see their effect on a macroscale although their influence is more obvious at higher confining pressures which may be due to changes in pore size.

Future research should attempt to incorporate suction changes from these two mechanisms into the shear strength-suction relationship.

7.9 Variation of Secant Modulus

It is common to infer the material stiffness of soil specimens from measurements of the secant modulus E_{50} which corresponds to the average stiffness up to a deviatoric stress of $q_f / 2$. Tables 7.1 and 7.2 show the values of E_{50} for the UU tests conducted. Figure 7.12 shows E_{50} vs. σ_3, for various degrees of saturation. In general, with increasing confining pressure the values of E_{50} increase. As can be seen in Figure 7.13 the value of E_{50} decreases with increasing degree of saturation. The changes in E_{50} tend to be small for 50% saturation. Recall from Chapter 4 that the initial secant modulus can be expressed as:

$$E_i = kp_a(\sigma'_3/p_a)^n \qquad (7.6)$$

where, $\sigma'_3 = [(\sigma'_3)_{applied} + ((u_a-u_w)\times S_r)_f]$ which means that with increasing

confining pressure the values of the secant modulus should increase. For a constant confining pressure, when water content increases the effective confining pressure decreases thus causing the secant modulus to decrease. Yuan and Nazarian (2003) performed some tests on subbase and subgrade material using resonant column tests to investigate the changes of elastic modulus with varying water content. The results are shown in Figure 7.14 where, for a fine-grained material the relationship resembles that of a typical moisture-density curve. For clean, coarse-grained material the modulus decreases with increasing water content. In general, independent of the type of material, a decrease in modulus with a progressive increase in the water content is inevitable. These results agree with the findings of this research.

As can be observed in Figure 7.15, the normalized E_{50} increases with increasing initial suction, and reaches maximum values at suctions around the air-entry-value (3.5 kPa). The slope then decreases for suctions greater than the air-entry-value, and E_{50}/σ_m no longer increases. Therefore, increasing suction does not result in continuously increasing normalized modulus. Note that the decrease in the slope is more pronounced for low cell pressure (4 kPa). Escario and Saez (1986) and Fredlund et al. (1987) observed increases in normalized stiffness with suction but the increase in normalized E_{50} with suction does not continue indefinitely (Yasuda et al. 1997).

7.10 Hyperbolic Stress-Strain Relationship

Figures 7.16 and 7.17 show the relationship between ε/σ_d and ε % when the water content is 4%, 7%, and 10%, and σ_3 is 4, 16 and 64 kPa. The graphs are not linear initially but approach linearity when ε % is between 0.5% and 0.75%. It is evident that by increasing σ_3, the slope of the linear section decreases. This is in accordance with what is shown by Desai and Siriwardane (1984), as illustrated in Figure 7.18. As described in Chapter 3, the hyperbolic stress-strain relationships can be represented by an equation of the form:

$$\frac{\varepsilon}{(\sigma_1-\sigma_3)}=\frac{1}{E_i}+\frac{\varepsilon}{(\sigma_1-\sigma_3)_{ult}}=a+b\varepsilon \tag{7.6}$$

where, $(\sigma_1-\sigma_3)_{ult}$ is the asymptotic value of stress difference, which is related closely to the strength of the soil. Therefore, the slope of the curves represents $1/q_f$ and as described in previous sections, q_f increases with increasing confining pressure resulting in the slope of the curve becoming flatter with increasing confining pressure.

Table 7.1: Monotonic Test Results – Material 1

Test #	Test Type	σ_3 (kPa)	S_r	ρ_d (g/cm^3)	%w	σ_d (kPa)	E_{50} (kPa)	σ_m (kPa)	E_{50}/σ_m	Initial Suction(kPa)
160	Monotonic	64	0.0	1.87	0	150.6	7370.9	114.2	64.5	26.5
161	Monotonic	64	0.0	1.9	0	307.0	9092.5	166.3	54.7	26.5
162	Monotonic	64	0.0	1.87	0	240.4	10770.7	144.1	74.7	26.5
8	Monotonic	4	25.6	1.89	4	69.5	3050.7	27.2	112.3	7.1
9	Monotonic	4	26.6	1.91	4	67.4	5380.4	26.5	203.3	7.1
34	Monotonic	16	26.1	1.90	4	132.6	15654	60.2	260.0	7.1
35	Monotonic	16	26.1	1.90	4	169.6	7496.2	72.5	103.3	7.1
36	Monotonic	16	26.6	1.91	4	158.8	14098.0	68.9	204.5	7.1
37	Monotonic	64	26.1	1.90	4	344.8	17562.3	178.9	98.1	7.1
38	Monotonic	64	26.1	1.90	4	339.7	21927.7	177.2	67.2	7.1
11	Monotonic	4	44.9	1.89	7	71.9	6627.6	28.0	237.0	4.7
16	Monotonic	4	45.7	1.90	7	68.9	6623.2	27.0	245.6	4.7
17	Monotonic	4	44.9	1.89	7	64.8	6533.5	25.6	255.2	4.7
1	Monotonic	16	47.4	1.92	7	121.7	5157.8	56.6	91.2	4.7
10	Monotonic	16	44.9	1.89	7	126.5	6963.2	58.2	119.7	4.7
12	Monotonic	16	46.5	1.91	7	146.7	11801.3	64.9	181.8	4.7
21	Monotonic	64	44.9	1.89	7	299.5	17536.0	163.8	107.0	4.7
22	Monotonic	64	47.4	1.92	7	236.5	19320.9	142.8	135.3	4.7
26	Monotonic	64	47.4	1.92	7	257.9	14803.4	150.0	98.7	4.7
4	Monotonic	4	67.8	2.00	8.6	139.8	9345.9	50.6	184.7	4.3
6	Monotonic	4	65.2	1.98	8.6	111.2	8405.6	41.1	204.7	4.3
13	Monotonic	16	66.5	1.99	8.6	159.6	11702.2	69.2	169.1	4.3
18	Monotonic	16	66.5	1.99	8.6	151.5	11986.0	66.5	180.2	4.3
23	Monotonic	16	66.5	1.99	8.6	154.9	10701.3	67.6	158.2	4.3
25	Monotonic	64	66.5	1.99	8.6	389.2	11184.6	193.7	57.7	4.3
28	Monotonic	64	67.8	2.00	8.6	353.2	13475.9	181.7	74.2	4.3
3	Monotonic	4	63.0	1.88	10	74.7	4824.6	28.9	166.9	4
7	Monotonic	16	65.3	1.90	10	119.1	6829.5	55.7	122.6	4
15	Monotonic	16	65.3	1.90	10	123.2	5630.4	57.1	98.7	4
19	Monotonic	16	65.3	1.90	10	106.7	5414.0	51.6	105.0	4
20	Monotonic	16	67.7	1.92	10	119.1	5291.2	55.7	95.0	4
24	Monotonic	16	67.7	1.92	10	115.5	12594.6	54.5	231.1	4
32	Monotonic	16	64.1	1.89	10	114.9	6855.8	54.3	126.3	4
27	Monotonic	64	66.5	1.91	10	260.6	14442.9	150.9	95.7	4
29	Monotonic	64	67.7	1.92	10	220.9	9558.0	137.6	69.4	4

Table 7.2: Monotonic Test Results – Material 2

Test #	Test Type	σ_3 (kPa)	%Sr	ρ_d (g/cm^3)	%w	U_a	σ_d (kPa)	E_{50} (kPa)	σ_m (kPa)	E_{50}/σ_m
156	Monotonic	64	0.0	1.90	0	N/A	210.1	9505.0	134.0	70.92
157	Monotonic	64	0.0	1.85	0	N/A	168.4	9704.6	120.1	80.78
159	Monotonic	64	0.0	1.97	0	N/A	283.1	10503.1	158.4	66.32
57	Monotonic	4	23.3	1.84	4	N/A	102.3	11341.3	38.1	297.67
58	Monotonic	16	23.3	1.84	4	N/A	145.1	12540.9	64.4	194.84
59	Monotonic	16	22.9	1.83	4	N/A	133.6	6802.8	60.5	112.38
65	Monotonic	16	22.9	1.83	4	N/A	163.5	8000.9	70.5	113.49
66	Monotonic	16	22.9	1.83	4	N/A	171.7	10744.0	73.2	146.71
67	Monotonic	64	23.7	1.85	4	N/A	327.2	20721.0	173.1	119.73
68	Monotonic	64	23.3	1.84	4	N/A	309.7	14346.7	167.2	85.79
63	Monotonic	4	40.1	1.83	7	N/A	123.9	8451.6	45.3	186.57
64	Monotonic	4	40.8	1.84	7	N/A	116.3	5797.7	42.8	135.57
83	Monotonic	4	40.8	1.84	7	N/A	58.8	3564.0	23.6	151.02
60	Monotonic	16	40.8	1.84	7	N/A	150.4	6240.7	66.1	94.37
75	Monotonic	16	38.7	1.81	7	N/A	131.1	4092.0	59.7	68.54
88	Monotonic	16	40.1	1.83	7	N/A	123.1	4669.8	57.0	81.88
61	Monotonic	64	41.5	1.85	7	N/A	255.7	17047.5	149.2	114.23
62	Monotonic	64	41.5	1.85	7	N/A	258.7	15580.1	150.2	103.71
69	Monotonic	4	56.0	1.91	8.5	N/A	110.5	6607.6	40.8	161.82
70	Monotonic	4	54.0	1.89	8.5	N/A	104.7	6296.8	38.9	161.87
72	Monotonic	4	53.1	1.88	8.5	N/A	150.6	7760.0	54.2	143.17
71	Monotonic	16	54.0	1.89	8.5	N/A	162.6	10001.5	70.2	142.47
73	Monotonic	16	52.1	1.87	8.5	N/A	181.8	7512.9	76.6	98.08
116	Monotonic	16	54.0	1.89	8.5	N/A	168.3	6981.4	72.1	96.83
117	Monotonic	16	55.0	1.90	8.5	N/A	157.1	5549.1	68.4	81.17
100	Monotonic	64	53.1	1.88	8.5	N/A	403.7	21523.2	198.6	108.39
107	Monotonic	64	53.1	1.88	8.5	N/A	268.2	12035.1	153.4	78.46
120	Monotonic	64	55.0	1.90	8.5	N/A	355.9	18230.7	182.6	99.82
124	Monotonic	64	52.1	1.87	8.5	N/A	340.1	19159.5	177.4	108.02
84	Monotonic	4	72.6	1.99	9.5	N/A	109.1	6552.1	40.4	162.31
87	Monotonic	4	69.9	1.97	9.5	N/A	120.0	6793.2	44.0	154.39
76	Monotonic	16	71.3	1.98	9.5	N/A	195.6	6412.2	81.2	78.97
85	Monotonic	64	71.3	1.98	9.5	N/A	410.1	15043.7	200.7	74.96
31	Monotonic	4	65.6	1.88	10.5	N/A	93.3	4124.6	35.1	117.51
77	Monotonic	4	67.9	1.90	10.5	N/A	65.9	3246.3	26.0	125.02
78	Monotonic	4	67.9	1.90	10.5	N/A	103.4	4040.8	38.5	105.05
80	Monotonic	4	65.6	1.88	10.5	N/A	77.5	3110.9	29.8	104.28
81	Monotonic	16	65.6	1.88	10.5	N/A	157.8	6717.9	68.6	97.93
86	Monotonic	16	64.4	1.87	10.5	N/A	153.6	5169.4	67.2	76.93
82	Monotonic	64	65.6	1.88	10.5	N/A	323.9	13339.7	172.0	77.57

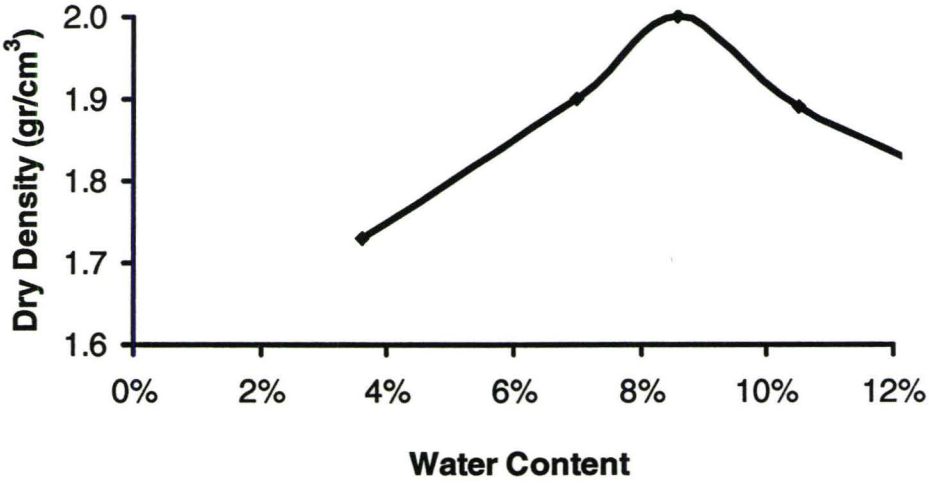

Figure 7.1: Compaction Curve - Material 1

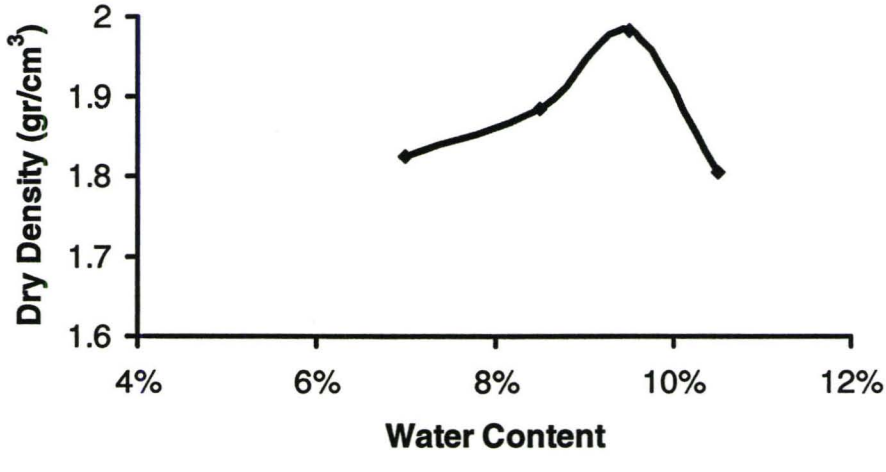

Figure 7.2: Compaction Curve - Material 2

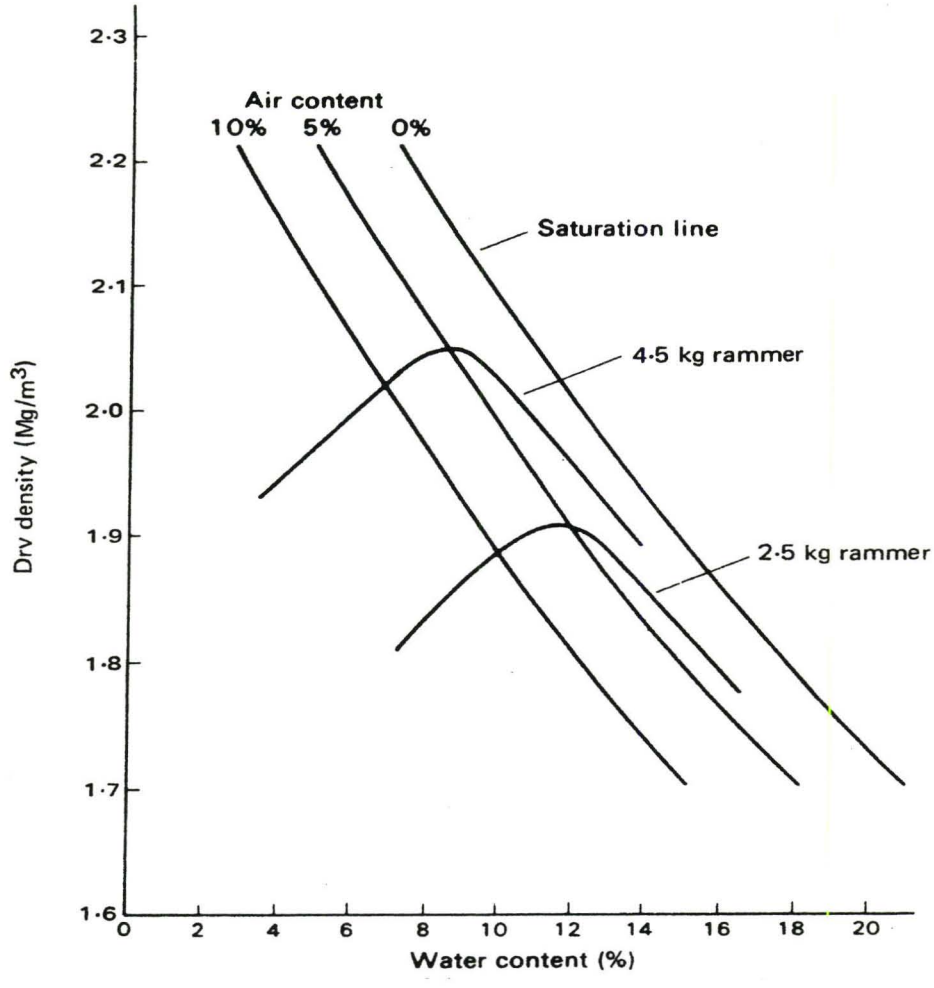

Figure 7.3: Dry Density-Water Content Curves for Different Compactive Efforts

(Craig, 1990)

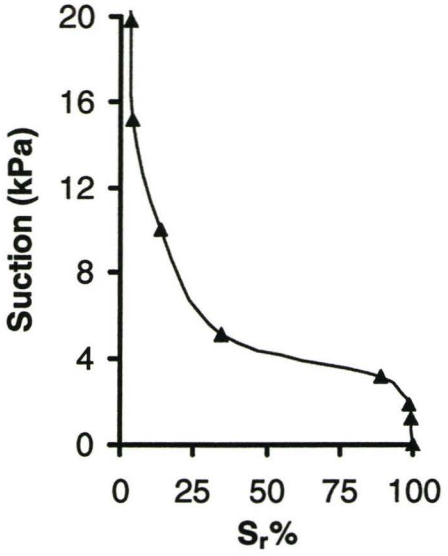

Figure 7.4: SWCC-Drying Curve - Material 1

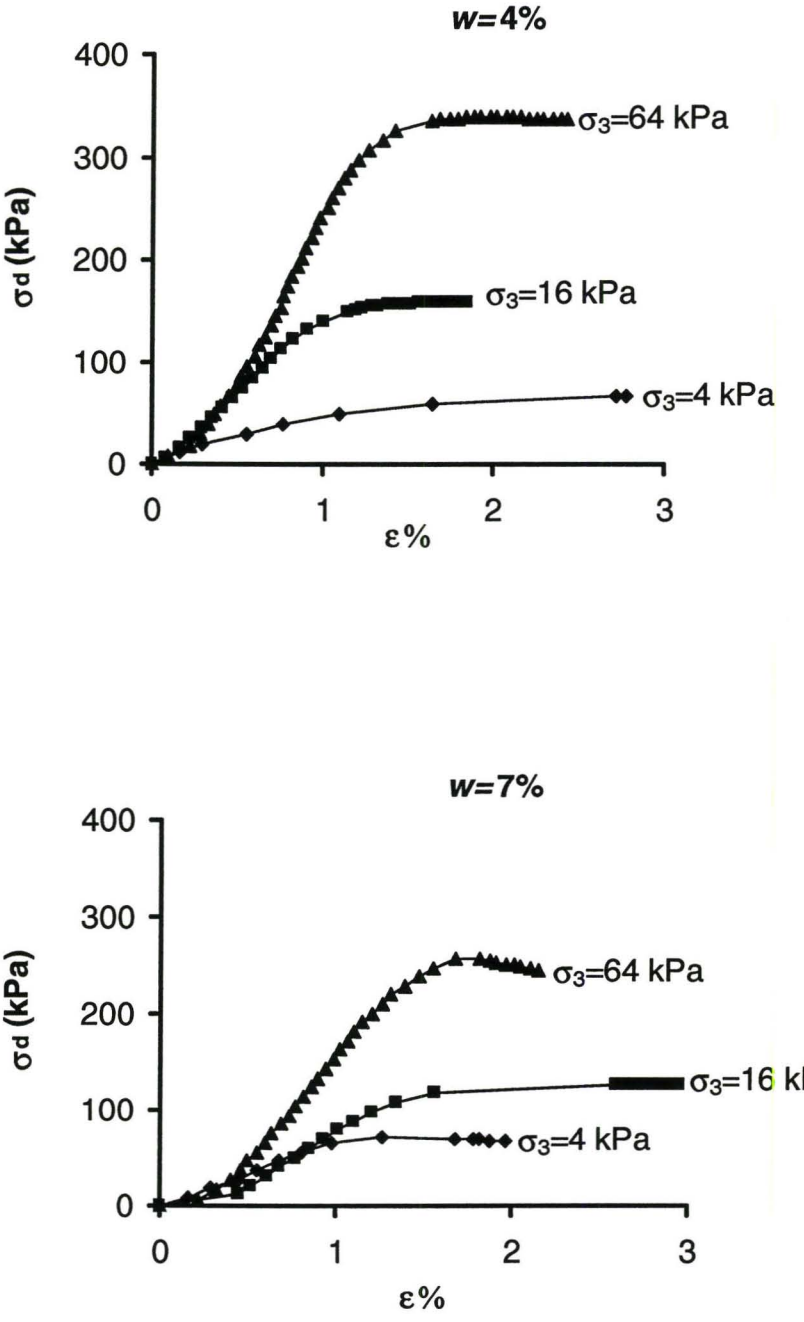

Figure 7.5: Deviatoric Stress vs. Axial Strain

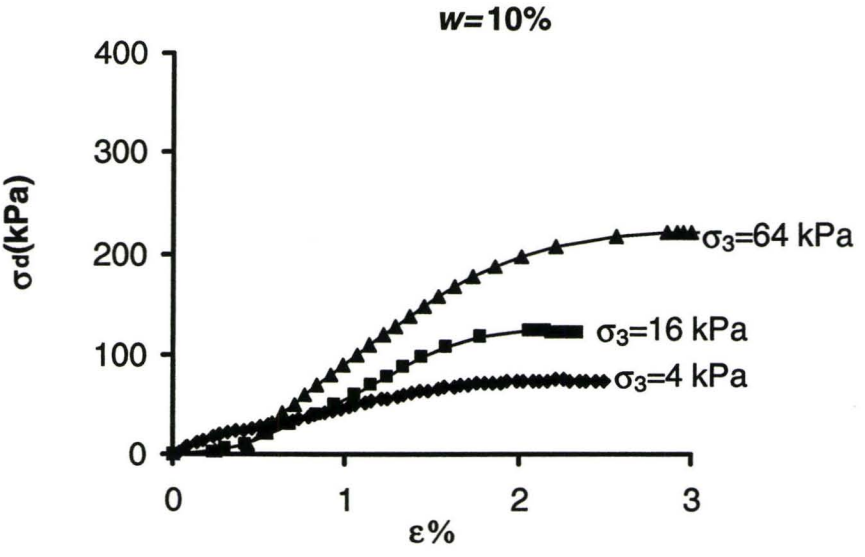

Figure 7.5: Deviatoric Stress vs. Axial Strain (continued)

Material 1 $w = 4\%$

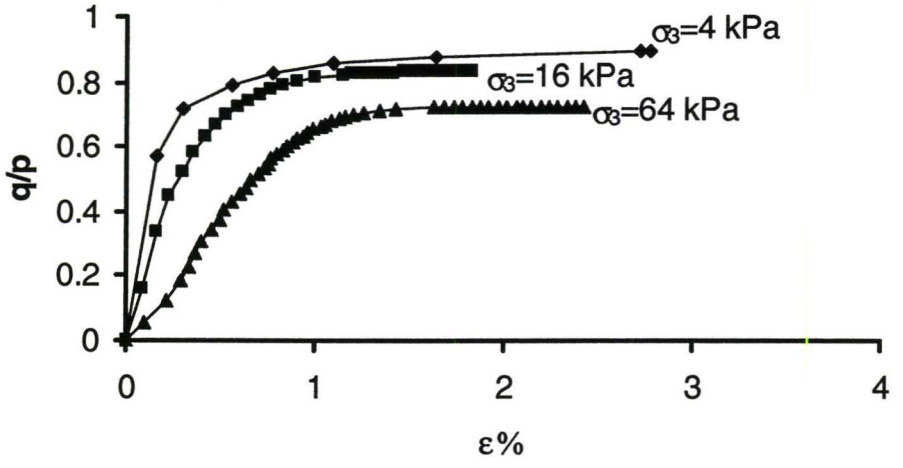

Material 2 $w = 4\%$

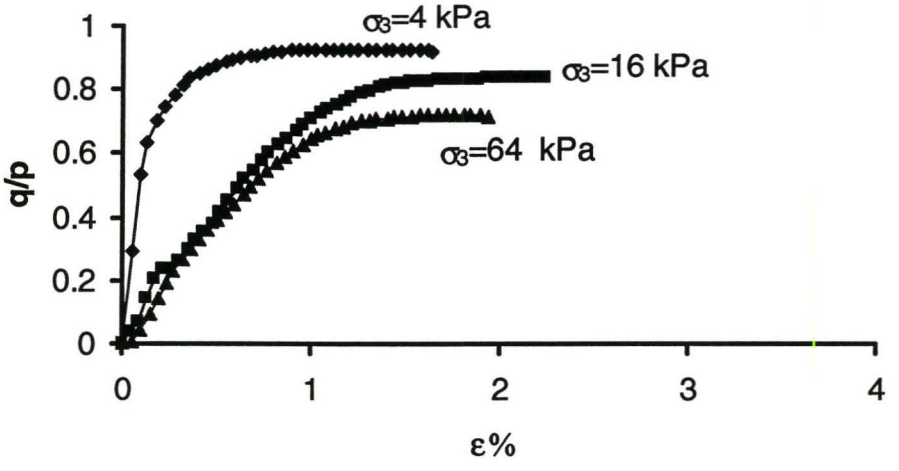

Figure 7.6: Variation of q/p with Confining Pressure

Material 1 $w = 7\%$

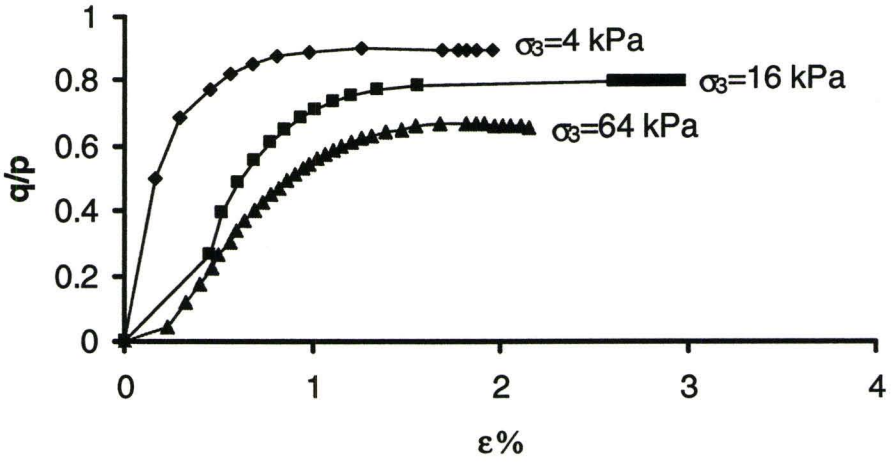

Material 2 $w = 7\%$

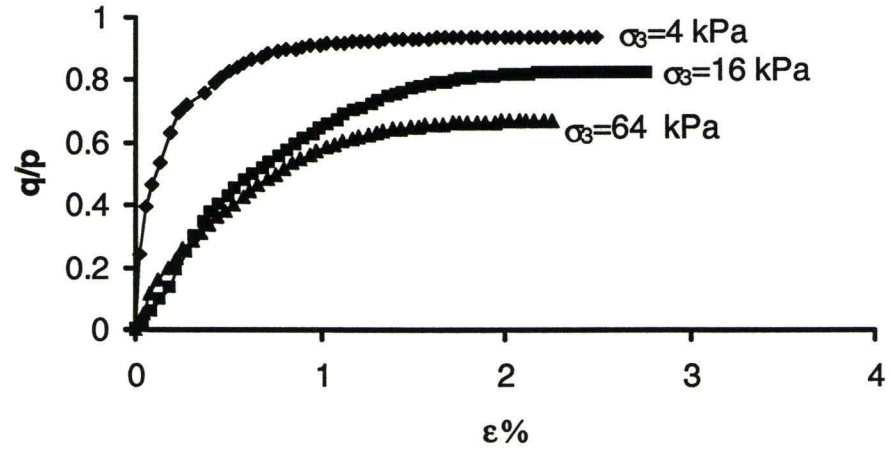

Figure 7.6: Variation of q/p with Confining Pressure (continued)

Material 1 $w = 10\%$

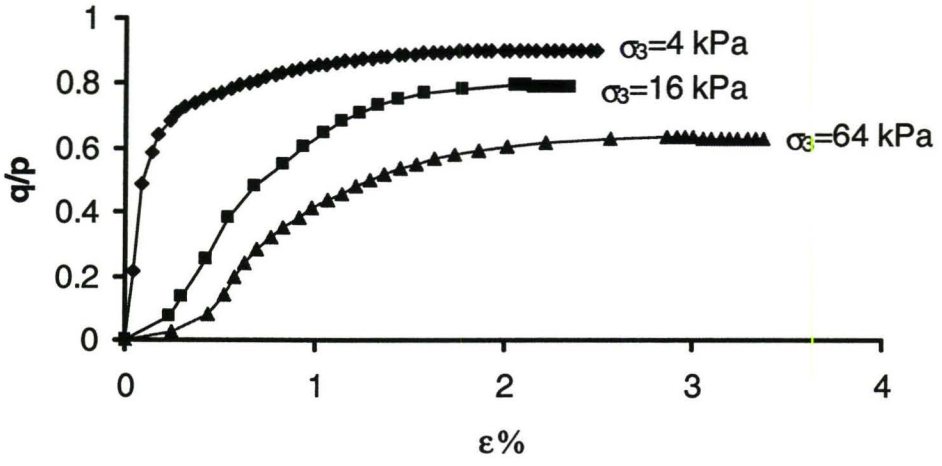

Material 2 $w = 9.5\%$

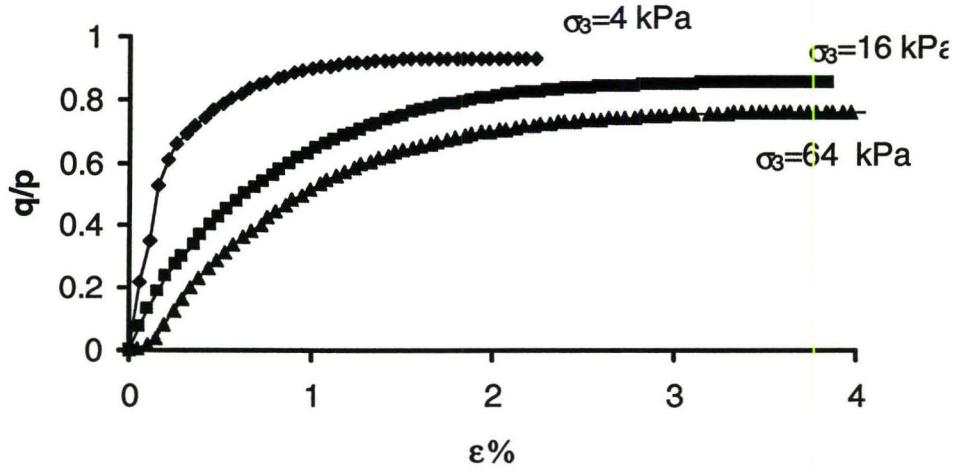

Figure 7.6: Variation of q/p with Confining Pressure (continued)

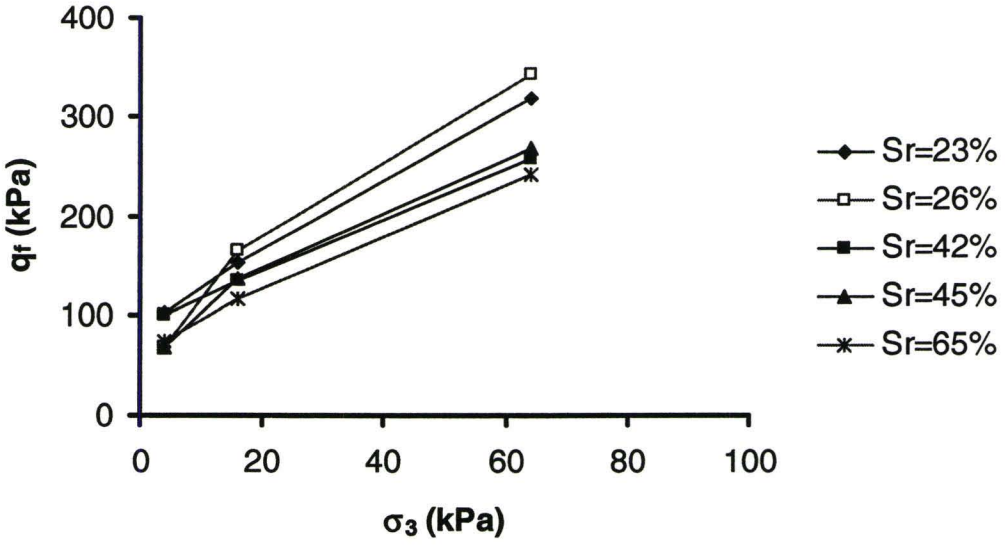

Figure 7.7: Relationship between Shear Strengths and Confining Pressure

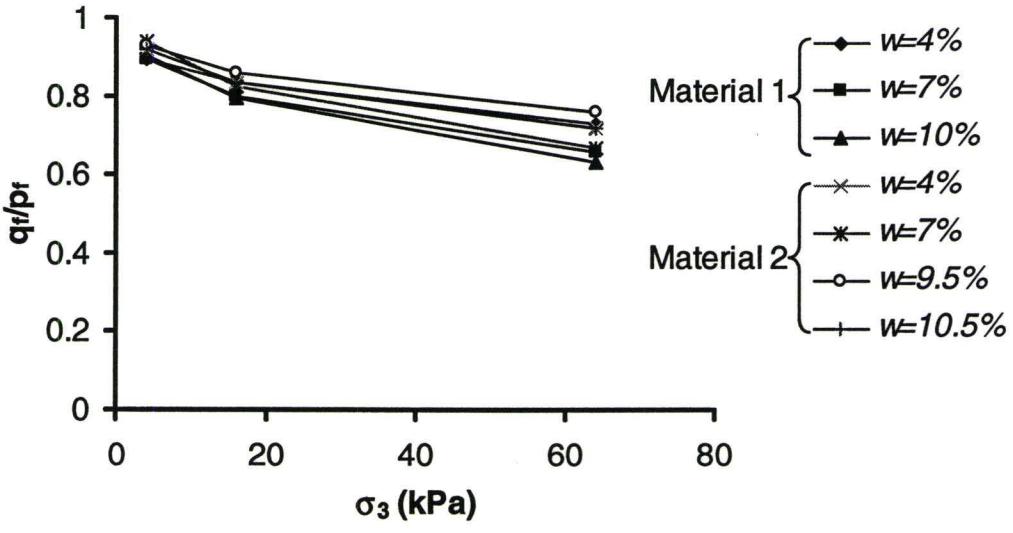

Figure 7.8: Variation of q_f/p_f with σ_3 for Different Moisture Contents

Material 1 σ_3=4 kPa

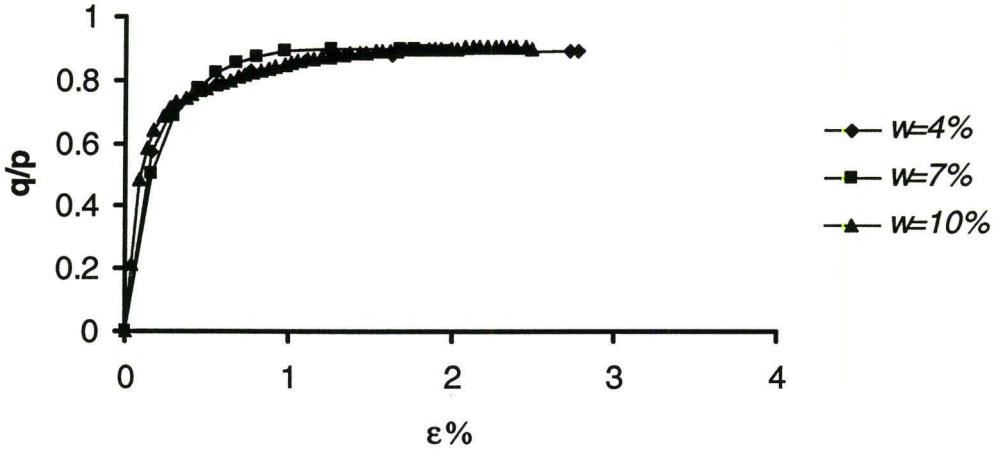

Material 2 σ_3=4 kPa

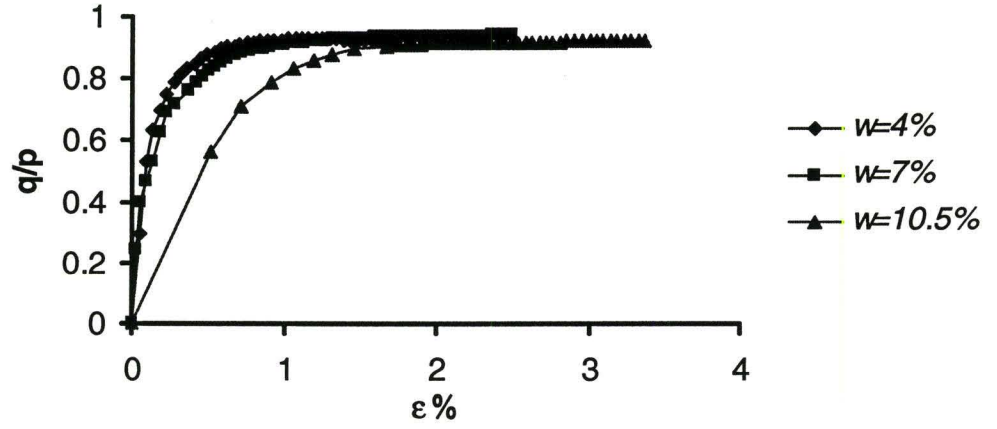

Figure 7.9: Variation of Normalized Shear Strength for Different Water Content

Material 1 σ_3=16 kPa

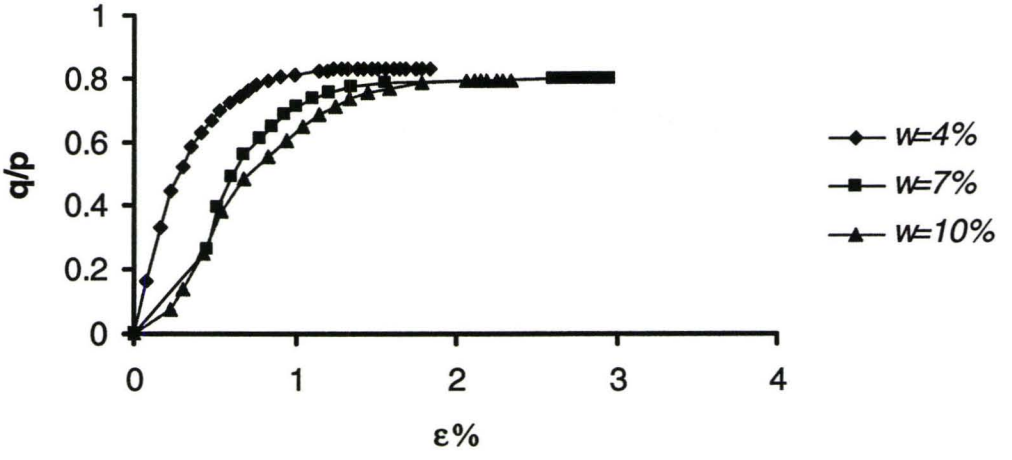

Material 2 σ_3=16 kPa

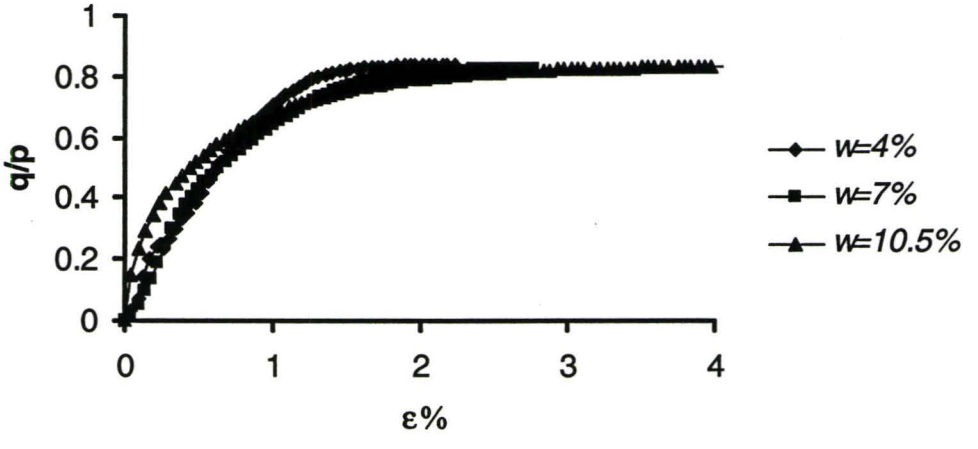

Figure 7.9: Variation of Normalized Shear Strength for Different Water Content

(continued)

Material 1 σ_3=64 kPa

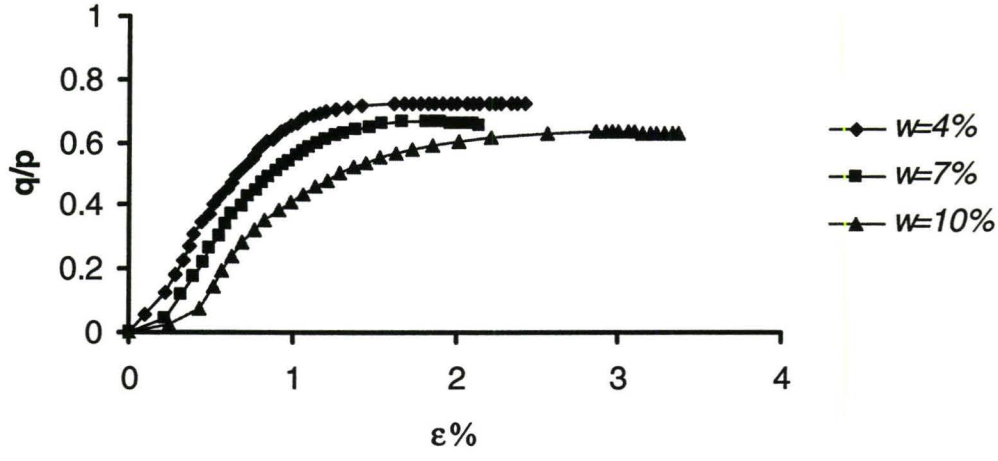

Material 2 σ_3=64 kPa

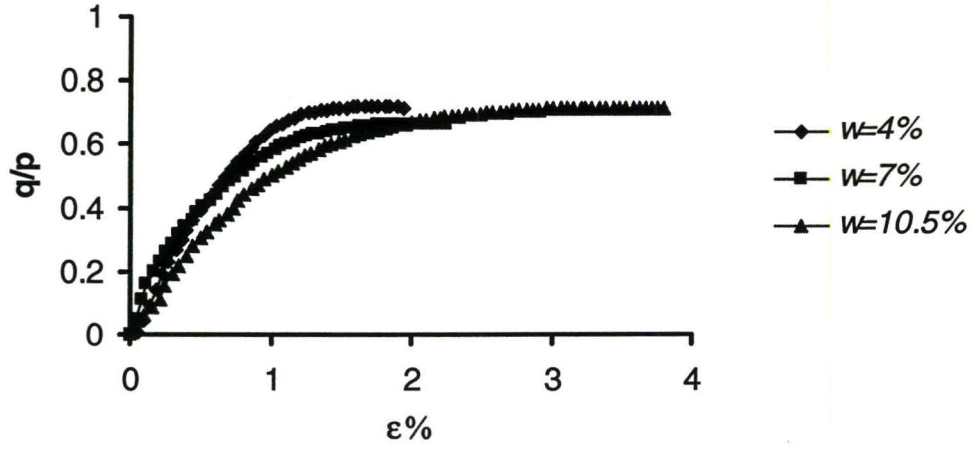

Figure 7.9: Variation of Normalized Shear Strength for Different Water Content

(continued)

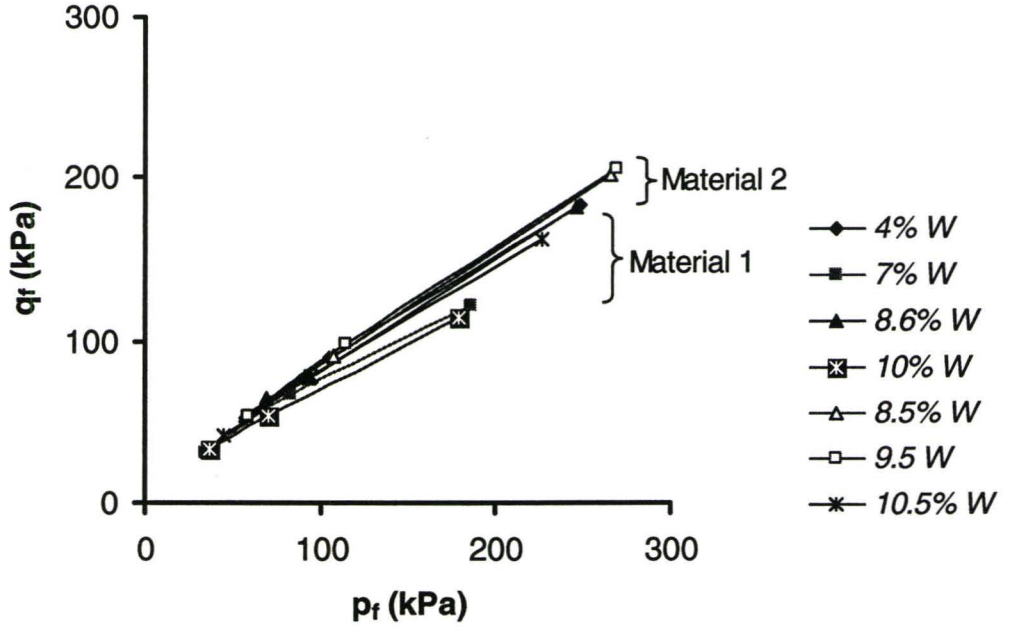

Figure 7.10: Failure Envelop for Material 1 and Material 2

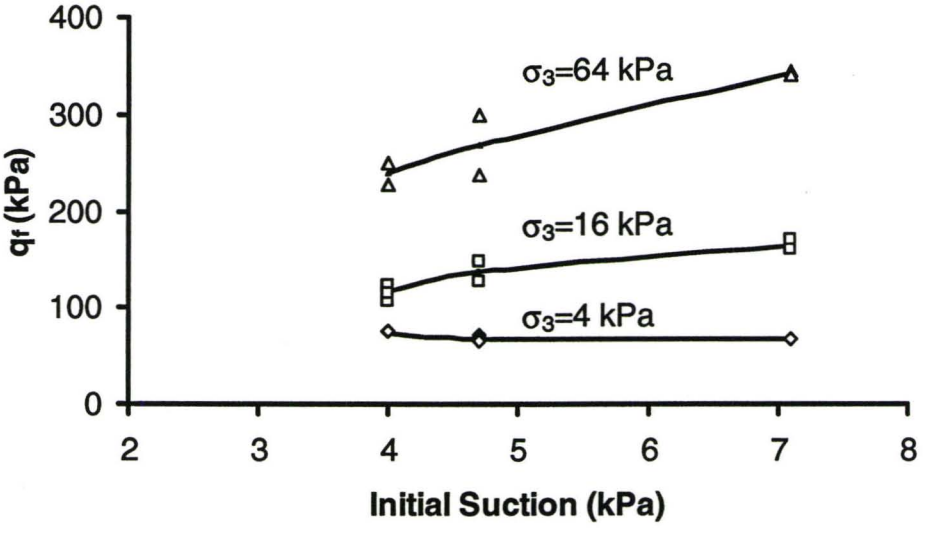

Figure 7.11: Changes in Shear Strength with Initial Suction - Material 1

Material 1

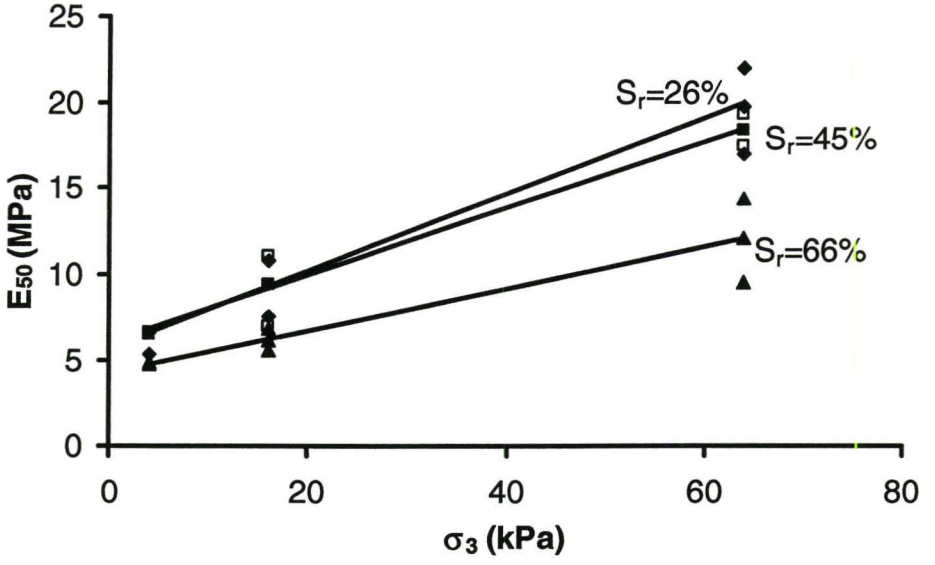

Material 2

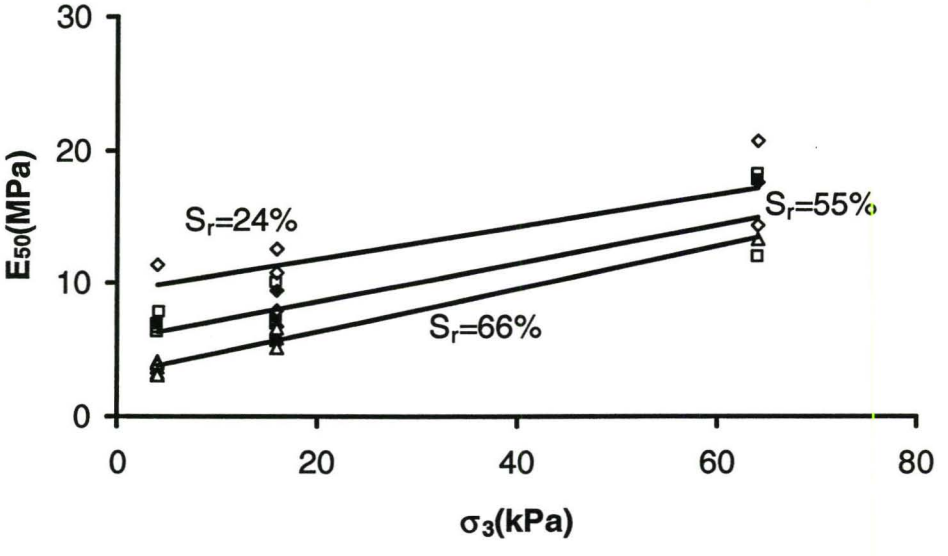

Figure 7.12: Variation of Secant Modulus with Confining Pressure

Material 1

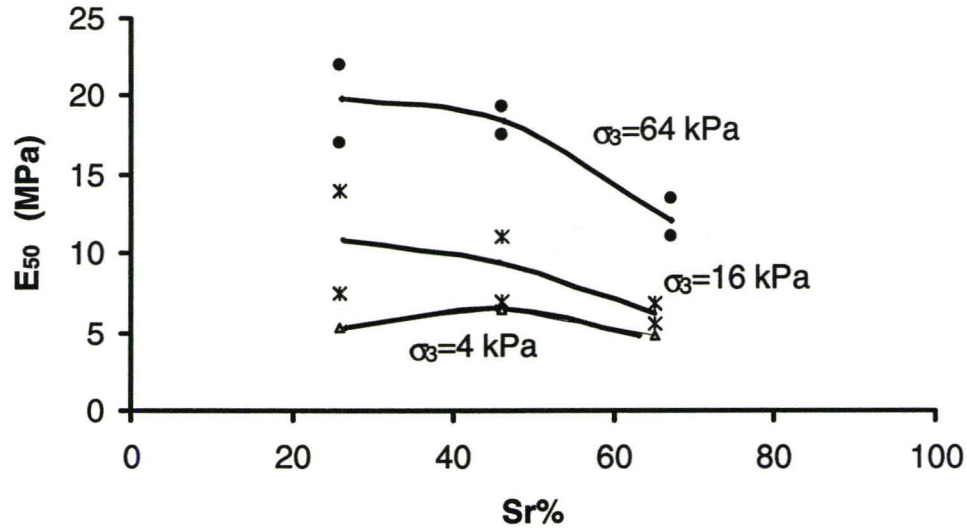

Material 2

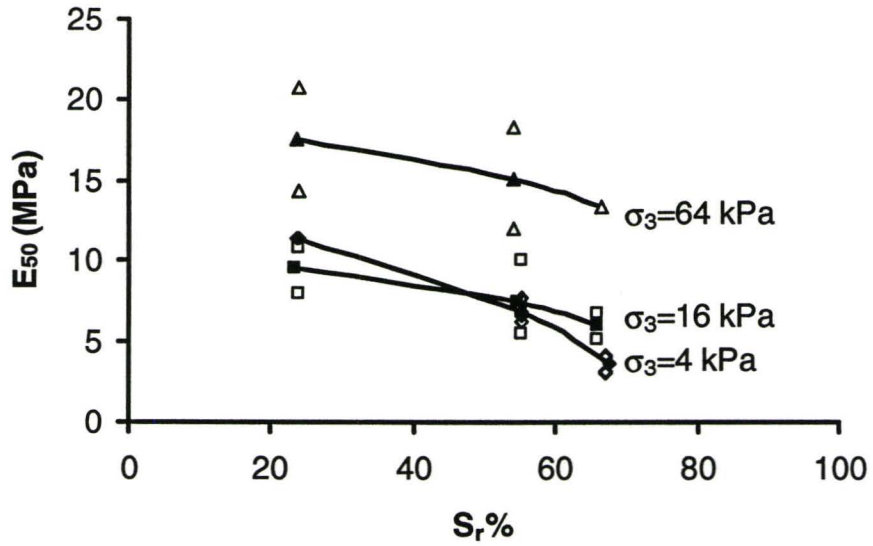

Figure 7.13: Variation of Secant Modulus with Degree of Saturation

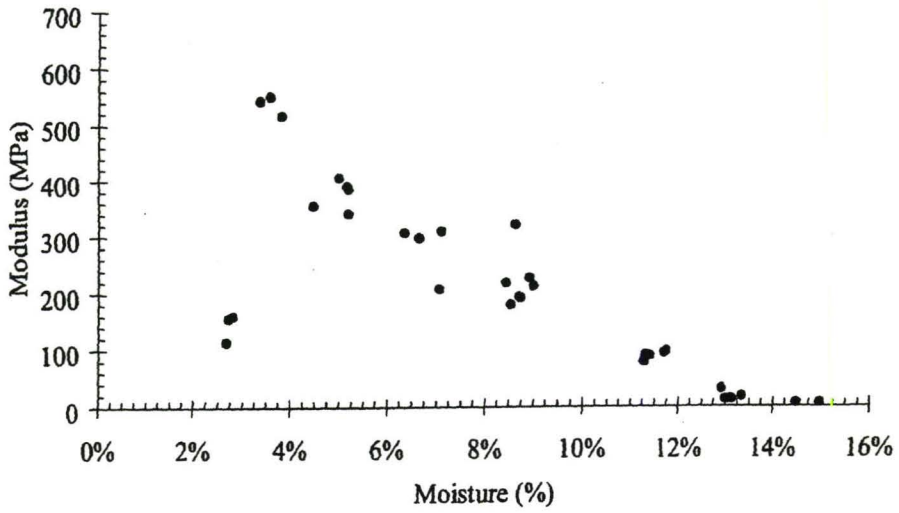

Figure 7.14: Variation in Elastic Modulus with Moisture Content for Granular Material (Nazarian 2003)

Material 1

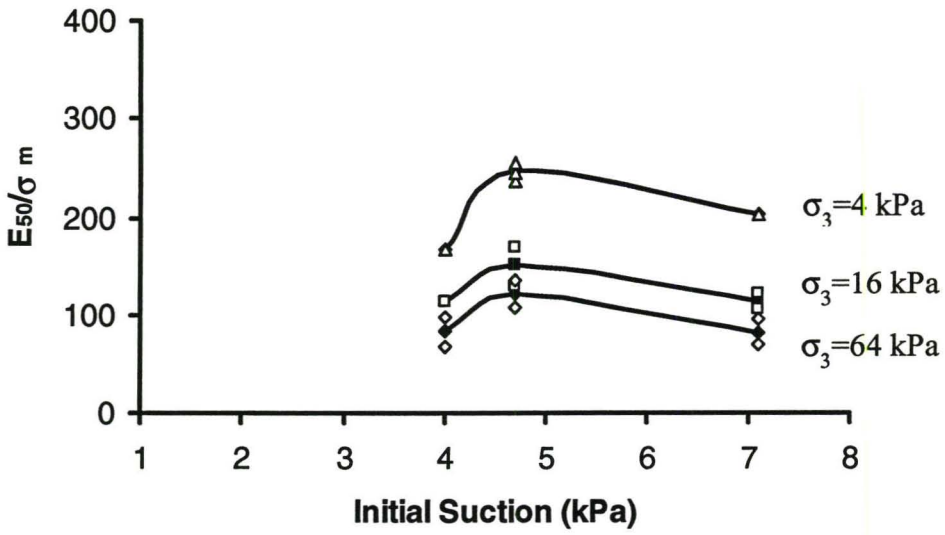

Figure 7.15: Variation of Normalized Secant Modulus with Initial Suction

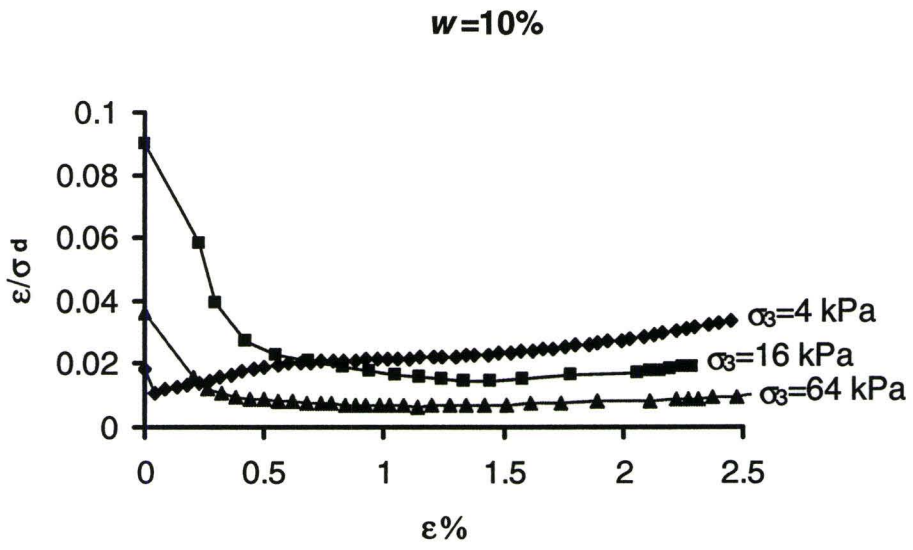

Figure 7.16: Transformed Plot for Constant Water Content (continued)

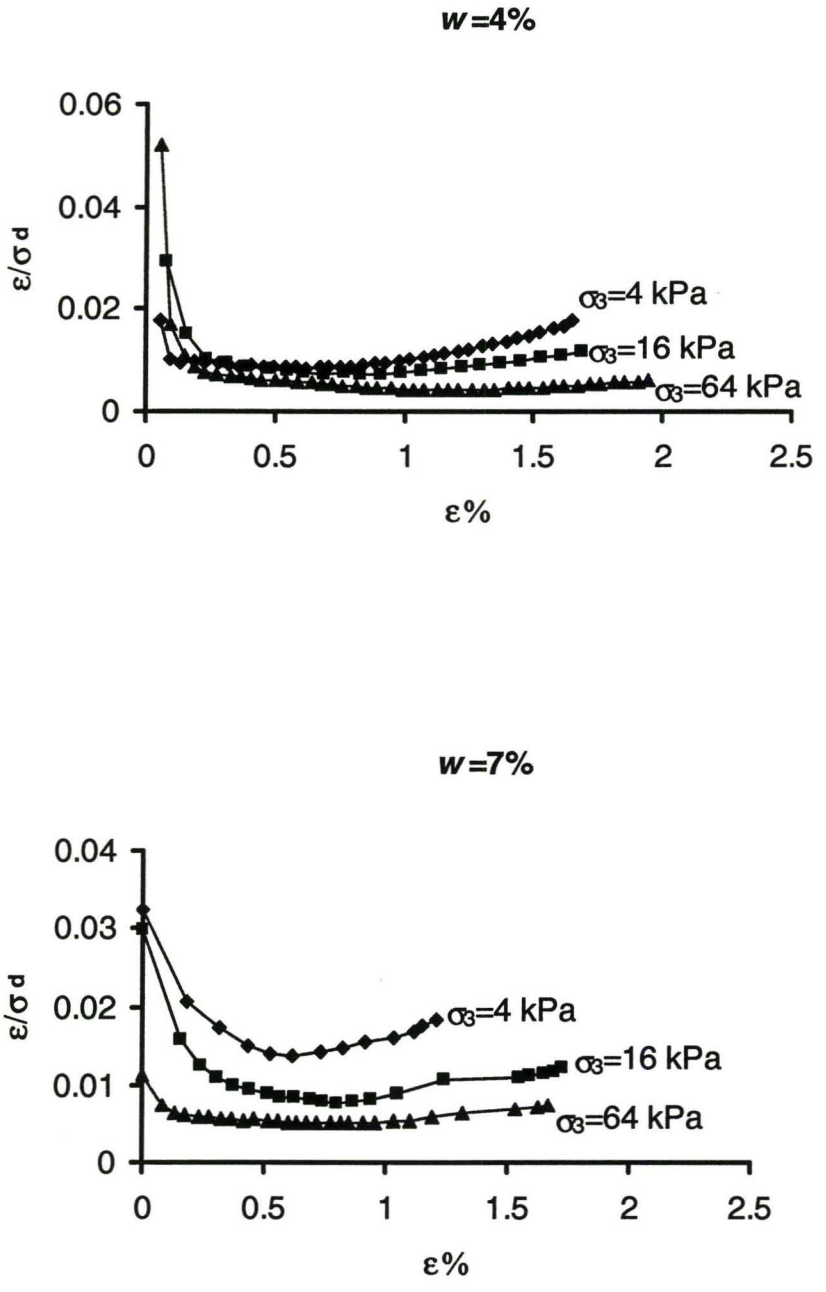

Figure 7.16: Transformed Plot for Constant Water Content

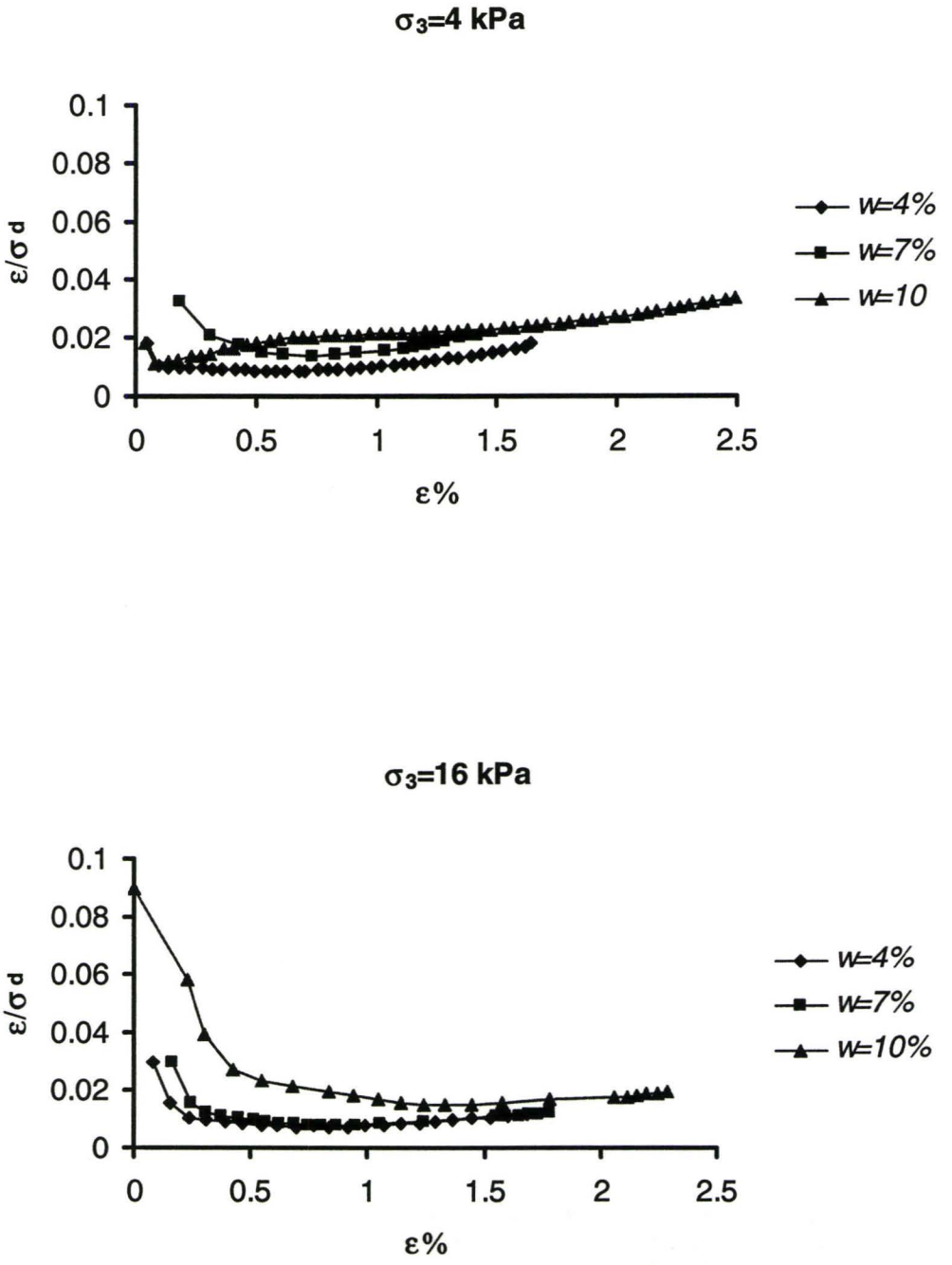

Figure 7.17: Transformed Plot for Constant Confining Pressure – Material 1

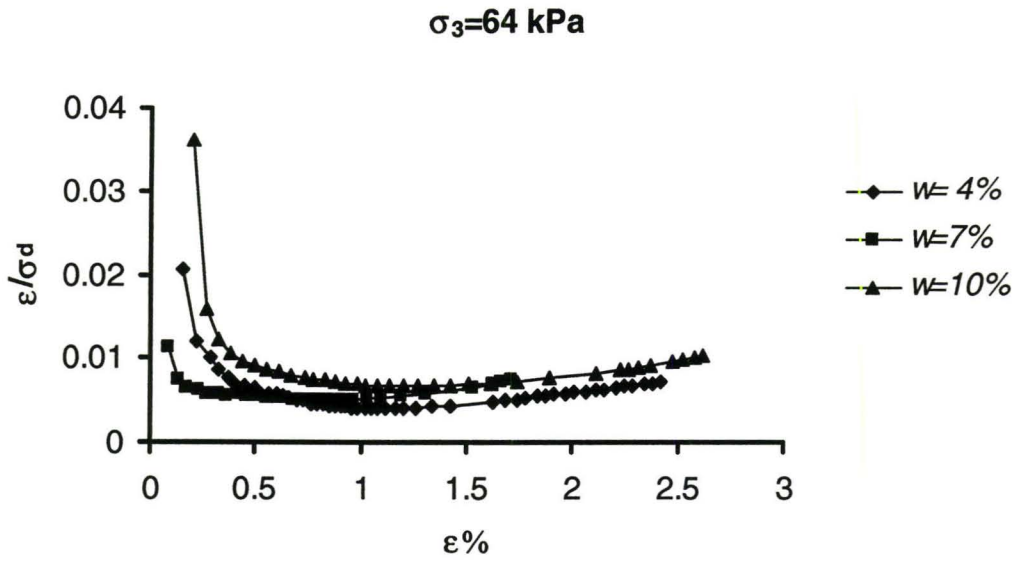

Figure 7.17: Transformed Plot for Constant Confining Pressure (continued)

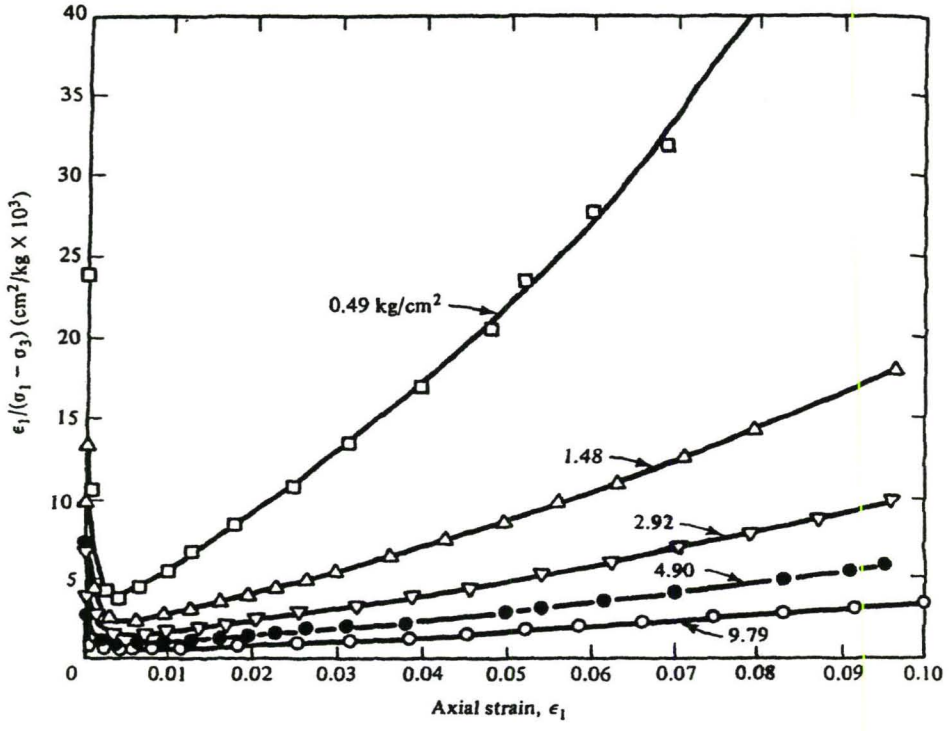

Figure 7.18: Transformed Hyperbolic Stress-Strain Relationship

CHAPTER 8

Results and Discussion of Cyclic Triaxial Tests

8.1 Introduction

A secondary objective of this thesis was to investigate the effects of cyclic loading and freeze-thaw on the plastic strain development of unsaturated modified material. First, this chapter presents a brief literature review. Next, the cyclic test results for different water content and confining pressure are summarized.

8.2 Permanent Deformation of the Base Layer

Pavement rutting is usually correlated to the deformation of the base/subbase and surface layers (Theyse 2000, Tseng and Lytton 1989). A mechanistic-empirical (ME) design model for the design of base layers was developed during the late 1970s (Maree, 1978). This model, however, was only calibrated for mechanically crushed material and not base quality natural aggregate.

8.3 Permanent Deformation Distress Mechanisms

Two permanent deformation mechanisms normally occur in pavement base/subbase layers. The first mechanism of permanent deformation occurs when the applied shear stress condition is well below the shear strength of the material. In this case, the base layer gradually deforms under repeated loading. This

mechanism of permanent deformation has an initial 'bedding-in' phase, during which the rate of deformation is relatively high. This soon declines with increased load repetitions until the rate of increase in permanent deformation enters a linear or stable phase and becomes constant with increased load repetitions (Theyse, 2000). This stable condition may be maintained for a substantial period if the conditions in the base layer do not change. Figure 8.1 shows a typical result from a cyclic test where this mechanism is active.

The second mechanism of permanent deformation occurs when the applied shear stress approaches the shear strength of the material. In this case, rapid permanent deformation of the base layer occurs under a relatively small number of load applications. The pavement base layer enters an unstable condition and the rate of permanent deformation increases (sometimes exponentially) with increased load applications. When this happens base layer material is shoved to the side of the wheeltrack. This mechanism of permanent deformation may be initiated for a base layer in a stable condition of permanent deformation when the shear strength of the material is suddenly reduced by the ingress of water or, in the case of an old road, when the material is sufficiently degraded by the mechanical action of the traffic loads to reduce the shear strength of the material.

8.4 Factors Affecting Permanent Deformation

Several important factors influence the permanent strain behaviour of

granular materials, which are discussed further in the following sections.

8.4.1 Stress Level

Research has shown that one of the most important factors affecting the development of permanent deformations is the stress level. They have reported that the permanent deformation is governed by some form of stress ratio consisting of both deviatoric and confining stresses. Other researchers have attempted to explain the permanent strain behaviour under repeated loading using the ultimate shear strength of the material.

In this latter approach the static failure line is considered as a boundary for permanent strain under repeated loading. This has been questioned by Lekarp and Isacsson (1998) who argue that failure in granular materials under repeated loading, is a gradual process and not a sudden collapse as in static failure tests.

8.4.2 Number of Load Applications

The number of load cycles is one of the most important factors to consider in the analysis of the long term behaviour of granular materials. Some researchers have reported continuously increasing permanent strain under repeated loading. Others suggest that plastic behaviour of granular materials gradually stabilises, making it possible to define a limit value for the accumulation of permanent strain. Lekarp and Dawson (1997) argue that stabilization is only achieved when the applied stresses are low. Application of high stress level results in a

continuous increase of permanent strain and gradual deterioration.

8.4.3 Moisture Content

It has been found that the combination of a high degree of saturation and low permeability, resulting in poor drainage, gives rise to pore pressure development, low effective stress and consequently, low stiffness and low deformation resistance. It has also been shown that a relatively small increase in water content can trigger a dramatic increase in permanent strain rate and that moisture sensitivity increases with an increase in fines content. The increase in rutting potential of granular materials due to wetting has also been observed during in-situ trials using the Heavy Vehicle Simulator (HVS).

8.4.4 Stress History

The permanent deformation behaviour of soils and granular materials at any instant is directly related to the stress history (the order of application of loads). It has been found that the permanent strain resulting from a successive increase in the stress level is considerably smaller than the strain that occurs when the highest stress level is applied first. Even though the effect of stress history on permanent deformation behaviour has been recognised, limited research has been done in this area.

8.4.5 Density

The effect of density, as described by degree of compaction, is regarded as being very important for the long-term behaviour of granular materials. Resistance to permanent deformation improves with a higher degree of compaction. The reduction of plastic strain resulting from increased density is particularly large for angular aggregates, that is provided that there is no accompanying increase in transient pore pressure during repetitive loading. For rounded aggregates, this decrease in strain with increasing density is considered to be much less significant, as they are initially of higher relative density than angular aggregates for the same density (Kim et al., 2001).

8.4.6 Grading and Aggregate Type

The differences in plastic strain for different aggregate types of the same density show that angular materials (crushed stone) undergo smaller plastic deformations compared to materials with rounded particles. This is said to be a result of the higher angle of shearing resistance in angular materials that is related to good particle interlock.

Some work has also been carried out in Linköping, Sweden (Arm, 1998) on determining the influence of material properties on the accumulation of permanent deformation. The following conclusions were drawn:

- As long as the material grading is within the required specification, there is no obvious change in permanent deformation properties. An open graded material

however, results in rapid deformation.

- The percentage of crushed rock in the mixture affects performance, with greater proportions of crushed material reducing the development of permanent deformations.
- Materials with lower than optimum water content offer the highest resistance to permanent deformation.
- The higher the degree of compaction, the better the material performance.
- Aggregate shape has little influence on performance.
- The petrography of the material may influence the performance, with crushed granite performing better than crushed limestone, which performs better than granite gravel. However some of this may be the result of aggregate crushing.

8.5 Permanent Deformations

Some modelling of permanent deformation behaviour was carried out by Van Niekerk et al. (1998). For each material tested, three triaxial tests were performed at three different stress levels. The samples were loaded for either 10^6 load repetitions (N) or until they accumulated more than 10% axial and/or radial strain. The axial and radial deformations were measured at increasing N values and from this, the axial and radial strains could be determined. The development of permanent strain with N, was found to depend strongly on the failure stress ratio (σ_1/σ_{1f}). It was observed that:

- Sands can be loaded to extreme ratios (σ_1/σ_{1f} = 0.9 - 0.95) before considerable

permanent strain develops,

- Mixed granulates develop considerable permanent strain at lower ratios (σ_1/σ_{1f}= 0.3 -0.5).

The observed permanent deformation behaviour has been modelled by means of the following equation for sand:

$$\varepsilon_p = a_1(R)^{a_2}\left[\frac{N}{1000}\right]^b \tag{8.1}$$

where: $b = b_1(R)^{b}{}_2$, $R = \sigma_1/\sigma_{1f}$, ε_p = permanent (axial or radial) strain, N = number of load repetitions, R = stress ratio, and a_1, a_2, b_1, b_2 are material parameters found from regression analysis, and σ_{1f} = maximum failure principal stress.

8.6 Selection of an Appropriate Stress Parameter

Several researchers have used the ratio between the applied shear stress and shear strength of base materials (q/q_f) as the stress parameter controlling the permanent deformation of the material. Maree (1978) used the "safety factor" for high quality crushed stone material and Huurman (1997) used a "stress ratio" for base and subbase materials. The stress ratio (R), used in the study carried out by Theyse (1999), was formulated in terms of deviator stress defined as:

$$R = \frac{\sigma_1^a - \sigma_3^m}{\sigma_1^m - \sigma_3^m} = \frac{q}{q_f} \tag{8.2}$$

where, σ = principle stress (kPa); σ_1^m = maximum allowable major principle stress (kPa) given c, ϕ and σ_3; σ_1^a = applied major principle stress (kPa); and

σ_3^m = minor principle stress or confining pressure for the triaxial test (kPa). This definition of stress ratio was adopted for this study.

8.7 Discussion of Cyclic Shear Tests

The cyclic test results are summarized in Tables 8.1 to 8.3.

8.7.1 Effect of Confining Pressure

Figure 8.2 and Figure 8.3 show the relationship between ε_p% and number of cycles (N) at different levels of water content. For a stress ratio ($R = q/q_f$) of 0.33, the tests entered a stable permanent deformation phase. The general trend indicates an increase in ε_p when σ_3 increases. However, there are anomalies in which this does not occur. The analysis of the data shows that at low confining pressures the growth of plastic strain levels off and the material behavior approaches an equilibrium state. At higher confining pressure (64 kPa), however, the material exhibits continuing deformation rather than leveling off. This phenomenon is more obvious as the water content/degree of saturation rises. When examining the figures it is clear that there appears to be a threshold value of water content, which when exceeded leads to large plastic strain development.

Figure 8.4 shows a linear relationship between plastic strain and confining pressure. However, the slope of the line increases with increasing water content. The stress dependency of plastic strain based on the static shear strength of the material was outlined in previous sections. As discussed in Chapter 7, the values

of q_f/p_f decrease with increasing confining pressure. So there seems to be a relationship between q_f/p_f and plastic strain, i.e., as this value decreases (i.e. when σ_3 increases) the plastic strain increases. However, the results for low confining pressures (i.e. 4 and 16 kPa) are very close to each other, which may be attributed to some errors occurring from testing at such a low confining pressure. The increase in plastic accumulated strain with increase in cell pressure should not be surprising since the applied cyclic deviatoric stress also increases, as indicated previously. What we observe is that plastic strain accumulation is not constant for constant stress ratio relative to failure, which had been originally assumed. This assumption implies that q_f/p_f is constant, which we now know is not true.

8.7.2 Effect of Water Content

Figure 8.5 shows the relationship between ε_p% and number of cycles (N) at varying water content and constant values of σ_3. For a constant value of σ_3, whether it is 4 kPa, 16 kPa or 64 kPa, when the water content increases the values of ε_p also rise. However, although water content is important it is concluded that plastic strain development is more influenced by water content.

Figure 8.6 shows the relationship between accumulated plastic strain after 10 cycles of loading/unloading vs. water content, for different confining pressure. As can be observed, the value of plastic strains increases with increasing water content for all cases.

This value was higher for Material 2, although it should be pointed out that

Material 2 had a higher q_f applied to it.

The same argument can be used for the evaluation of the effect of water content on plastic strain under a constant confining pressure. As was evident in Chapter 7, when water content increases, the values of q_f/p_f decrease because of changes in matric suction. Therefore, plastic strain increases with increasing water content.

8.8 Freeze/Thaw

8.8.1 Effects of Saturation Level

Figure 8.7 shows the relationship between ε_p vs. number of cycles of loading/unloading, for σ_3 = 4, 16 and 64 kPa. Between cycle five and six, which corresponds to the freeze-thaw cycle, there is a sharp rise in the values of ε_p and a leveling off thereafter. It is quite clear that with increasing water content the amount of plastic strain increases. It is also clear that freeze-thaw action increases plastic strain accumulation. When water content decreases from 10% to 4% the plastic strain decreases by 17% for a confining pressure of 16 kPa, and by 30% for a confining pressure of 64 kPa.

Figure 8.8 shows the relationship between ε_p% vs. water content for different values of σ_3 after freezing and thawing. As can be seen, with increasing water content the plastic strain increases and also, increased confining pressure causes an increase in plastic strain, which is consistent with what was discussed previously. Figure 8.9 shows the relationship between water content and $\Delta\varepsilon_p$ for

different σ_3, where $\Delta\varepsilon_p$ is the difference between ε_p after 10 cycles and ε_p after 5 cycles. A graph of $\Delta\varepsilon_p$ vs. water content was drawn for cyclic loading and after freezing/thawing and it appears to be linear in nature. As can be seen, after freezing and thawing, the $\Delta\varepsilon_p$ values are higher than those at cyclic loading at the various levels of water content. The increase in percentage of the average plastic strain ranges from 0.16% to 0.29% for σ_3 = 4, 16 and 64 kPa. The reason $\Delta\varepsilon_p$ was used, instead of accumulated plastic strain, is that it made the results more comparable and also more accurate.

It was mentioned in Chapter 4 that freezing/thawing can change suction in the specimen. In addition, as water freezes due to the vapor pressure of ice being much lower than that of water, a high degree of suction is created. When thawing takes place, the moisture inside the soil sample will not remain uniformly distributed. This may lead to a change in suction and shear strength under cyclic loading. Another important effect of freezing/thawing is that when water freezes its volume increases by about 9%, thus the volume of the soil increases by about 2% to 6% (Lambe and Whitman, 1979) making the dry density decrease to 94% of the original value. However, after freezing/thawing the suction probably could be increased but the effect of decreased dry density is more governed by the increasing plastic strain. From what was observed in this stage of the experimental study, the freeze-thaw action likely contributes to a loss of material memory with respect to strain hardening. Thus properties such as M_r can be changed by a freeze-thaw cycle.

Table 8.1: Cyclic Test Results – Material 1

Test #	Test Type	σ_3 (kPa)	$\%S_r$	ρ_d (g/cm^3)	$\%w$	$(p/q)_f$	N=0 $\%\varepsilon_p$	N=1 $\%\varepsilon_p$	N=5 $\%\varepsilon_p$	N=10 $\%\varepsilon_p$
41	Cyclic	4	27.1	1.92	4	0.8145	0	0.29	0.36	0.36
55	Cyclic	4	26.6	1.91	4	0.8164	0	0.45	0.52	0.58
56	Cyclic	4	27.1	1.92	4	0.7778	0	0.29	0.36	0.36
122	Cyclic	4	25.6	1.89	4	0.7715	0	0.30	0.38	0.37
39	Cyclic	16	25.6	1.89	4	0.6151	0	0.21	0.23	0.35
40	Cyclic	16	25.6	1.89	4	0.6094	0	0.21	0.23	0.32
123	Cyclic	16	25.2	1.88	4	0.6068	0	0.43	0.50	0.56
42	Cyclic	64	26.1	1.90	4	0.4696	0	0.52	0.65	0.69
121	Cyclic	64	26.6	1.91	4	0.4623	0	0.47	0.52	0.55
43	Cyclic	4	44.9	1.89	7	0.7271	0	0.15	0.19	0.19
132	Cyclic	4	44.9	1.89	7	0.6891	0	0.71	0.78	0.83
44	Cyclic	16	44.9	1.89	7	0.5869	0	0.78	1.05	1.20
53	Cyclic	16	47.4	1.92	7	0.5624	0	0.38	0.52	0.70
133	Cyclic	16	46.5	1.91	7	0.5851	0	0.47	0.51	0.52
46	Cyclic	64	47.4	1.92	7	0.3893	0	0.29	0.36	0.38
54	Cyclic	64	45.7	1.90	7	0.3785	0	0.38	0.41	0.47
134	Cyclic	64	45.7	1.90	7	0.3882	0	0.58	0.84	1.06
47	Cyclic	4	65.2	1.98	8.6	0.8434	0	0.65	0.87	1.14
137	Cyclic	4	66.5	1.99	8.6	0.8271	0	0.54	0.63	0.7
48	Cyclic	16	65.2	1.98	8.6	0.6100	0	0.43	0.53	0.62
138	Cyclic	16	65.2	1.98	8.6	0.6116	0	0.28	0.35	0.37
49	Cyclic	64	66.5	1.99	8.6	0.4755	0	0.31	0.43	0.53
139	Cyclic	64	66.5	1.99	8.6	0.4794	0	0.6	1.21	1.88
50	Cyclic	4	65.3	1.90	10	0.7319	0	0.52	0.71	0.86
140	Cyclic	4	64.1	1.89	10	0.7225	0	0.24	0.32	0.36
51	Cyclic	16	66.5	1.91	10	0.5330	0	0.29	0.46	0.64
141	Cyclic	16	66.5	1.91	10	0.5144	0	0.65	0.89	0.96
52	Cyclic	64	65.3	1.90	10	0.4896	0	0.64	0.96	1.51
142	Cyclic	64	65.3	1.90	10	0.3712	0	1.21	1.59	1.92

N: Number of cycles of loading

ε_p: Plastic strain at that certain cycle

Table 8.2: Cyclic Test Results – Material 2

Test #	Test Type	σ_3 (kPa)	$\%S_r$	ρ_d (g/cm^3)	$\%w$	$(p/q)_f$	N=1 $\%\varepsilon_p$	N=5 $\%\varepsilon_p$	N=10 $\%\varepsilon_p$
101	Cyclic	4	65.6	1.88	10.5	0.7976	0.56	0. 64	0.70
145	Cyclic	4	65.6	1.88	10.5	0.7960	0. 61	0. 76	0.83
104	Cyclic	16	64.4	1.87	10.5	0.6100	0. 28	0. 36	0.40
112	Cyclic	16	64.4	1.87	10.5	0.7300	0. 67	0. 84	0.93
113	Cyclic	16	64.4	1.87	10.5	0.4960	0.64	0. 76	0.80
146	Cyclic	16	64.4	1.87	10.5	0.6370	0.71	0. 87	0.96
125	Cyclic	64	66.7	1.89	10.5	0.4644	1.25	2.16	3.00
147	Cyclic	64	67.9	1.90	10.5	0.4561	0.38	0. 75	1.00
89	Cyclic	4	69.9	1.97	9.5	0.8180	0.70	0.82	0.90
150	Cyclic	4	72.6	1.99	9.5	0.8090	0.47	0.65	0.66
90	Cyclic	16	71.3	1.98	9.5	0.6616	0.53	0.76	0.80
110	Cyclic	16	69.9	1.97	9.5	0.5180	1.05	1.24	1.31
111	Cyclic	16	69.9	1.97	9.5	0.7400	1.60	1.90	2.03
151	Cyclic	16	71.3	1.98	9.5	0.6560	0.52	0.63	0.65
92	Cyclic	64	72.6	1.99	9.5	0.5090	0.41	0.55	0.60
152	Cyclic	64	69.9	1.97	9.5	0.5100	0.59	0.72	0.90
93	Cyclic	4	54.0	1.89	8.5	0.7535	0.66	0.76	0.78
153	Cyclic	4	53.1	1.88	8.5	0.7580	0.46	0.57	0.64
94	Cyclic	16	53.1	1.88	8.5	0.5920	0.70	0.93	1.10
154	Cyclic	16	55.0	1.90	8.5	0.6050	0.39	0.57	0.68
96	Cyclic	64	54.0	1.89	8.5	0.4359	0.89	1.25	1.53
155	Cyclic	64	52.1	1.87	8.5	0.4350	0.84	1.33	1.68

Table 8.3: Cyclic Test Results – Material 1

(Freeze and Thaw)

Test #	Test Type	σ_3 (kPa)	$\%S_r$	ρ_d (g/cm^3)	$\%w$	N=1 $\%\varepsilon_p$	N=5 $\%\varepsilon_p$	N=6 $\%\varepsilon_p$	N=10 $\%\varepsilon_p$
136-143	Cyc.F/Th	4	24.7	1.87	4	0.14	0.18	0.28	0.29
144-148	Cyc.F/Th	16	25.6	1.89	4	0.18	0.20	0.28	0.33
149-158	Cyc.F/Th	64	25.6	1.89	4	0.63	0.77	1.13	1.24
97-98	Cyc.F/Th	4	48.3	1.93	7	0.63	0.72	0.96	1.00
127-128	Cyc.F/Th	16	44.1	1.88	7	0.50	0.57	1.05	1.07
131-135	Cyc.F/Th	64	44.1	1.88	7	0.75	0.92	1.20	1.20
106-108	Cyc.F/Th	4	65.2	1.98	8.6	0.54	0.72	0.91	0.94
109-114	Cyc.F/Th	16	66.5	1.99	8.6	0.68	0.85	1.12	1.14
115-118	Cyc.F/Th	64	64.0	1.97	8.6	0.48	0.55	0.75	0.85
119-126	Cyc.F/Th	4	65.3	1.90	10	0.61	0.79	1.10	1.20
99-102	Cyc.F/Th	16	66.5	1.91	10	0.29	0.32	0.64	0.73
103-105	Cyc.F/Th	64	64.1	1.89	10	0.55	0.74	1.08	1.13

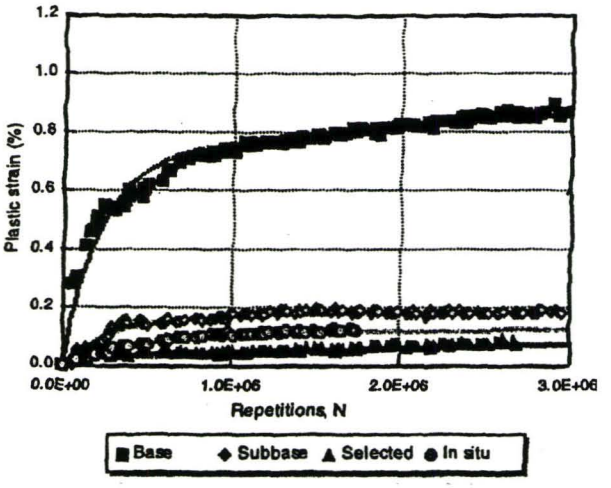

Figure 8.1: Plastic Strain – Number of Loads (Theyse, 2000)

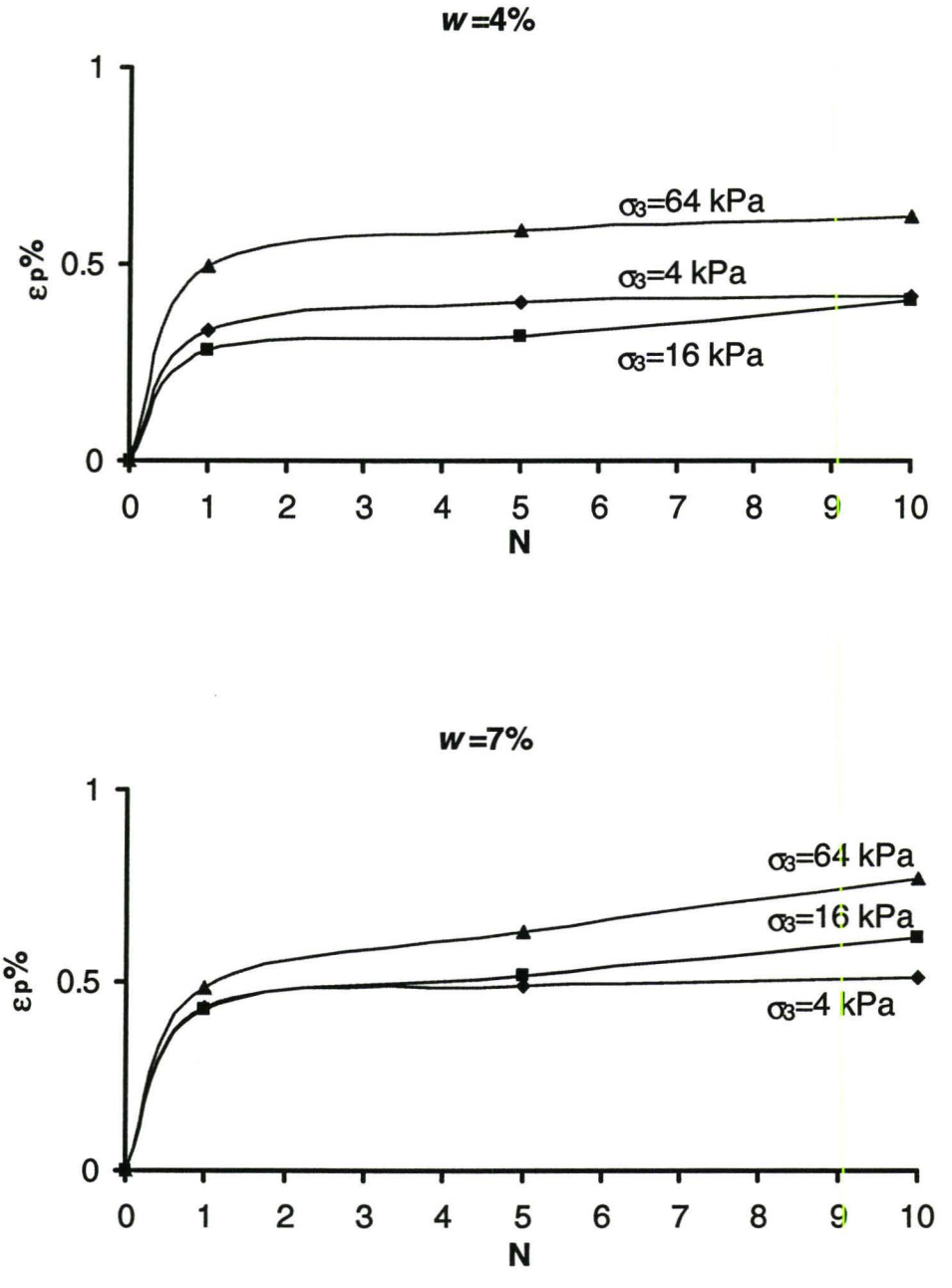

Figure 8.2: Plastic Strain vs. Number of Loads - Material 1

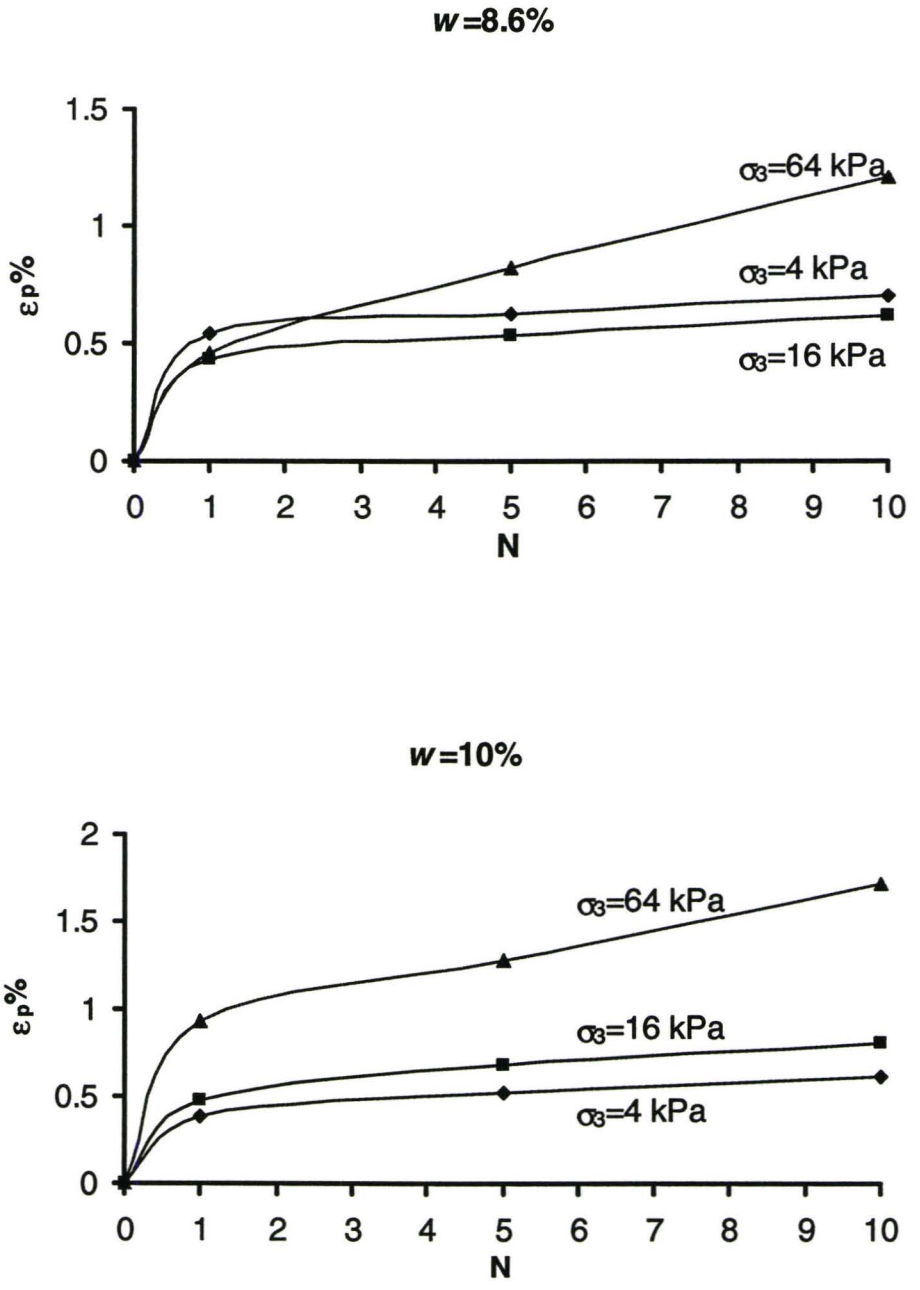

Figure 8.2: Plastic Strain vs. Number of Loads - Material 1 (continued)

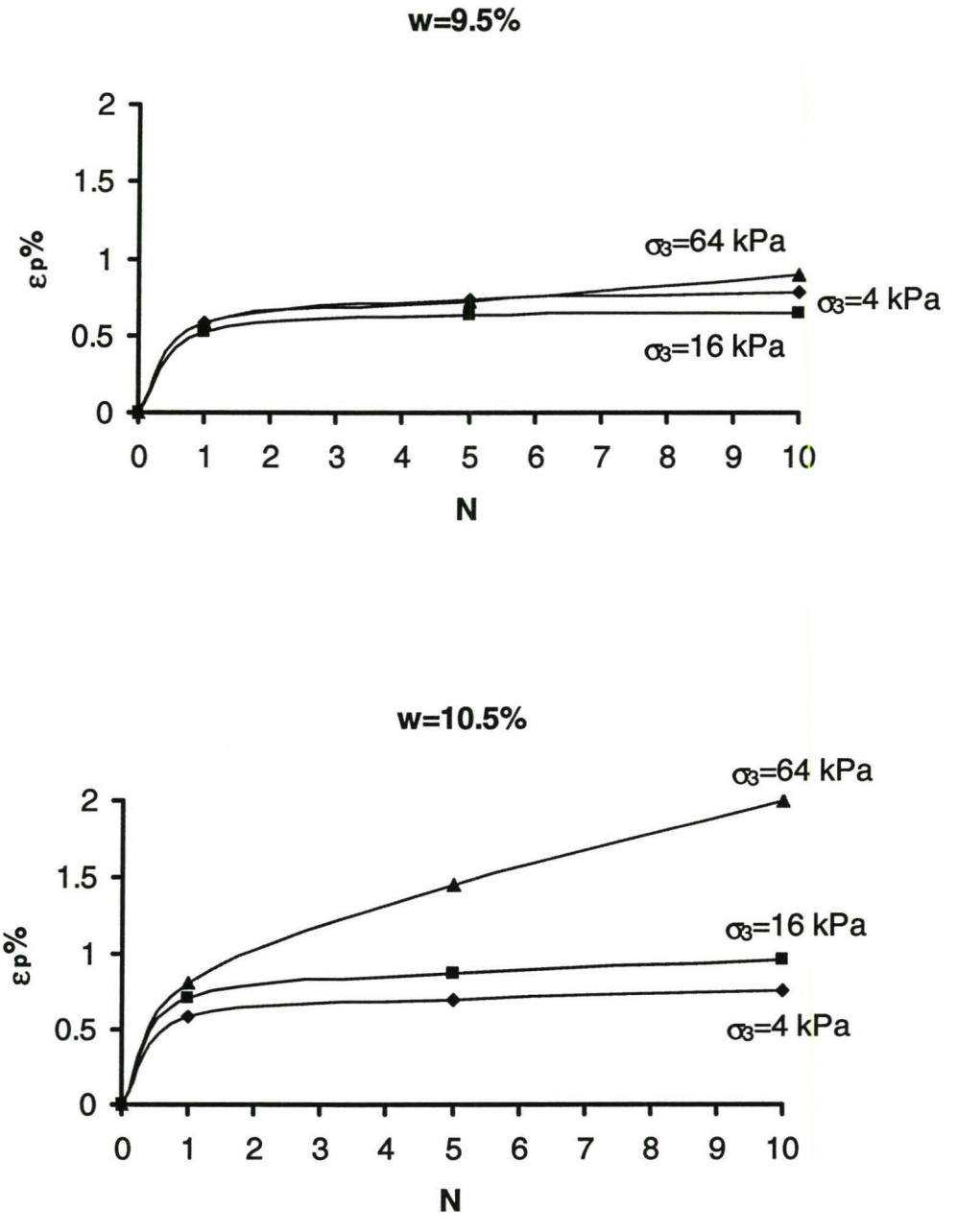

Figure 8.3: Plastic Strain vs. Number of Loads - Material 2

Material 1

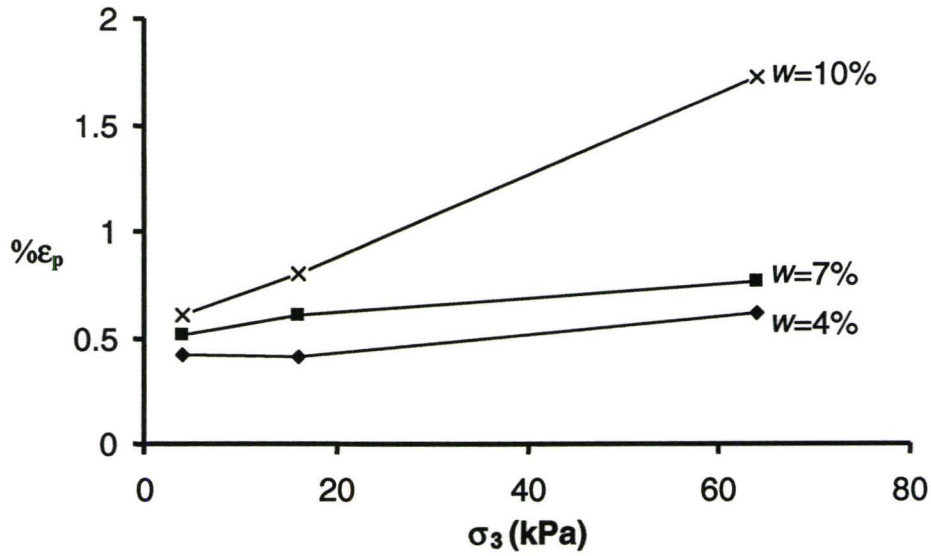

Material 2

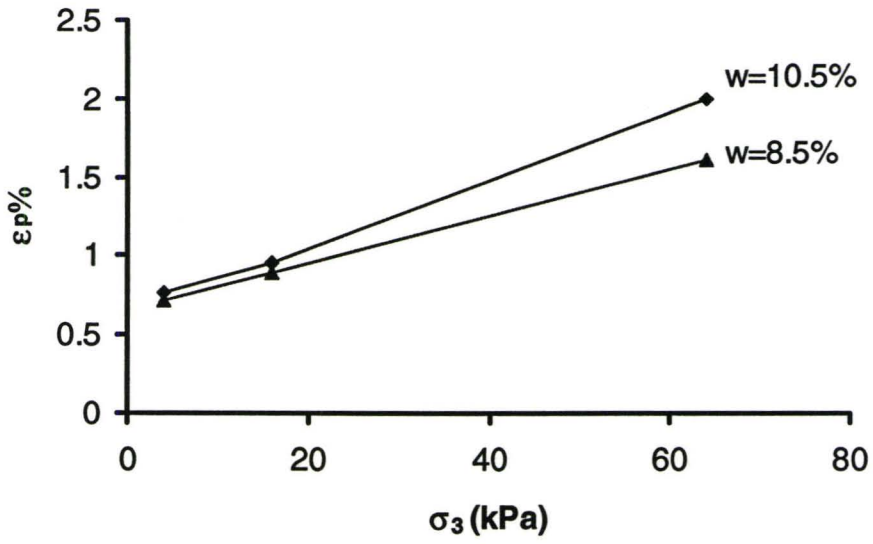

Figure 8.4: Variation of Plastic Strain with Confining Pressure

Material 1 σ_3=4 kPa

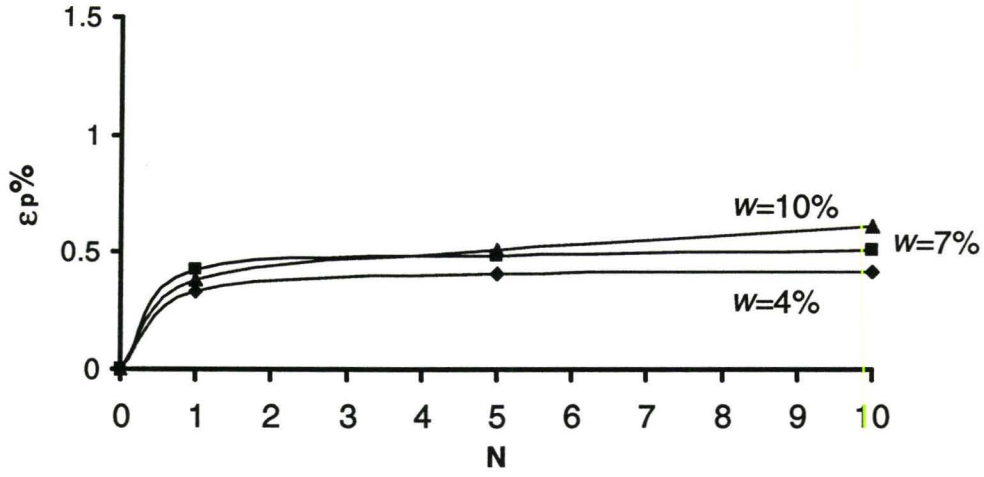

Material 1 σ_3=16 kPa

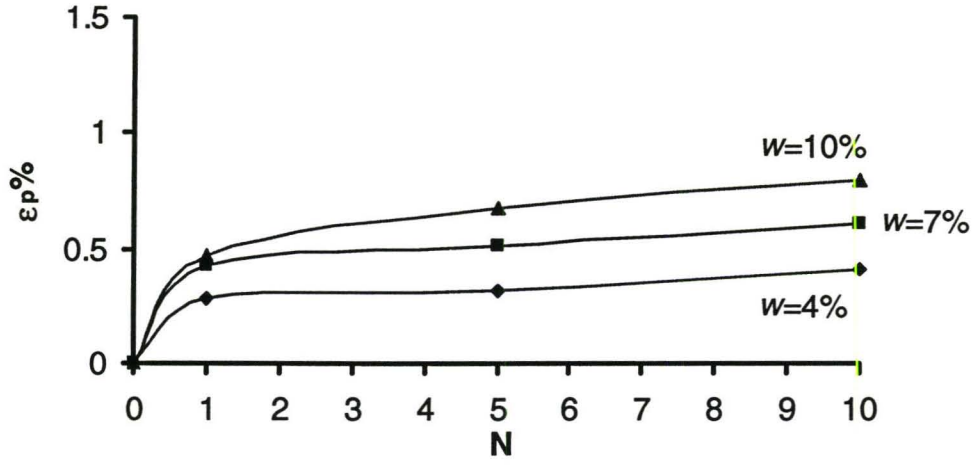

Figure 8.5: Plastic Strain vs. Number of Loads

Material 1 σ_3=64 kPa

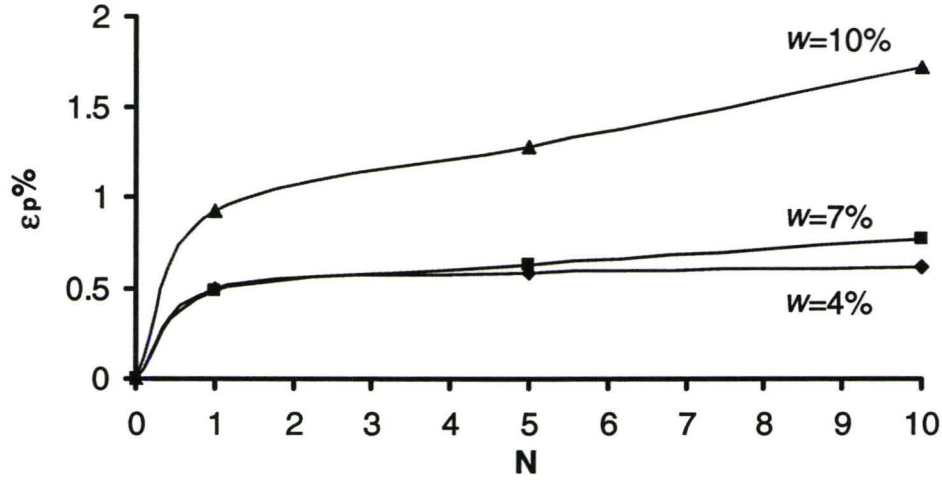

Material 2 σ_3=4 kPa

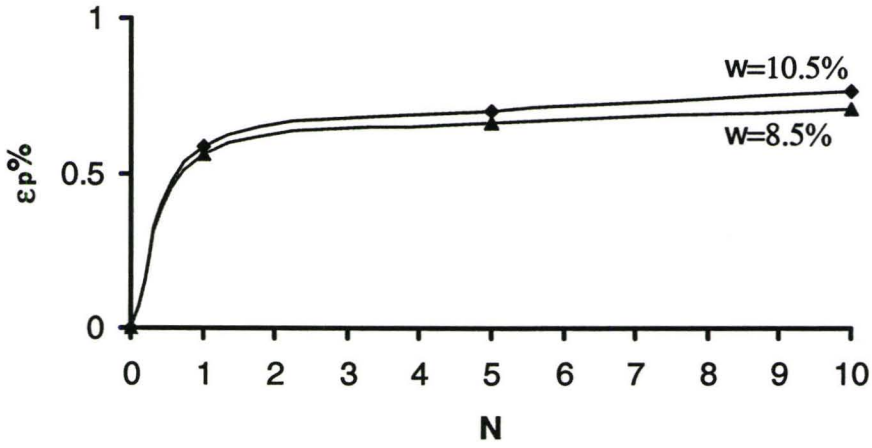

Figure 8.5: Plastic Strain vs. Number of Loads (continued)

Material 2 σ_3=16 kPa

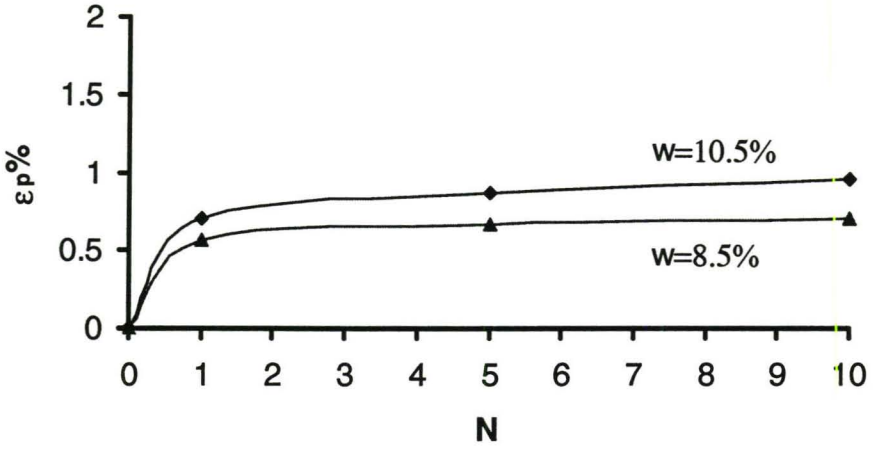

Material 2 σ_3=64 kPa

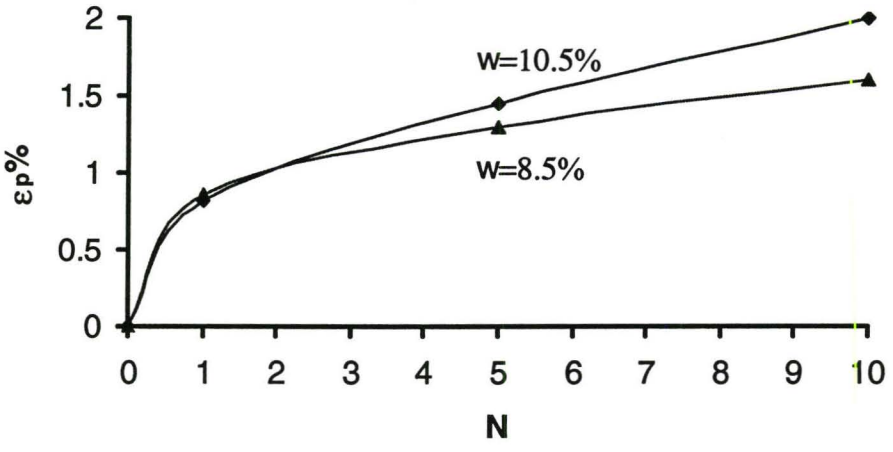

Figure 8.5: Plastic Strain vs. Number of Loads (continued)

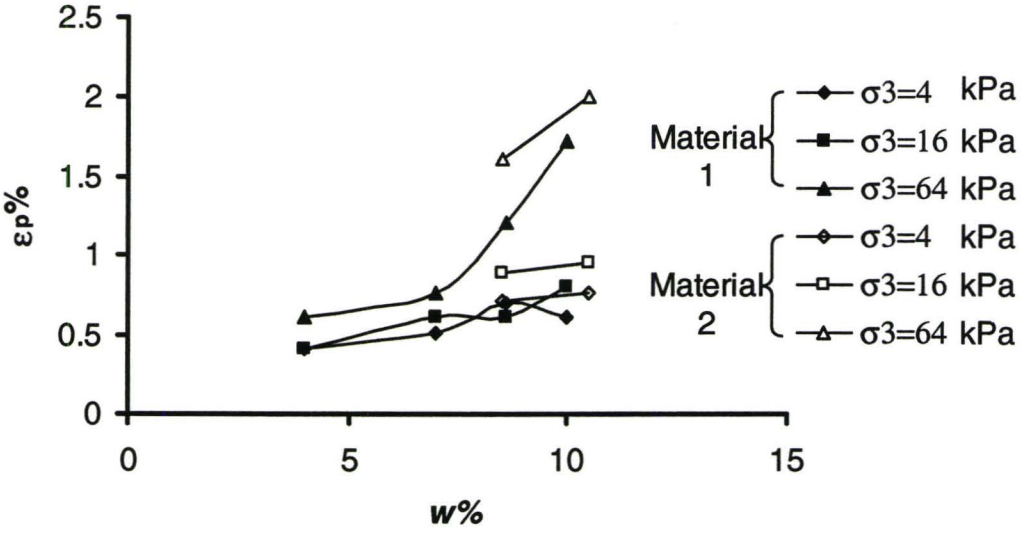

Figure 8.6: Plastic Strain vs. Water Content

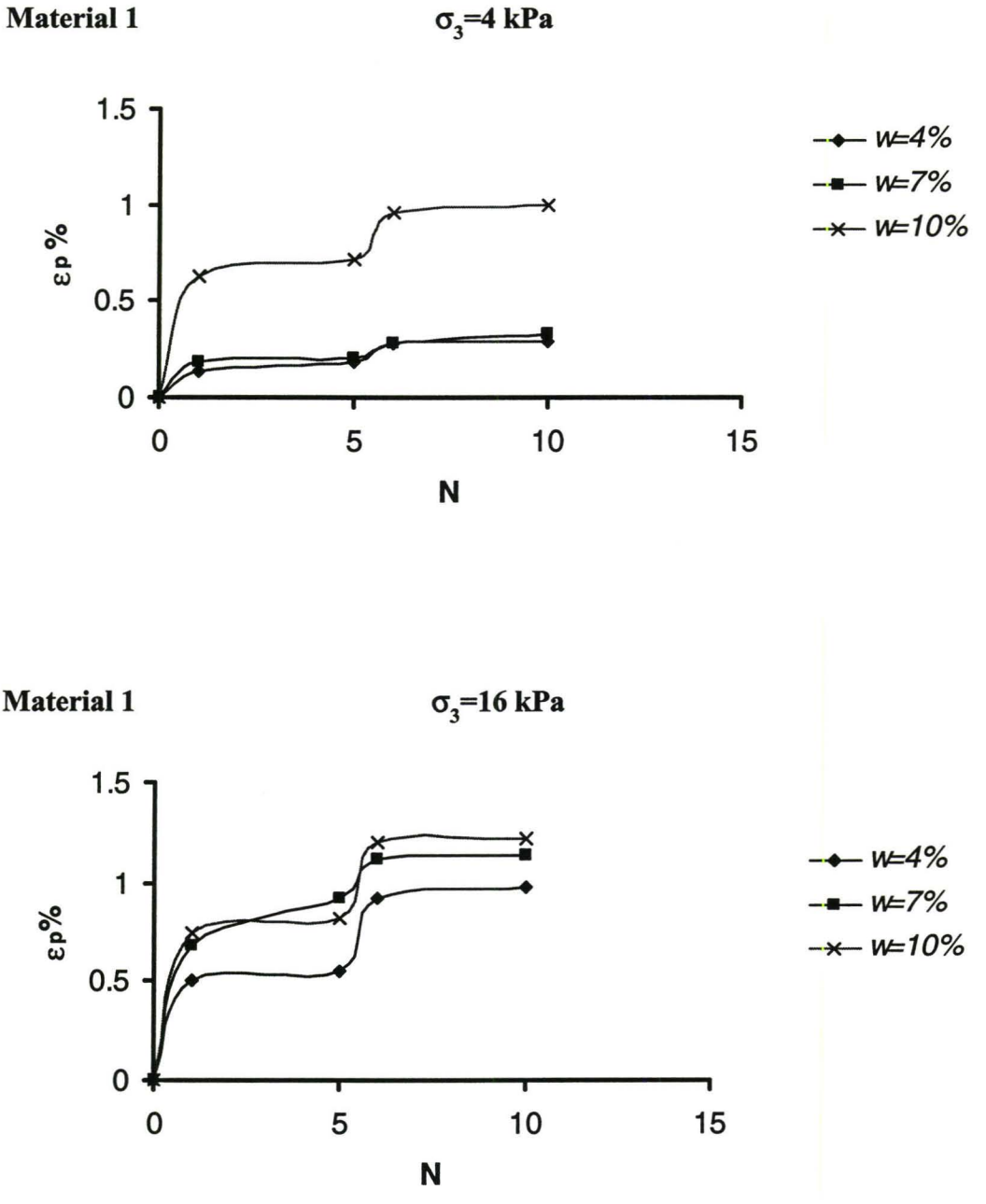

Figure 8.7: Plastic Strain vs. Number of Loads

(Freeze - Thaw)

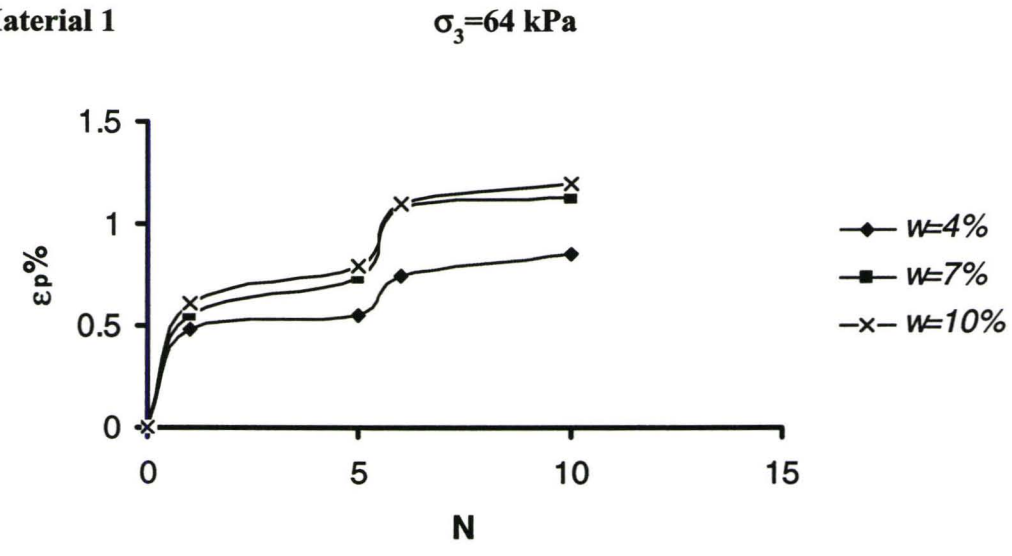

Figure 8.7: Plastic Strain vs. Number of Loads (continued)

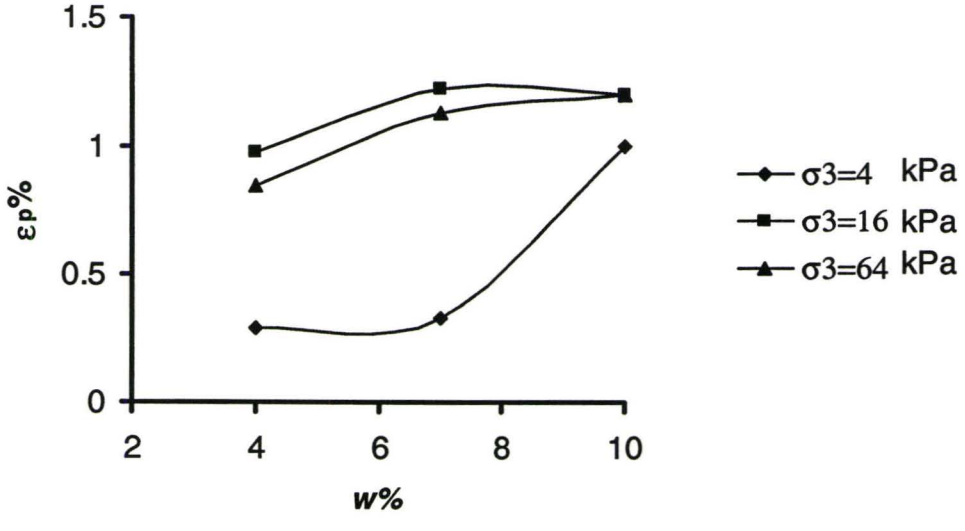

Figure 8.8: Accumulated Plastic Strain vs. Water Content

(Freeze-Thaw)

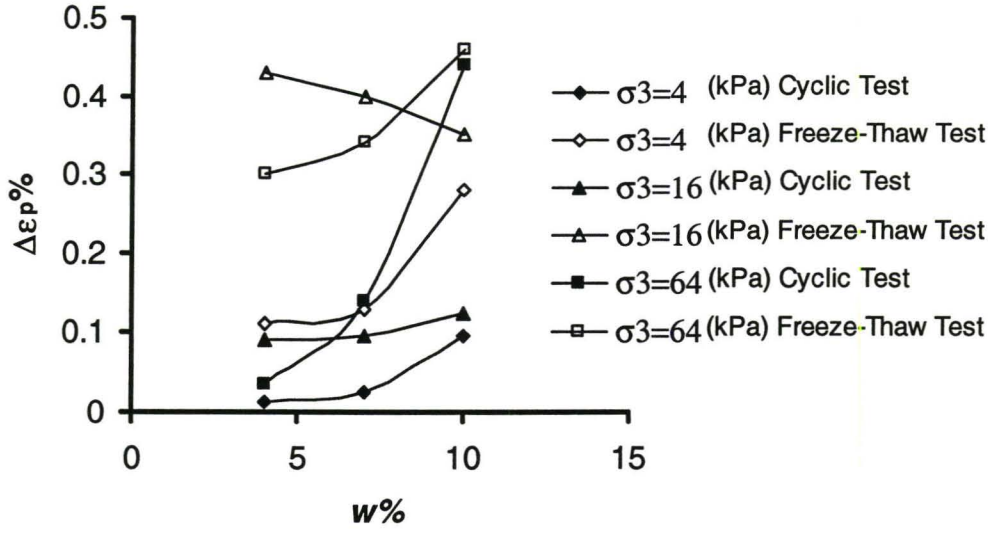

Figure 8.9: Variation of Differential Plastic Strain with Water Content

CHAPTER 9

Conclusions and Recommendations

9.1 Introduction

This study was designed to identify characteristics of the stress-strain behavior of unsaturated modified granular material at different initial water content, degrees of saturation and confining pressures. Throughout the study, the tests focused on undrained, unsaturated behavior. The objectives of the study were listed in Chapter 1 and the results presented in Chapters 7 and 8 indicate that the objectives have generally been met. Therefore, the following conclusions are made.

9.2 Observations and Conclusions

1. The stress-strain response of unsaturated modified granular material is affected by the confining pressure applied. Results show that as cell pressure was increased, the stiffness (E_{50}) and shear strength (q_f) observed at a given degree of saturation increased, as expected.

2. The shear strength and stiffness decreased with increasing saturation. This was true for the entire range of test conditions. Variations in strength and stiffness are therefore direct consequences of the molding water content. Increasing the degree of saturation from 25% to 66% causes a 30% reduction

in q_f and 50% reduction in E_{50} for $\sigma_3 = 16$ and 64 kPa, and almost no changes in q_f and E_{50} for $\sigma_3 = 4$ kPa.

3. Results show that the relation between q_f and p_f appears to be linear in nature, although it has a slight curvature which can be attributed to its unsaturated condition. This was clearer for samples at higher water content (7%, 10%). The lines for 8.6% and 9.5% water content had higher values of dry density that justify the higher shear strength. It can be interpreted that a change in suction is not as effective as a change in confining pressure when it comes to producing an increase in shearing resistance.

4. A comparison of the results for Material 1 and Material 2 suggests that angular aggregates with good particle interlock may reduce the lubrication effect of water content and minimize the effect of increasing water content on the reduction in shear strength.

5. A comparison of the normalized stress-strain curves for varying water contents at constant cell pressures shows that for low confining pressure (4 kPa), the effect of changing water content is minimal but with increasing confining pressure, it is reasonably clear that q_f / p_f decreases as the water content increases.
6. A comparison of the normalized stress-strain curves, for varying confining

pressures at constant water content, indicates that with increasing confining pressure the value of normalized shear strength decreases and the behavior becomes more ductile.

7. Initial suction was found to have little influence on shear strength at low confining pressure (4 kPa).

8. The normalized modulus (E_{50}/σ_m) was found to increase with increasing initial suction, reaching maximum values at suctions at about the air-entry-value (3.5 kPa) and then levelling off. Therefore, increasing suction does not necessarily result in continuously increasing normalized modulus. Note that the decrease in the slope was more pronounced for low cell pressure (4 kPa). For confining pressures of 4 kPa and 64 kPa, and when moisture content changes from 7% to 10%, E_{50}/σ_m decreases by 20%, and 10% respectively.

9. The test results show that the hyperbolic stress-strain relation is applicable to unsaturated modified granular material at large strains (1% to 2%). Ductility also increases with increasing confining pressure.

10. Based on results corresponding to cyclic load tests performed at a stress ratio of 0.33, the materials entered a stable permanent deformation phase and the general trend indicates an increase in ε_p when σ_3 increases. However, there

are anomalies in which this does not occur. In fact, plastic strain accumulation is not constant for a constant stress ratio relative to failure, which had been originally assumed.

11. Analysis of the data showed that at low confining pressures the growth of plastic strain levels off after 5 cycles of loading/unloading and the material behavior approached an equilibrium state. At higher confining pressure (64 kPa), however, the material exhibited continuing deformation rather than stabilization. This phenomenon is more obvious as the water content/ degree of saturation rises.

12. Analysis of the data showed that the plastic strain (ε_p %) increased as the water content increased. However it is evident that with increasing confining pressure this effect is more noticeable. For confining pressures of 16 and 64 kPa, when moisture content changes from 10% to 4%, the plastic strain decreases by 17% and 30% respectively.

13. For material 1 at 4% and 7% moisture content, cyclic loading causes about a 33% decrease in plastic strain when the confining pressure decreases from 64 kPa to 4 kPa. However there is a decrease of about 64% in the plastic strain for material 1 and material 2 at 10 % moisture content.

14. It is clear from the cyclic tests that plastic strain accumulation is not a simple function of stress ratio, R, which had been originally assumed. The accumulated plastic strain is a function of confining pressure, suction, dilatancy, number of load cycles, and stress ratio. However, both suction and dilatancy are significantly affected by confining pressure. Therefore it appears that the effect of confining pressure on plastic strain is significant.

15. There is an approximate linear relation between plastic strain development and confining pressure for different water content. It was observed that with increasing confining pressure, the value of the plastic strain increases. However, the slope of the line increases with increasing water content.

16. It was found that freeze-thaw cycles increase the accumulated plastic strains. However, it appears that strain hardening memory may be lost due to freeze-thaw loading.

17. Results show that there is an almost linear relation between plastic strain and water content after freeze-thaw or cyclic tests.

18. The research also shows that there is an almost linear relation between $\Delta\varepsilon_p$ and moisture content after cyclic tests or freeze-thaw. For all cases, the $\Delta\varepsilon_p$ is higher after freeze-thaw.

19. The computer analysis showed that the surface deflection is relatively insensitive to the properties of the base layer, which in turn implies that deflection measurements are not a good indicator of changes in the properties of the base/subbase due to possible changes in moisture.

9.3 Minor Observations and Conclusions

1. The compaction energy, used to compact the samples prepared for this study, was 2.45 times less than that of the standard Proctor test. Based on compaction theory, this is expected to cause an increase in the optimum water content (w_{opt}) and a decrease in the maximum dry density (ρ_{dmax}). It should be mentioned that in spite of increasing the w_{opt} and decreasing the dry density, the air content was found to be between 7% and 8%. This is the same air content range of material tested in the standard Proctor test.

2. Three samples were prepared by applying suction during the preparation of specimens for the triaxial test and the results show that water content decreased on average from 10% to 7%.

3. The samples could not be prepared with water content 2% higher than w_{opt}, because during compaction and preparation of the samples the excess water would reach the top of the sample making it loose and unstable.

4. A SWCC test was conducted on Material 1 (drying curve) and the results show a bubbling pressure of about 3.5 kPa, which is in accordance with the characteristic results for sandy material.

9.4 Recommendations for Future Research

1. Greater attention should be given to the measurement of volume and suction changes that occur during shearing procedures (both quick undrained, consolidated undrained, and drained procedures) to more precisely understand the mechanisms responsible for shearing resistance.

2. Changes in suction should be measured during shear application. The following questions should be examined: Does the change in suction behave linearly with respect to changes in confining pressure and net mean stress? Does the change in suction that occurs with changes in pressure depend on the initial suction (water content) of the specimen before testing?

3. The changes in suction that occur specifically as a result of freeze-thaw of the unsaturated granular material should be examined.

4. The relation between normalized shear strengths and plastic strain of the granular material should be identified.

5. The adjustment to the normalized shear strengths-plastic strain relationship due to freeze-thaw phenomena should be investigated further.

LIST OF REFERENCES AND BIBLIOGRAPHY

Al-Douri, R. H. and Poulos, H. G. "Static and Cyclic Direct Shear Tests on Carbonate Sands." *Geotechnical Testing Journal*, 15 (1991): 138-157.

American Association of State Highway and Transportation Officials (AASHTO). *AASHTO Guide for Design of Pavement Structures,* American Association of State Highway and Transportation Officials. Washington, D.C. 1993.

Anderson, W. F. "Equipment for One-Dimensional Compression and Triaxial Testing of Unsaturated Granular Soils at Low Stress Levels." *Geotechnical Testing Journal*, 20 (1997): 74-89.

Barbour, S. L. "Nineteenth Canadian Geotechnical Colloquium: The soil-water characteristic curve: a historical perspective." *Canadian Geotechnical Journal*, 35 (1998): 873-894.

Barksdale, R. D. "Laboratory Evaluation of Rutting in Basecourse Materials." *Proceedings from the 3rd International Conference on the Structural Design of Asphalt Pavements*, London. 1 (1972): 161-174.

Bergan, A. T. and Monismith, C. L. "Characterization of Subgrade Soils in Cold Regions for Pavement Design Purposes." *Transportation Research Board Record*

No. 431. 1973: 25-37.

Bishop, A. W. "The principle of effective stress." *Tecknisk Ukeblad*, 106 (1959): 859-863.

Blatz, J. and Graham, J. "A system for controlled suction in triaxial tests." *Géotechnique*, 50 (2000): 1-5.

Blatz, J. et al. "Psychrometer Techniques for Measuring Suction in the Triaxial Test" [Electronic version]. *52nd Canadian Geotechnical Conference, Regina, SK.*1999.

Brooks, R. H. and Corey, A. T. "Hydraulic Properties of Porous Media." *Colorado State University Hydrology Paper*, No. 3. 1964.

Brown , S. F. and Pappin, J. W. "Analysis of Pavements with Granular Bases, Layered Pavement Systems." *Transportation Research Record No. 810.* 1981: 17-23.

Chamberlain, E. J. "Frost Susceptibility of Soil." *Review of Index Tests,* USA Cold Regions Research and Engineering Laboratory. 1983: 81-82.

Cole, D. M. et al. "Effect of Freezing and Thawing on Resilient Modulus of a

Granular Soil Exhibiting Nonlinear Behavior." *Transportation Research Board Record No. 809.* 1981: 19-26.

Cole, D. M. et al. "Resilient Modulus of Freeze-Thaw Affected Granular Soils for Pavement Design and Evaluation." *Laboratory Tests on Soils from Winchendon, Massachusetts, Part 1, Test Sections*.1986: 1-39.

Craig, R. F. Soil Mechanics. 4th ed. London: Chapman and Hall, 1990.

Croney, D. and Coleman, J. D. "Soil Thermodynamics Applied to the Movement of Moisture in Road Foundations." *Proceedings from the 7th International Congress of Applied Mechanics*, 3 (1948): 163-177.

Desai, C. S. and Siriwardane, H. J. Constitutive Laws for Engineering Materials. Englewood Cliffs, New Jersey: Prentice-Hall, 1984.

Drumm, E. C. et al. "Estimation of Subgrade Resilient Modulus from Standard Tests." *Journal of Geotechnical Engineering*, 116 (1990): 774-789.

Drumm, E. C. et al. "Alternative Test Method for Resilient Modulus of Fine-Grained Subgrades." *Geotechnical Testing Journal*, 19 (1996): 141-154.

Drumm, E. C. et al. "Subgrade Resilient Modulus Correction for Saturation Effects." *Journal of Geotechnical and Geoenvironmental Engineering*.1997: 663-670.

El-Naggar, H. M. Design of Equipment Foundations (Short Course). Continuing Education Units, Program Innovations Center, Toronto. 2003.

Erlingsson, S. and Magnusdottir, B. "Dynamic Triaxial Testing of Unbound Granular Base Course Materials." *Proceedings from the 6th International Conference on the Bearing Capacity of Roads, Railways and Airfields BCRA'02,* Lisbon, Portugal. 2002: 989-1000.

Erlingsson, S. et al. "Seasonal variation of moisture and bearing capacity in roads with a surface dressing wearing course." *Proceedings from the 9th International Conference on Asphalt Pavements,* Copenhagen, Denmark. 2002.

Erlingsson, S. "Mechanistic Pavement Design Methods-A Road to Better Understanding of Pavement Performance" [Electronic version –www.vegag.is]. *ViaNordica,* 2004.

Escario, V. and Juca. "Shear strength and deformation of partly saturated soils." *Proceedings of the 12th International Conference on Soil Mechanics and Foundation Engineering*, Rio de Janeiro, Brazil. 2 (1989): 43-46.

Escario, V. and Saez, J. "The Shear Strength of Partly Saturated Soils." *Géotechnique*, 36 (1986): 453-456.

Finn, F.N., et al. The Use of Distress Prediction Subsystems for the Design of Pavement Structures. *Proceedings*, 4th International Conference on the Structural Design of Asphalt Pavements, University of Michigan. Ann Arbor, MI. 1977.

Fredlund, D. G. et al. "Deformation Characterization of Subgrade Soils for Highways and Runways in Northern Environments." *Canadian Geotechnical Journal*, 12 (1975): 213-223.

Fredlund, D. G. et al. "Relation Between Resilient Modulus and Stress Conditions for Cohesive Subgrade Soils." *Transportation Research Record 652*, National Research Council, Washington, D.C. 1977: 73-81.

Fredlund, D. G. et al. "The shear strength of unsaturated soils." *Canadian Geotechnical Journal*, 15 (1978): 313-321.

Fredlund, D. G. et al. "Nonlinearity of Strength Envelope for Unsaturated Soils." *Proceedings of the 6th International Conference on Expansive Soils*, New Delhi, India. 1 (1987): 49-54.

Fredlund, D. G. "The Character of the Shear Strength Envelope for Unsaturated Soils." *The 12th International Conference on Soil Mechanics and Foundation Engineering*, Rio de Janeiro, Brazil, The Victor de Mello Volume. 1989: 142-149.

Fredlund, D. G. and Rahardjo, H. Soils Mechanics for Unsaturated Soils. New York: John Wiley & Sons, Inc., 1993.

Fredlund, D. G. and Xing, A. "Equations for the Soil-Water Characteristic Curve." *Canadian Geotechnical Journal*, 31 (1994): 533-546.

Fredlund, D. G. et al. "The relationship of the unsaturated soil shear strength to the soil-water characteristic curve." *Canadian Geotechnical Journal*, 33 (1996): 440-448.

Fredlund, D. G. "The 1999 R.M. Hardy Lecture: The implementation of unsaturated soil mechanics into geotechnical engineering." *Canadian Geotechnical Journal*, 37 (2000): 963-986.

Fredlund, M. D. et al. "Prediction of the Soil-Water Characteristic Curve from Grain-Size Distribution and Volume-Mass Properties" [Electronic version]. *3rd Brazilian Symposium on Unsaturated Soils,* 1997: 22-25.

Gan, J. K. M. and Fredlund, D. G. "Multistage direct shear testing of unsaturated soils." American Society for Testing Materials, *Geotechnical Testing Journal*, 11 (1988): 132-138.

Gens, A. et al. "A Constitutive Model for Partially Saturated Soils," *Géotechnique*, 40 (1990): 405-430.

Guthrie, S. and Scullion, T. "Using Dielectric Measurements to Predict Cold Weather Performance of Unstabilized Aggregate Base Materials" [Electronic version]. *Annual Meeting of the Transportation Research Board*, Washington, D.C. 2000.

Habibagahi, G. and Mokhberi, M. "A hyperbolic model for volume change behavior of collapsible soils." *Canadian Geotechnical Journal*, 35 (1998): 264-272.

Harris, J. S. Ground Freezing in Practice. London: Thomas Telford Services Ltd., 1995.

Haynse, J. H. and Yoder, E. J. "Effects of Repeated Loading on Gravel and Crushed Stone Base Material used in the AASHO Road Test." *Highway Research Board*, Record 39. 1963.

Heath, A. C. et al. "Normalizing the Behavior of Unsaturated Granular Pavement Materials." *Institute of Transportation Studies*, University of California. 2002.

Hicks, R. G. and Monismith, C. L. "Factors Influencing the Resilient Response Granular Materials." *Highway Research Record No. 345*, Highway Research Board, Washington, D. C. 1971: 14-31.

Holtz, W. G. and Gibbs, H. J. "Engineering Properties of Expansive Clays." Trans. ASCE, 121 (1956): 641-663.

Holtz, R.D. and Kovacs, W.D. An Introduction to Geotechnical Engineering. Prentice-Hall, Inc. Englewood Cliffs, NJ. 1981.

Huang, Y. H. Pavement Analysis and Design. Englewood Cliffs, New Jersey: Prentice Hall, 1993.

Huebner, K.H. et al. The Finite Element Method for Engineers, 4th ed. John Wiley & Sons, Inc. New York, 2001.

Huurman, M. "Permanent Deformation in Concrete Block Pavements." *Ph.D. Thesis*, Technical University of Delft, The Netherlands. 1997.

Irick, P. et al. "Characteristics of Load Equivalence Relationships Associated with

Pavement Distress and Performance, Phase II Study- Executive Summary". *Trucking Research Institute*, ATA Foundation, Inc., Alexandria, VA. 1991.

Jones, D.E. and Holtz, W.G. "Expansive Soils - the Hidden Disaster." *Civil Engineering,* 43(1973): 49-51.

Kallas, B. F. and Riley, J. C. "Mechanical Properties of Asphalt Pavement Materials." *Proceedings from the 2nd International Conference on the Structural Design of Asphalt Pavements*, Ann Arbor, Michigan. 1967.

Khallili, N. and Khabbaz, M. H. "A unique relationship for the determination of the shear strength of unsaturated soils." *Géotechnique*, 48 (1998): 681-687.

Kim, D. S. et al. "Alternative method of determining resilient modulus of subbase soils using a static triaxial test." *Canadian Geotechnical Journal*, 38 (2001): 117-124.

Knutsson, S. et al. "Analysis of Large Scale Laboratory and In Situ Frost Heave Tests." *Proceedings of the Fourth International Symposium on Ground Freezing*, Sapporo, Japan. 1985. 65-70.

Kono, F. et al. "Pavement Design in Cold Areas." *Proceedings, Symposium on*

Frost Action on Roads, Norwegian Road Research Laboratory. Oslo, Norway. 1973.

Lambe, T. W. and Whitman, R. V. Soil Mechanics. New York: Wiley, 1979.

Lekarp, F. and Dawson, A. "Analysis of Permanent Deformation Behavior of Unbound Granular Materials" [Electronic version]. *International Symposium on Thin Pavements, Surface Treatments, Unbound Roads*. 1997.

Lekarp, F. et al. "Permanent Strain Response of Unbound Aggregates." *Journal of Transportation Engineering*. 2000: 76-83.

Leong, E. C. and Rahardjo, H. "Review of Soil-Water Characteristic Curve Equations." *Journal of Geotechnical and Geoenvironmental Engineering*. 1997: 1106-1117.

Lytton, R.L. "Backcalculation of Pavement Layer Properties." *Nondestructive Testing of Pavements and Backcalculation of Moduli,* ASTM STP 1026. American Society for Testing and Materials. Philadelphia, PA. 1989: 7-38.

Mandal, J. N. and Divshikar, D. G. Soil Testing in Civil Engineering. New Delhi: Oxford & IBH, 1994.

Maree, J. H. "Ontwerpparameters vir klipslag in plaviesels (Design Parameters

for crushed stone in pavements)." *M.Eng. Thesis*, University of Pretoria, South Africa. 1978.

McCarthy, D. F. Essentials of Soil Mechanics and Foundations. Columbus: Prentice-Hall, 1998.

Miao, L. et al. "Empirical Function Representing the Shear Strength of Unsaturated Soils." *Geotechnical Testing Journal*, 24 (2001): 220-223.

Mitchell, J. K. Fundamentals of Soil Behavior. New York: John Wiley & Sons Inc., 1976.

Moran, M.J. and H.J. Shapiro. Fundamental of Engineering Thermodynamics. New York: Wiley and Sons. 1996.

Öberg, A. –L. and Sällfors, G. "Determination of Shear Strength Parameters of Unsaturated Silts and Sands Based on the Water Retention Curve." *Geotechnical Testing Journal*, 20 (1997): 40-48.

Rada, G. and Witczak, M.W. "Comprehensive Evaluation of Laboratory Resilient Modulus Results for Granular Materials." *Transportation Research Record No. 810*, Transportation Research Board, Washington, D. C. 1981: 23-33.

Rampino, C. et al. "Laboratory testing on an unsaturated soil: equipment, procedures, and first experimental results." *Canadian Geotechnical Journal*, 36 (1999): 1-12.

Rassam, D. W. and Williams, D. J. "A relationship describing the shear strength of unsaturated soils." *Canadian Geotechnical Journal*, 36 (1999): 363-368.

Saarenketo, T. et al. "Moisture Susceptibility and Electrical Properties of Base Course Aggregates." *Fifth International Conference on the Bearing Capacity of Roads and Airfields*, Trondheim, Norway. 1998: 1401-1410.

Said S. F. and Wahlström, J. "Validation of Indirect Tensile Method for Fatigue Characterizing of Bituminous Mixes." *2nd Eurasphaslt & Eurobitume Congress,* Barcelona. 2000: 772-778.

Said S. F. et al. "Evaluation of Permanent Deformation in Bituminous Mixes." *2nd Eurasphaslt & Eurobitume Congress,* Barcelona. 2000: 779-785.

Seed, H. B. et al. "Resilience characteristics of subgrade soils and their relation to fatigue failures in asphalt pavements." *Proceedings of the 1st International Conference on Structure Design of Asphalt Pavements*, Ann Arbor, Michigan. 1967.

Sweere, G. T. H. "Unbound Granular Bases for Roads." *Ph.D. Thesis*, University of Delft, Delft. 1990.

Tang, G. X. et al. "Volume Changes in Unsaturated Sand-Bentonite Caused by Suction-Controlled Drying and Wetting" [Electronic version]. *51st Canadian Geotechnical Conference, Edmonton, Alberta.* 1998.

Theyse, H. L. "Laboratory design models for materials suited to labour-intensive construction." *Transportek CSIR CR-99/038*, South Africa. 1999.

Theyse, H. L. "The development of mechanistic-empirical permanent deformation design models for unbound pavement materials from laboratory and accelerated pavement test data." *Unbound Aggregates in Road Construction.* Dawson (ed). Balkema, Rotterdam. 2000: 285-293.

Tomlinson, M. J. Foundation Design and Construction. 5th ed. New York: John Wiley & Sons Inc., 1991.

Tseng, K. H. and Lytton, R. L. "Prediction of Permanent Deformation in Flexible Pavement Materials." *Implication of Aggregates in Design, Construction, and Performance of Flexible Pavements, ASTM STP 1016.* H. G. Schrauders and C. R. Marek (eds.), American Society for Testing and Materials, Philadelphia. 1989:

154-172.

Vaid, Y. P. et al. "Laboratory Characterization of Stress-Strain Behavior of Soils by Stress and/or Strain Path Loading." *Geotechnical Testing Journal*, 24 (2001): 200-208.

Vaid, Y. P. et al. "Confining stress and static shear effects in cyclic liquefaction." *Canadian Geotechnical Journal*, 38 (2001): 580-591.

Vanapalli, S. K. et al. "The Relationship Between the Soil-Water Characteristic Curve and the Unsaturated Shear Strength of a Compacted Glacial Till." *Geotechnical Testing Journal*, 19 (1996): 259-268.

Vanapalli, S. K. et al. "Model for the prediction of shear strength with respect to soil suction." Canadian Geotechnical Journal, 33 (1996): 379-392.

Vanapalli, S. K. and Fredlund, D. G. "Comparison of Different Procedures to Predict Unsaturated Soil Shear Strength" [Electronic version]. *3rd Brazilian Symposium on Unsaturated Soils*. 1997.

Wan, A. W. L. et al. "On the relations of suction, moisture content and soil structure in compacted clays." *In Proceedings of the 1st International Conference on Unsaturated Soils*, Paris, France. E. E. Alonso, P. Delage and A. A. Balkema

(eds.), Rotterdam, The Netherlands. 1995: 215-222.

Watson, D. K. and Rajapakse, R. K. N. D. "Seasonal variation in material properties of a flexible pavement." *Canadian Journal of Civil Engineering*, 27 (2000): 44-54.

Wiebe, B. et al. "Influence of pressure, saturation, and temperature on the behavior of unsaturated sand-bentonite." *Canadian Geotechnical Journal*, 35 (1998): 194-205.

Wolff, H. and Visser, A. T. "Incorporating Elasto-plasticity in Granular Layer Pavement Design." *Proceedings of Institution of Civil Engineers*, Transport. 105 (1994): 259-272.

Wong, K. S. and Duncan, J. M. "Hyperbolic Stress-Strain Parameters for Nonlinear Finite Element Analyses of Stresses and Movements in Soil Masses." *University of California Report No. TE-74-3*. 1974: 1-58.

Yasuda, N. et al. "Undrained monotonic and cyclic strength of compacted rockfill material from triaxial and torsional simple shear tests." *Canadian Geotechnical Journal*, 34 (1997): 357-367.

Yoder, E.J. and Witczak, M.W. Principles of Pavement Design. 2nd ed. John Wiley and Sons. New York, 1975.

Yoshimine, M. et al. "Undrained shear strength of clean sands to trigger flow liquefaction." *Canadian Geotechnical Journal*, 36 (1999): 891-906.

Yuan, D. and Nazarian, S. "Variation in Moduli of Base and Subgrade with Moisture." Center for Highway Materials Research, The University of Texas at El Paso. 2003.